

**POLISH ACADEMY OF SCIENCES – WROCLAW BRANCH**  
**WROCLAW UNIVERSITY OF TECHNOLOGY**

---

# **ARCHIVES OF CIVIL AND MECHANICAL ENGINEERING**

**Quarterly**  
**Vol. II, No. 1**

**WROCLAW 2002**



## Mechanism of chipping of silicon carbide grains during grinding

J. BORKOWSKI, P. BORKOWSKI

Technical University of Koszalin, Raławicka 15–17, 75-620 Koszalin

The character of chipping of the abrasive grain edges is one of the most important factors affecting grinding efficiency. Such a kind of wear is possible when mechanical and thermal tensions exceed an abrasive material resistance. The mechanism of chipping of silicon carbide grains, which was emphasized by the theory of thermal stresses domination, was discussed in the paper. Both temperature and thermal stresses' distributions inside the abrasive grains during grinding were analyzed. The test results of the abrasive grains' heat load fatigue strength allow evaluation of the chipping character as well as the durability of silicon carbide grains. This enables us to define the mechanism of silicon carbide chipping during grinding process.

Keywords: *abrasive grain, silicon carbide, wear, grinding*

### 1. Introduction

The grinding of metal is usually accompanied by abrasive tool wear, which markedly affects the grinding performance. Tool wear may involve abrasive grain wear by attritions or fracture, the former being the major effect. The wear of grains, which are distributed over the cutting surface of an abrasive tool during its operation, is a very complex physicochemical and mechanical process that embraces all effects of brittle fracture, plastic strain, heating and oxidation of the grain as well as its chemical reactions with the surface layers of the work material [3]. An additional complication is that all these effects take place under periodically variable conditions which produce dynamic modifications of the properties of the grain, the bond and the work material [15].

Of major importance in the complicated process of grinding is thus the kind of abrasive and bond used and the physicochemical properties of the work material as well as the medium in which the process takes place [10, 11]. In grinding practice, also the interactions between the grain and the work, which takes place during grinding, are important. Consequently, knowledge of the elementary effects determining the wear processes as they affect the grain and binder material is most essential for rational planning and efficient implementation of the grinding process [6, 10].

An external manifestation of grain wear is the shape it takes in the course of abrasive machining. Most frequently grain wear involves:

- attrition of grain edges,
- surface microchipping,
- grain chipping and cracking.

The way this basic grain wear manifests itself depends first of all on the grinding conditions, which determine the cutting resistance, temperature, length of grinding zone, and so forth, and on the kind of abrasive material used.

The present work was aimed at explaining the decisive mechanisms of breaking chips from one of the most often used abrasives, i.e. silicon carbide. Investigations of such abrasives, including the grinding conditions, were carried out in order to determine the effect of mechanical and thermal stresses on a rate of chipping and, by the same token, a rate of self-sharpening of the grinding wheel.

## 2. Silicon carbide as an abrasive material

One of the most often used abrasives is silicon carbide. Its small expansion coefficient, which decreases with increasing temperature, high hardness, and sharp crystal edges make it a very efficient abrasive. The material is synthesized from silica and carbon at a temperature exceeding 2300 K in the Acheson resistance furnaces. Silicon carbide crystallizes in a hexagonal system sometimes forming monocrystalline ( $\alpha$ -SiC) platy grains (Figure 1). Such platy grains are characterized by structural homogeneity, a regular geometry forming cutting points at an angle of  $120^\circ$  (Figure 2), smooth lateral surfaces and edge sharpness (Figure 3).

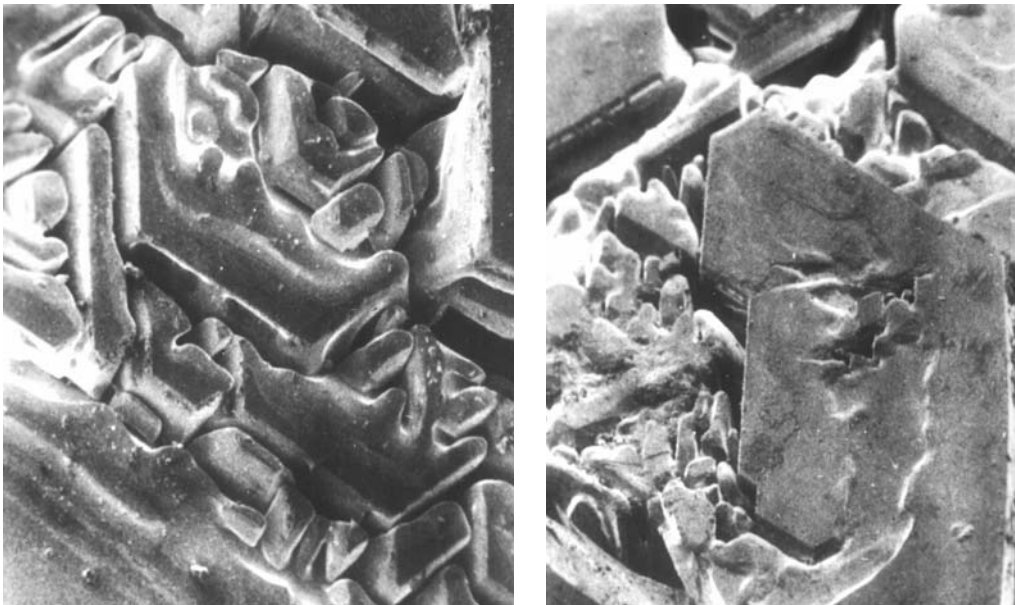


Fig. 1. Group of hexagonal  $\alpha$ -SiC monocrystals in various phases and degrees of crystallization

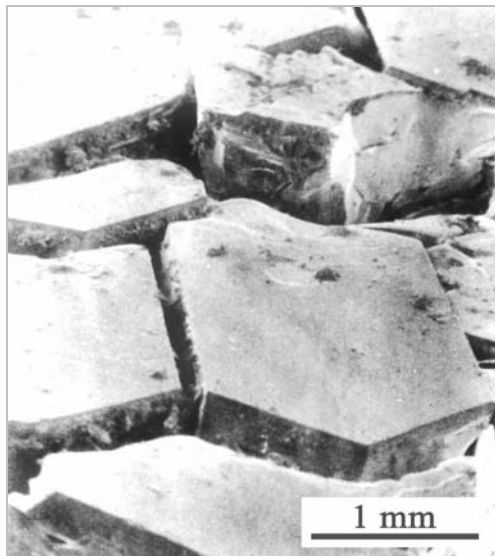


Fig. 2. Hexagonal  $\alpha$ -SiC monocrystals in identical phases and degrees of crystallization

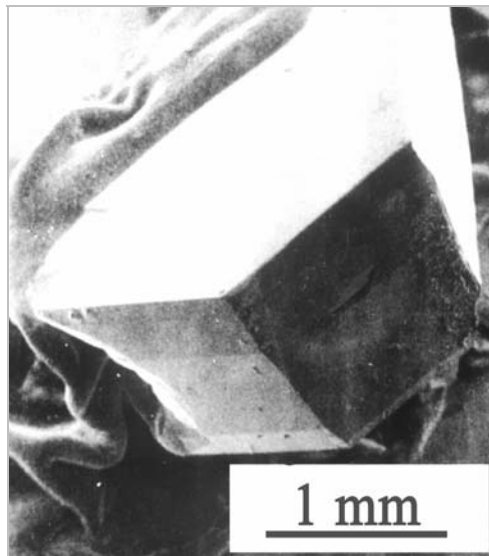


Fig. 3. Monocrystal of  $\alpha$ -SiC grain with naturally crystallized regular edges

This type of SiC grains' crystallization often affects an analogous way of their chipping during grinding and the wear behaviour of the whole grinding wheel [2, 4] making its life long. Therefore, it is necessary to carry out appropriate simulation tests allowing us to evaluate the extent of wear due to fatigue and thermal-fatigue loading of such abrasive grains in order to determine mechanisms of silicon carbide grain chipping in the course of grinding.

### 3. Fatigue chipping of silicon carbide grain particles

Fatigue chipping of silicon carbide grains in the course of grinding results from chipping of abrasive grain particles subjected to cyclic interaction produced by grinding forces. In order to determine more precisely the mechanisms of fatigue chipping of abrasive grains, one should analyze their behaviour under conditions of fatigue compression with the forces whose values are close to those applied in the process of grinding.

A special stand for testing the fatigue chipping of abrasive grains was constructed. Its working element is an electro-dynamic inductor controlled by a sine oscillator. The grain under study is subjected to compression between plates made of sintered tungsten carbide which are connected to the inductor terminals and an anvil of a piezoelectric dynamometer.

The tests on fatigue chipping of grain particles [2] revealed that the frequency of grain loading – within a standard rotational speed of grinding wheels – did not have

any practical effect on the fatigue resistance of the abrasive being tested. With an increase of the normal component of the cutting force  $F_N$ , the fatigue resistance of the grain – determined by a number of loading cycles at which the grain chipping or cracking occurs – decreases, whereas with an increase in the size of grains (expressed by their characteristic dimension  $a$ ), their fatigue resistance is on the increase. All the above interactions can be described by the following general dependence:

$$N_z = C_1 F_N^{-u_1} a^{w_1}. \quad (1)$$

This formula expresses the relationship between the fatigue strength of the grains and the fundamental parameter of loading  $F_N$  and the abrasive grain dimension  $a$ . A factor of proportionality  $C_1$ , indices  $u_1$  and  $w_1$  applied to this formula are determined by empirical methods.

The above investigations prove that a main factor deciding the fatigue resistance of the grains is their crystalline structure. Regular structure of monocrystalline silicon carbide grains contributes to their repeatedly higher resistance to fatigue chipping compared to standard grains. Average sizes of such grain fractures mostly do not exceed 3% of a dimension specific to abrasive grains. Therefore, volumetric elementary fatigue chipping of the grains can reach the following value:

$$\Delta V_{zz} = 0.25 \cdot 10^{-3} a^3. \quad (2)$$

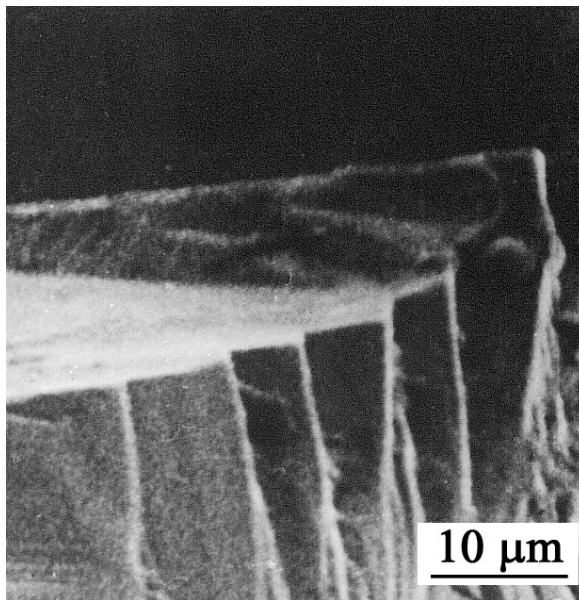


Fig. 4. Type of silicon carbide multi-edges spalling

Such grain chipping, affected by fatigue loadings, usually occurs in a slip plane of the  $\alpha$ -SiC crystal. It affects duplicating of external grain configurations in the form of new numerous cutting points (Figure 4).

#### 4. Thermal-fatigue chipping of silicon carbide grain particles

Thermal-fatigue chipping of grains occurs as a result of breaking chips from the bond under the influence of fatigue-producing thermal loads in the course of grinding. To determine such a form of silicon carbide grain wear one has to analyze the thermal stresses occurring in abrasive grains during grinding and carry out experimental investigations of the thermal-fatigue chipping of abrasive grains under the influence of fatigue produced by heat pulses applied.

##### 4.1. Analysis of thermal stresses in abrasive grains

The quality of the abrasive machining primarily depends on thermal phenomena, especially on the grinding temperature which determines the quality of the workpiece and the rate of adhesive wear. Investigations of the sources of grinding energy [8, 12] have revealed that they are as follows: chip-forming, sliding of grains and plastic deformation [9].

A great amount of heat is generated as a result of plastic deformation of material and friction between the grain and the work material, and the chip flowing along the abrasive grain [13]. Due to this fact, the temperature of cutting points often reaches [1] and even exceeds [12] the melting point of the work material under standard service conditions. The existing thermal stress concentration, because of the specific nature of grinding, brings about the state of thermal stresses which intensify the process of abrasive grain wear [9]. The value of thermal stresses generated in the surface layers of the work material and the abrasive grain is influenced by the thermal decomposition and the flow of heat fluxes in the grinding region [6, 13].

Undertaking the analysis of the thermal decomposition in single grains one should assume that under standard grinding conditions the temperature of cutting points is equal to that of the melting point of the work material ( $T_0$ ). Since some grain edges have flat worn surfaces [3], the flat thermal field could be also assumed. Then, the thermal decomposition prevailing in abrasive grains is only a function of time and place coordinates according to the following relation:

$$T = \frac{2}{\pi} T_0 \int_{\frac{r}{2\sqrt{K_0 t}}}^{\infty} e^{-x^2} dx, \quad (3)$$

where:

$T$  – temperature of the grain element under study at a given moment,

$T_0$  – melting point of the work material,  
 $r$  – distance between the grain and the heat source,  
 $t$  – time constant,  
 $K_0$  – coefficient of temperature compensation.

The results of these calculations (Figure 5) show that the deeper these layers under the surface of grains, the lower their temperature. It should be also stressed that at a shorter time of contact, the temperature difference will be larger.

Assuming that the grain surface, while coming out the grinding region, takes the ambient temperature, the thermal field obtained can be described by the following relation:

$$T = \frac{2}{\pi} T_0 \left( \int_{\frac{r}{2\sqrt{K_0 t}}}}^{\infty} e^{-x^2} dx - \int_{\frac{r}{2\sqrt{K_0(t-t_k)}}}}^{\infty} e^{-x^2} dx \right), \quad (4)$$

where  $t_k$  is duration of grain–work contact. At the same time this relation is valid for the time  $t$  in the interval from  $t_k$  to infinity.

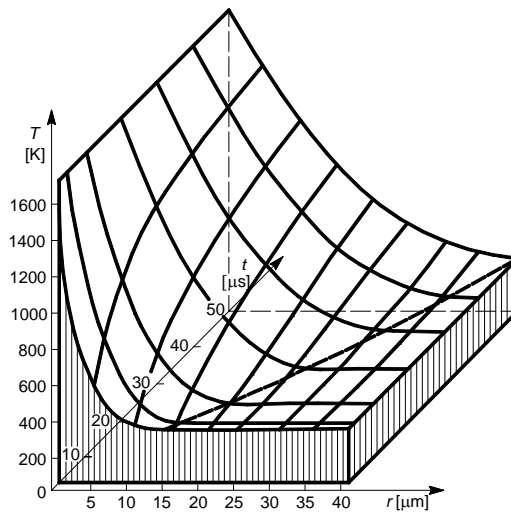


Fig. 5. Distribution of temperature in silicon carbide grains in the course of grinding, i.e. while heating the grain surface

After leaving the grinding region the grain surface cools down which brings about its different thermal decomposition. As the depth of penetration under the grain surface was growing, the temperature rose at the beginning and after reaching the maximum value it dropped again. The temperature values are very crucial for the duration of grain in the grinding region, while cooling down. At higher rates of grinding, corresponding to shorter time of grain heating in the grinding region, the

temperature of the grain is dropping more rapidly after its leaving this region. This behaviour justifies the use of higher grinding rates [14].

Moreover, the heat transmitted to the abrasive grain induces a thermal gradient which enables us to determine the tangential stresses in accordance with the following relation [2]:

$$\sigma_t = Gd\alpha_z\beta_z\left(\frac{dT}{dr}\right), \quad (5)$$

where:

$\sigma_t$  – tangential stress in the surface layers of the abrasive grain,

$G$  – rigidity modulus of abradant,

$d$  – size of the grain element under study,

$\alpha_z$  – coefficient of thermal expansion,

$\beta_z$  – coefficient of the regularity of tension distribution,

$T, r$  – symbols employed in relation (3).

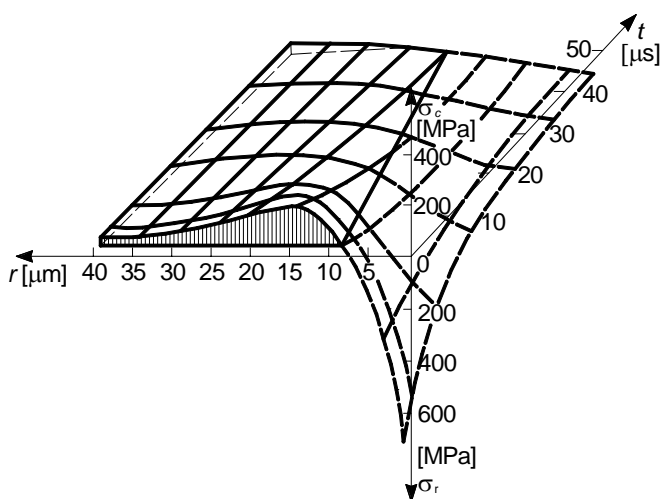


Fig. 6. Distribution of thermal stresses in silicon carbide grains after their leaving the grinding region

Based on the analysis of thermal stresses induced in grains, while they are in contact with the work material, we arrive at conclusion that the maximum values of these stresses occur in surface layers of grains at the initial stage of their contact, i.e. for shorter periods of time. At the same time, while cooling off the grain in surface layers of abradant, the diversification of thermal stresses appeared (Figure 6). Tensile stresses occurred on the grain surface, while compressive stresses were in deeper layers of



abradant. The maximum values of tensile stresses occurred on the grain surface at an initial stage of cooling. This can bring about grain cracking because the abrasive resistance to tensile stresses is twice lower than that to compressive ones.

Cyclic repetition of stress patterns occurring in surface layers of grains makes the abrasive grains crack not on their surface, but in deeper layers of material [5]. Taking account of the above, the grain strength is higher because under such conditions it is easier for small cracks to be reinforced by diffusion. Only after exceeding some boundary value the chipping of grain edges takes place.

#### 4.2. Investigation of thermal-fatigue abrasive grain chipping

Investigation of the thermal-fatigue abrasive grain chipping allowed analysis of thermal phenomena occurring in the grinding region. This analysis was carried out at the same assumptions as above. Values of unit heat pulses affecting single abrasive grains in the course of grinding were calculated on the basis of [5] from the following formula:

$$Q_e = \frac{1.125}{J} \frac{K_2 \cdot L \cdot \sigma_t}{\sqrt{K_1 \cdot c_1 \cdot \rho_1 \cdot v \cdot l_s^{-3}}}, \quad (6)$$

where:

$J$  – Joule's constant,

$K_1, K_2$  – thermal conductivity of the workpiece and the abrasive material, respectively,

$L$  – length of the grain interference zone in the workpiece,

$l_s$  – dimension of the heat source,

$c_1$  – specific heat of the workpiece,

$\rho_1$  – density of the workpiece,

$v$  – velocity of the moving source (cutting speed),

$\sigma_t$  – interface shearing stress.

Thermal pulses generated by an electronic micro-machine BMF 100 (Carl Zeiss Oberkochen) were applied to separate the thermal interactions. These investigations [2, 4] confirmed that intensity of thermal-fatigue grain wear was mainly affected by the changes in energy of single heat pulses. For example, fatigue wear of  $\alpha$ -SiC monocrystal surfaces under thermal conditions similar to these of grinding appears only after application of heat pulses in the range from 28000 to 100000. The relation between a number of these pulses (Figure 7) and their energy is given by the following formula:

$$N_{tz} = C_2 \cdot Q_e^{-w_2}, \quad (7)$$

where:

$C_2, w_2$  were determined experimentally,  
 $Q_e$  – energy of single heat pulses expressed by (6).

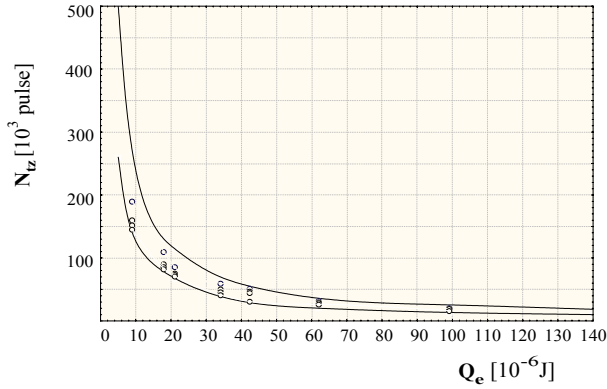


Fig. 7. Thermal life of  $\alpha$ -SiC monocrystal versus a single heat pulse (pulse duration  $t_e = 5\mu\text{s}$ )

On the other hand, longer duration of single heat pulse – which is connected with a decrease in grinding rate – is considered to be the major cause of more extensive grain chipping (Figure 8). Such heat pulses lasting as long as a single grain–work contact produces relatively extensive areas of grain wear within 30–200  $\mu\text{m}$ . Thus, mean volumetric wear of abrasive grains influenced by thermal-fatigue pulses with the energy  $Q_e$  and the duration  $t_e$  can be expressed by general relation:

$$a_e = C_3 \cdot Q_e \cdot e^{u_2 t_e}. \quad (8)$$

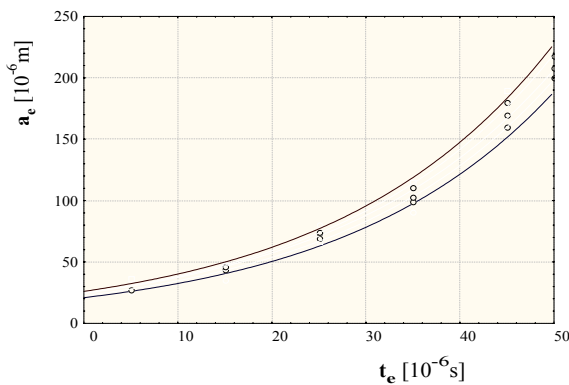


Fig. 8. Wear of  $\alpha$ -SiC monocrystal surface versus pulse duration

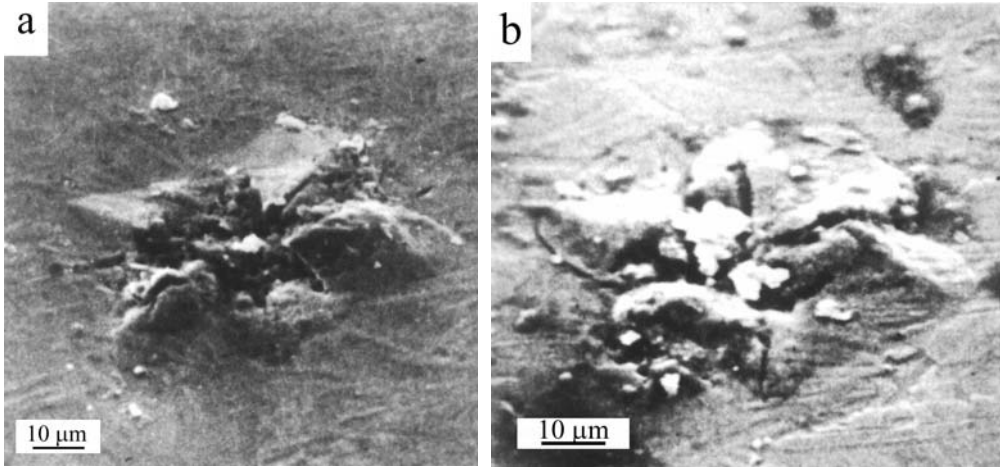


Fig. 9. Examples of thermal breakdown of silicon carbide monocrystal surfaces.  
Experimental conditions:  $Q_e = 133 \times 10^{-6}$  J,  $N_t = 7000$  (a),  $Q_e = 34 \times 10^{-6}$  J,  $N_t = 50000$  (b)

These cracks on the grain surface arrange themselves into symmetric six-pronged stars that conform to hexagonal structure of  $\alpha$ -SiC crystals (Figure 9). Taking into consideration this structure of silicon carbide it is possible to determine volumetric single grain chipping. It is approximated by the following relation:

$$\Delta V_{tz} = 0.076 \cdot a_e^3. \quad (9)$$

Inserting Equation (8) to the above relation, the following formula for volumetric single grain chipping is obtained:

$$\Delta V_{tz} = C_4 \cdot Q_e^3 \cdot e^{u_3 t_e}, \quad (10)$$

where:

$C_4$  – proportionality factor (equal to  $0.076 \cdot C_3^3$ ),

$u_3$  – index (equal to  $3u_2$ ),

$t_e$  – duration of a single heat pulse,

$e$  – base of the Neperian logarithm,

$Q_e$  – quantity as in (7).

The above experimental results are mainly applied to  $\alpha$ -SiC monocrystals of relatively good technological properties. Therefore, it is worth noting that thermo-fatigue wear of standard abrasive grains in the course of grinding is remarkably higher and under specified conditions self-sharpening of the grinding wheel can take place [2, 4].

## 5. Chipping mechanism of silicon carbide grain particles

The chipping mechanism of abrasive grains repeatedly exposed to small forces can be explained by wedging them apart with gases trapped in grain pores and cracks. Due to grain compression these pores and cracks are stopped and gas cushions are forced deeper intensifying this effect as a number of load cycles increase. Still more effective grain wedging is caused by cutting the fluid that gets inside cracks in the course of grinding.

However, a real chipping mechanism of abrasive grains can be determined on the basis of tests on single grains carried out under conditions similar to those of grinding. Typical wear of abrasive grain consists in chipping and cracking of abrasive grains, or of their top layers, under the influence of the stress induced by grinding conditions (Figure 10). Wear of this kind takes place when mechanical or thermal stresses or, most usually, their combined action, produce in the abrasive a state of effort exceeding its strength. Such grain wear is found to be dominant mostly under conditions of high performance grinding.

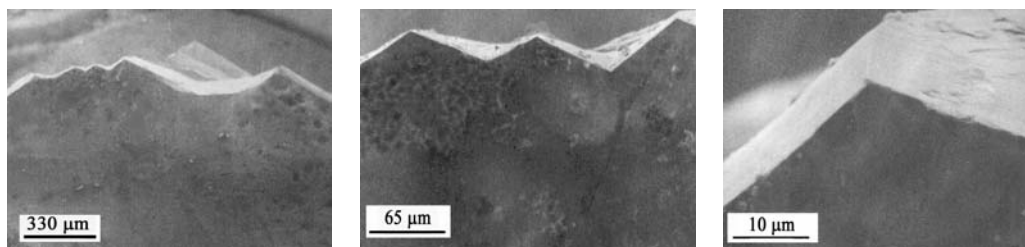


Fig. 10. Character of  $\alpha$ -SiC monocrystal grain top spallings. Enlargements of particular grain areas

Standard grains formed of aggregates of fine crystal structure in general crack along grain boundaries exposing new cutting edges random in shape [7], whereas wear in  $\alpha$ -SiC monocrystals of hexagonal crystal structure proceeds along slip planes. Consequently, a larger number of small edges with typical apex angles of  $120^\circ$  (Figure 4) mostly appear in place of chipped edges. Furthermore, point corner radii of new edges are usually equal to those of initial ones which enables us to maintain similar technological properties of grains within the grinding wheel life.

All micrographs presented here make evident distinct anisotropy of the properties of silicon carbide due to its hexagonal structure. Moreover, the mechanism of microcrack formation induced by thermal-fatigue grain wear (Figure 9) consists in the fact that interactions of consecutive heat pulses make the earlier cracks spread and the new cracks come into being which also spread with application of further heat loads. This way “a star” of cracks (Figure 11) is formed where prongs conform to the planes of closely packed atoms in hexagonal crystal structure of silicon carbide grains.

Based on these models of silicon carbide grain wear it is possible to do calculations allowing assessment of the sizes of  $\alpha$ -SiC grain chipping.

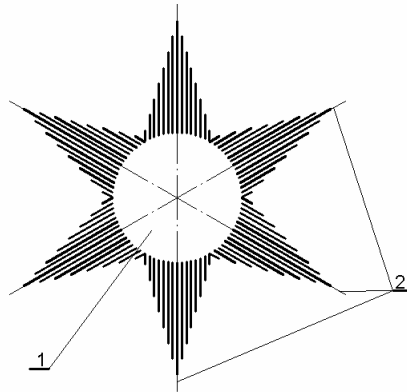


Fig. 11. Diagram of thermal-fatigue wear of silicon carbide monocrystal surface: 1 – electron beam impact trace, 2 – surface directions of closely packed atoms filled with traces of the first crystal cracks

In order to determine the abrasive grain wear, one has to make allowances for volumetric single grain chipping described by Equations (2) and (10) and maximum number of loading cycles with pulsating force (Equation (1)) and heat pulses (Equation (7)). It allows us to determine total values of volumetric wear of silicon carbide grains during grinding time under the influence of mechanical stress along with thermal stress. Hence, such volumetric wear of abrasive grain is given by the following relation:

$$\Delta V = n \cdot t \cdot \left( \alpha \cdot C_5 \cdot F_N^{u_1} \cdot a^{3-w_1} + \beta \cdot C_6 \cdot Q_e^{3+w_1} \cdot e^{u_2 t_e} \right), \quad (11)$$

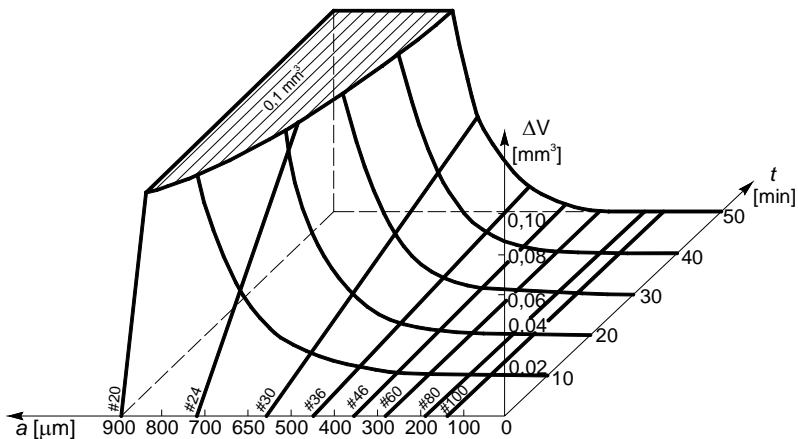


Fig. 12. Formation of volumetric thermal-fatigue wear of abrasive grain as a function of grinding time and abrasive grain size ( $D = 300$  mm,  $v = 30$  m/s,  $v_w = 15$  m/min,  $g = 0.05$  mm)

where:

$\alpha, \beta$  – the factors of interference in both forms of abrasive grain wear,

$n$  – rotational speed of grinding wheel,

$t$  – duration of grinding process,

$F_N$  – normal cutting force component,

$a$  – characteristic abrasive grain dimension,

empirical factors  $C_5 = 0.0042 \cdot 10^{-3} C_1^{-1}$  and  $C_6 = C_4/60C_2$ .

Plots of these relations as a function of grain size and grinding duration are presented in Figure 12. According to this diagram the total magnitude of volumetric fatigue abrasive grain wear occurring under the joint influence of mechanical and thermal stresses increases in direct proportion to cutting time. On the other hand, an increase in abrasive grain size produces a rapid increase in volumetric wear of abrasive grain, because its growing contact area with work material contributes to an increase in heat pulses inducing thermal stresses which constitute a major mechanism of self-sharpening of  $\alpha$ -SiC abrasive grains.

## 6. Conclusions

The experimental investigations of the wear of silicon carbide grains under grinding conditions and detailed theoretical analyses of the grain wear enabled us to determine the mechanisms of silicon carbide grain chipping in the grinding process. The explanation of different types of wear formation under the influence of anisotropy of physical properties of silicon carbide grains allowed development of the useful models of their wear. Due to them it is possible to do respective calculations in order to determine the extent of silicon carbide grain wear and total volumetric wear of these grains that which occur under the joint influence of mechanical and thermal stresses. This enabled us to put forward the following essential theses of general character:

- Process of silicon carbide wear is of a beneficial character because it tends to produce numerous cutting edges. Such grain chipping usually occurs in a slip plane of  $\alpha$ -SiC crystal revealing its hexagonal crystal structure. Consequently, new apex angles of  $120^\circ$  with sharp edges formed by smooth lateral surfaces ensure high durability of the abrasive grains.

- Rate and specific character of silicon carbide wear are determined by mechanical and thermal stresses induced by fatigue interaction. Then, the extent of wear mainly depends on the range of heat sources affecting the individual abrasive grains. From the practical point of view, the extent of thermal-fatigue grain wear is under the influence of its contact area with the work material which mainly depends on a grain size and a state of wear. Thus, this wear process is getting more intense with an increasing attritious wear of grain. The more extensively the areas of cutting edges are worn, the more intensive is the process of thermal-fatigue abrasive grain wear.

- The above phenomena have a beneficial influence on the self-sharpening mechanism of the abrasive tool in the grinding process. Silicon carbide grain chipping uncovers new and numerous cutting edges and points ensuring a high grinding performance of the grinding wheel.

## References

- [1] Bokučava G.V.: *Temperatura rezanija pri šlifovanii*, Vestnik Mašinstroenija, 1963, nr 11, s. 62–66.
- [2] Borkowski J.: *Zużycie i trwałość ściernic*, PWN, Warszawa, 1990.
- [3] Borkowski J., Borkowski P.: *Physical aspects of attritious grain wear in grinding conditions*, Scientific Publication of Mechanical Department: Modern techniques and technologies, Technical University of Koszalin, Koszalin, 2001, pp. 54–66.
- [4] Borkowski J., Szymański A.: *Uses of abrasives and abrasive tools*, Ellis Horwood Ltd., New York–London–Toronto–Sydney–Tokyo–Singapore, 1992.
- [5] Hahn R.S.: *On the nature of the grinding process*, 3<sup>rd</sup> Intern. MTDR Conf., Birmingham, Pergamon Press, 1963, pp. 129–154.
- [6] Kim N.K., Guo C., Malkin S.: *Heat flux distribution and energy partition in creep-feed grinding*, Annals of the CIRP, Vol. 46, 1997, No. 1, pp. 227–232.
- [7] Koziański A.: *Czynna powierzchnia ściernicy. Metody badań makro- i mikogeometrii*. Wydawnictwo Politechniki Łódzkiej, Łódź, 1996.
- [8] Malkin S.: *Grinding technology. Theory and applications of machining with abrasives*, Ellis Horwood Ltd., New York–Chichester–Brisbane–Toronto, 1989.
- [9] Oczóś K., Porzycki J.: *Szlifowanie. Podstawy i technika*, WNT, Warszawa, 1986.
- [10] Rowe W.B., Jin T.: *Temperatures in high efficiency deep grinding (HEDG)*, Annals of the CIRP, Vol. 50, 2001, No. 1, pp. 205–208.
- [11] Rowe W.B., Morgan M.N., Black S.C.E.: *Validation of thermal properties in grinding*, Annals of the CIRP, Vol. 47, 1998, No. 1, pp. 275–279.
- [12] Ueda T., Sato M., Sugita T., Nakayama K.: *Thermal behaviour of cutting grain in grinding*, Annals of the CIRP, Vol. 44, 1995, No. 1, pp. 325–328.
- [13] Warnecke G., Zitt U.: *Kinematic simulation for analyzing and predicting high-performance grinding processes*, Annals of the CIRP, Vol. 47, 1998, No. 1, pp. 265–270.
- [14] Weiss Z.: *Szlifowanie szybkościowe*, Wydawnictwo Politechniki Poznańskiej, Poznań, 1987.
- [15] Zheng H. W., Gao H.: *A general thermal model for grinding with slotted or segmented wheel*, Annals of the CIRP, Vol. 43, 1994, No. 1, pp. 287–290.

## Mechanizm wykruszania się ziaren ściernych węgliku krzemu podczas szlifowania

Na efektywność szlifowania znacząco wpływa charakter zużycia ściernic. Ten zaś zależy przede wszystkim od zużycia ziaren ściernych, które może występować w postaci wyruszeń cząstek materiału ściernego. Z takim zużyciem mamy do czynienia, gdy naprężenia mechaniczne lub cieplne, a najczęściej ich wspólne oddziaływanie, wywołują stan wyteżenia materiału ściernego przekraczający jego wytrzymałość. Ten typ zużycia ziaren dominuje najczęściej w warunkach wysoko wydajnej obróbki ściernic.

W artykule przedstawiono wyniki badań i analiz dotyczące mechanizmu powstawania zjawiska samoostrzenia ściernic z węgla krzemu, które uwypuklają teorię dominacji naprężeń cieplnych. Opisano kształtowanie się temperatury w ziarnach ściernych, określając rozkład pola temperatur w ziarnach ściernych podczas skrawania i chłodzenia w warunkach szlifowania z różnymi prędkościami. Obliczono także analogiczne rozkłady pola naprężeń cieplnych i omówiono ich wpływ na wykruszanie się ziaren. Zbadano również odporność ziaren ściernych na zmęczeniowe obciążenia cieplne, aby wyodrębnić jedynie wpływ zjawisk cieplnych na trwałość ziaren ściernych, a pominięto inne rodzaje oddziaływania.

Badania intensywności i charakteru zużycia ziaren węgla krzemu, przeprowadzone przy użyciu pojedynczych ziaren ściernych skrawających w warunkach odpowiadających szlifowaniu pozwoliły wyjaśnić rzeczywisty mechanizm ich zużycia. Pod wpływem zmęczeniowego oddziaływania naprężeń mechanicznych i cieplnych wykruszenia ziaren węgla krzemu występują zwykle po płaszczyznach poślizgu kryształu  $\alpha$ -SiC. Takie uzewnętrznienie heksagonalnej budowy kryształów sprzyja powstawaniu licznych wierzchołków ziarna o kącie  $120^\circ$  i ostrych krawędziach utworzonych przez gładkie powierzchnie. Jest to korzystne, gdyż zapewnia ziarnom odpowiednie własności skrawne w całym wydłużonym okresie trwałości ściernicy.

Na podstawie powyższych wyników opracowano użyteczne modele zużycia ziaren węgla krzemu umożliwiające zadowalająco dokładne obliczanie wielkości i intensywności zużycia takich ziaren i całych ściernic.



## The influence of elementary effects on grinding wheel wear

J. BORKOWSKI, P. BORKOWSKI

Technical University of Koszalin, Raławicka 15-17, 75-620 Koszalin

In the paper, there have been presented the dependences that describe the intensity of grinding wheels wear which occurs due to elementary processes of grains wear and bond fracture. The interactions between these elements during the grinding process were also analysed. This allowed describing the formulas which render the resulting intensity of grinding wheel wear calculated various grinding conditions. The results presented enabled evaluation of the influence of chosen parameters and characteristic elements on the intensity of grinding wheel wear and proportional shares of individual elementary wear processes.

Keywords: *abrasive grains wear, elementary wear processes, grinding wheels wear, wear*

### List of notations

$a$	– grinding depth,
$h$	– number of layers of the grinding wheel working surface,
$m$	– coefficient of the limiting wear of the abrasive grain,
$n$	– rotational speed of grinding wheel,
$n_a$	– number of the active grains on the working surface of the grinding wheel,
$r$	– radius of the surface wear of the abrasive grain edge,
$t_e$	– duration of the thermal impulse,
$u_1, u_2, u_3$	– empirical indices,
$v_s$	– grinding velocity,
$w_1, w_2, w_3$	– empirical indices,
$x$	– wear degree of the abrasive grain,
$y$	– coefficient of linear wear of the abrasive grain,
$\alpha$	– interference coefficient of the main forms of grinding tool wear,
$\beta$	– interference coefficient of various forms of grinding tool wear,
$C_1, C_2, C_3$	– empirical constants,
$D$	– diameter of grinding wheels,
$F_N$	– maximum value of the pulsating force compressing the abrasive grain,
$H$	– width of grinding wheels,
$K_z$	– number of grains in a unit of the grinding wheels surface,
$P_a$	– probability of activity of abrasive grains,
$P_d$	– probability of immediate chipping of grain particles,
$Q_t$	– intensity of the grinding wheel wear due to the thermofatigue wear of grains,
$R$	– radius of a spherical model of abrasive grain,
$T_{WN}$	– numerical equivalent of grinding wheel hardness,

$T_{\max}$	– maximal duration of the grinding wheel life, whose grains are subjected to wear through mechanical abrasion of vertices,
$T_s$	– duration of the grinding wheel life with the mechanical abrasion of grains only within the range of technological norms,
$T_B$	– duration of the grinding wheel life with taking account of the cracking of the bond bridges,
$T_G$	– duration of grinding wheel life with taking account of wear of all abrasive grains,
$T_N$	– duration of grinding wheel life,
$W_B$	– intensity of grinding wheel wear due to bond fracture,
$W_d$	– intensity of the grinding wheel wear due to immediate wear of abrasive grains,
$W_G$	– intensity of grinding wheel wear due to the interaction between all forms of grinding wheel wear,
$W_f$	– intensity of grinding wheel wear due to fatigue cracking of the bond bridges,
$W_N$	– global intensity of grinding wheel wear,
$W_s$	– intensity of grinding wheel wear due to abrasion of grain edges,
$W_{sz}$	– intensity of “grains shell” from the grinding wheel subjected to abrasive wear,
$W_t$	– intensity of grinding wheel wear due to thermofatigue wear of grains,
$W_w$	– intensity of grinding wheel wear due to immediate cracking of the bond bridges,
$W_z$	– intensity of grinding wheel wear due to fatigue wear of abrasive grains,
$V_{zk}$	– volume of a spherical model of abrasive grain,
$\Delta V_{dz}$	– volume unit chipping of a grain due to its immediate wear,
$\Delta V_{zz}$	– volume unit chipping of a grain due to its fatigue wear.

## 1. Introduction

Earlier analysis of elementary wear processes [1] allows defining the influence of individual grinding parameters and grinding conditions on wear of abrasive grains [3], the bond fracture [2] and, consequently, wear of the whole grinding wheels [4]. This enables a detailed recognition of the wear mechanisms resulting from the interactions between definite kinds of elementary processes [5, 9]. If, however, mechanical or thermal [12, 13] loads are taken into account separately, they cause that wheel wear occurs after relatively high number of cyclic interactions [7]. On the other hand, simultaneous influence of both these factors produces a considerable increase in the global wear [11]. Thus, under normal grinding conditions [8] a great role is played by the global wear which consists in partial influences of individual elementary processes. That is why it is necessary to be familiar with the influence of individual elementary processes on the degree of global grinding wheel wear [10]. This allows recognition of elementary processes' influence in given grinding conditions as well as it gives the opportunity to define the interrelations between separate processes and to compare their interactions. So far the processes which are responsible for the physical process of tool wear have not been taken into account despite the fact that these processes have a decisive influence on the intensity of wheel wear.

This paper is meant to give an explanation of the role of these processes in physical bases of grinding wheel wear.

## 2. Wear of grinding wheels in respect to individual elementary processes

A detailed analysis of the grinding wheel wear process allowed us to select the most important elementary processes which have a decisive influence on the intensity of grinding wheel wear. Due to specific structure of grinding wheels their lives depend on the wear of abrasive grains and on bond fracture [2]. On the basis of research [1] conducted in isolated conditions there were defined and described [4] types of physical processes which were responsible for the two processes of grinding wheel wear. To define the interrelations between individual elementary processes and their role in wheel wear it is necessary to find a common basis of comparison of those elementary quantities' influence [6]. In order to formulate analytically this topic, the influences of individual elementary processes should be established, starting with the base quantity, i.e. intensity of wear.

In paper [1], it has been proved that among wear processes of abrasive grains, the main selected are as follows:

- grains attrition, which occurs with the intensity of  $W_s$ ,

$$W_s = \frac{500\pi}{3h} v \Delta R H K_z \left\{ (3r^2 + A^2 R^2) + (AR + \Delta R) [6Br + 2AR + (1 + 3B^2) \Delta R] \right\} \sum_{i=1}^h P_{ai}, \quad (1)$$

where:

$$A = 1 - \cos\left(\arcsin \frac{r}{R}\right),$$

$$B = \cot\left(\arcsin \frac{r}{R}\right);$$

- immediate chipping of grains particles, which occurs with the intensity of  $W_d$ ,

$$W_d = 1000v \frac{H}{h^2} K_z \Delta V_{dz} \sum_{i=1}^h P_{ai} P_{di}; \quad (2)$$

- fatigue chipping of grains particles, which occurs with the intensity of  $W_z$ ,

$$W_z = 1000v \frac{H}{h} \frac{F_N^{u_1}}{C_1 R^{w_1}} K_z \Delta V_{zz} \sum_{i=1}^h P_{ai}; \quad (3)$$

- thermal-fatigue chipping of grains particles, which occurs with the intensity of  $W_t$ ,

$$W_t = 1000 C_2 v \frac{H}{h} Q_t^{3+w_2} e^{u_2 l_c} K_z \sum_{i=1}^h P_{ai} . \quad (4)$$

On the other hand, the main processes of wheel wear associated with bond spalling are brought about by [2]:

- immediate breaking of the bonding bridges, which occurs with the intensity of  $W_w$ ,

$$W_w = 1000 v \frac{H}{h^2} K_z V_k \sum_{i=1}^h P_{ai} P_{wi} ; \quad (5)$$

- fatigue-induced breaking of the bonding bridges, which occurs with the intensity  $W_f$ ,

$$W_f = 1000 \frac{1}{C_3} v \frac{H}{h} \frac{F_N^{u_3}}{R^{w_3} T_{WN}^z} K_z V_k \sum_{i=1}^h P_{ai} . \quad (6)$$

If we assume that there is only unilateral influence of the elementary process being investigated (abrasive wear in this case), duration of the tool life can be defined from a comparison of the active grains with the intensity of their relative wear. The intensity of relative wear of grains should be interpreted as the relation between the intensity of wearing up and the admissible volume of the grain subjected to wear, i.e. in practice it is the intensity of “grains shell” out of the grinding wheel, which is expressed by the dependence:

$$W_{sz} = \frac{W_s}{m V_{zk}} . \quad (7)$$

In this dependence, the coefficient of the admissible wear of abrasive grain is a number within the range from 0 to 1. This number provides information that with exceeding a specified degree of grain wear there occurs damage of the bonding bridges and the remaining part of the grain falls out despite of its not fully used abrasive potential.

The number of the active grains existing on grinding wheel cutting surface are expressed by the following formula [1]:

$$n_a = D H h^{-1} \cdot K_z \cdot \sum_{i=1}^h P_{ai} . \quad (8)$$

Thus the duration of abrasive grain life examined in this way is expressed by the ratio of the number of grains participating in the grinding process to the intensity of

wear, the so-called “grains shell” of the active grains, that is:

$$T_{\max} = \frac{n_a}{W_{sz}} \quad (9)$$

But this duration of life is calculated from the moment of full wear of one layer of abrasive grains. In reality, however, the life of grinding wheels being subjected to attrition wear of grains is decisively affected not by full wear of the grains, but by their such partial wear that causes the tool bluntness. Usually such wear occurs already at relatively small linear wear of the grain defined by the product of the radius  $R$  of a spherical model of the grain and the coefficient of the linear wear ( $y$ ), as is shown in Figure 1.

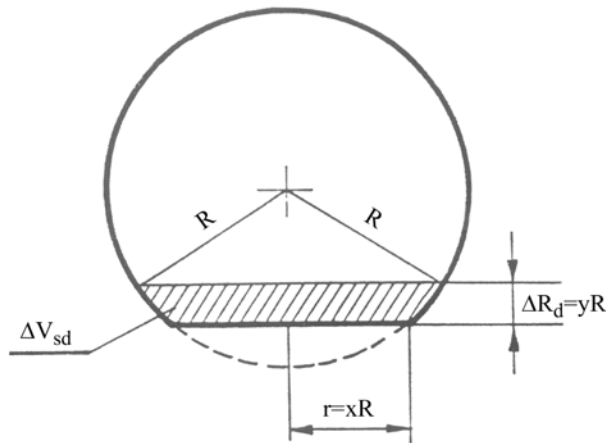


Fig. 1. Diagram of the spherical model of an abrasive grain illustrating the way of defining the linear degree of its wear

Thus for such a case the admissible volume wear of the grain is expressed by the following dependence:

$$V_{sd} = \frac{yR^3}{3} \cdot \left[ (2x^2 + 1) - (y - 1 - x^2) \right]^2 \quad (10)$$

In this expression, the coefficient of the admissible linear wear  $y$  of the grain, in regard to admissible grain wear up to 10% of its nominal dimension, equals 0.2, and the values of the coefficient  $x$ , which define the degree of grain wear, range from 0 to 1.

If instead of the grains volume in dependence (7) we take into account the admissible volume wear of the grain expressed by dependence (10), then we can define the so-called technological duration of the grinding wheel life according to the principle (11):

$$T_s = \frac{n_a V_{sd}}{W_s}. \quad (11)$$

The above procedure of calculating the duration of the grinding wheel life refers only to the first elementary process of wear. In all other cases – when we deal with the fracture grain wear and cracking of the bonding bridges – the calculating procedure is simplified. It comprises the procedure described in the above example with adequately adapted, to meet the needs, general formulas like equations (7)–(9).

Between the above-mentioned elementary quantities there exist interrelations which – with simultaneous run of elementary processes – increase the intensity of the grinding wheel wear leading, in consequence, to the decrease of their lives.

### 3. Definition of the global wear intensity

In papers [1, 2] it was shown that simultaneous interaction between individual elementary processes leads to accumulation of the wear intensity. As a result of that phenomenon the intensity of the grinding wheel wear due to the abrasive grain wear is described by equation:

$$W_G = W_s + W_d + W_z + W_t. \quad (12)$$

The intensity of the wheel wear process due to crush dressing of the bond bridges is expressed by the formula:

$$W_B = W_w + W_f. \quad (13)$$

If we take into account the fact that the grinding wheel wear processes caused by the wear of abrasive grains and the bond spalling overlap partially, then the joined intensity of wheel wear can be expressed by the function:

$$W = \alpha \cdot W_G + \beta \cdot W_B, \quad (14)$$

in which  $\alpha$  and  $\beta$  are the coefficients of both forms of grinding wheel wear interference. To define their values the following argumentation should be done.

From the analysis of the process of grinding wheel wear it appears that if the grain does not fall out at the beginning of the first cycle of the grinding, then its partial wear will occur. Thus in a big set of active abrasive grains practically every grain undergoes partial wear. If we assume uniform intensity due to the accumulation of interactions between individual elementary processes then the average volume wear of a single grain in a unit of time is expressed as:

$$\Delta V'_z = \frac{W_s + W_d + W_z + W_t}{n_a} dt. \quad (15)$$

In the same time interval, due to cracking of the bond bridges in cutting surface of the grinding wheel there falls out number of grains which is defined by the following expression:

$$\Delta n_a = \frac{W_w + W_f}{V_{zk}} dt. \quad (16)$$

To be frank, each of the falling out grains was subjected earlier to wear on the scale defined by dependence (15), but regardless of the wear degree of the grain due to its falling out of the grinding tool there is a loss of the abrasive material not bigger than that which the grain comprises itself. Based on the above, part of the intensity of grinding wheel wear, which occurs due to the wear of abrasive grains, can be defined as equal to:

$$W'_G = \left( n_a - \frac{W_w + W_f}{V_{zk}} dt \right) \frac{W_s + W_d + W_z + W_t}{n_a}. \quad (17)$$

Due to transformation of this formula by including the expression  $n_a$  to in the brackets and by comparing the result obtained with the first part of the general expression (14) we arrive at the expression which defines the momentary value of the coefficient of interference:

$$\alpha' = 1 - \frac{W_w + W_f}{V_{zk} \cdot n_a} dt. \quad (18)$$

By integrating the above momentary value in the whole duration of grinding wheel life ( $T_N$ ) and by taking into account the fact that elementary intensities of the tool wear due to cracking of the bond bridges occur in that period as constant average values, we can define the coefficient of wear intensity as:

$$\alpha = 1 - \frac{W_w + W_f}{V_{zk} \cdot n_a} T_N. \quad (19)$$

We must also consider the fact that regardless of the degree of grains' wear, their falling-out of the tool will not cause a loss of abrasive material bigger than that which is contained in the abrasive grain, and then we can accept the coefficient of wear interference as  $\beta = 1$ . Such a value of the coefficient  $\beta$  can be also defined by a procedure

analogous to that adopted for the coefficient  $\alpha$ , with taking into account proper interchangeable values of the elementary processes.

By appropriate association of Equations (12), (13), (14) and (19) we can define the final shape of the average wear intensity of the grinding wheels as:

$$W_N = \left( 1 - \frac{W_w + W_f}{V_{zk} \cdot n_a} T_N \right) (W_s + W_d + W_z + W_t) + W_w + W_f. \quad (20)$$

Investigating the wear of grinding wheels in its physical aspect we should notice different forms of wear caused by the wear of grains and bond fracture. Wear of grains causes abrasion or crushing up the grain ( $mV_{zk}$ ) in part only, which results in weakening of its fastening in the tool, thus causing the falling out of the remaining part of the grain. Cracking of the bond bridges causes a falling out of the whole grain of the wheel cutting surface regardless of the present degree of its wear. Because of simultaneous occurrence of all wear processes and taking account of the fact that an abrasive volume of the value  $V_{zk}n_a$  corresponds to the wear of all active grains present on the grinding wheel cutting surface the number of all worn grains (equal to the number of active grains) can be expressed by the following equation:

$$n_a = \frac{\alpha \cdot W_G T_N}{mV_{zk}} + \frac{\beta \cdot W_B T_N}{V_{zk}}. \quad (21)$$

If in the above equation we include the component quantities given by dependencies (12), (13) and (19) and arrange them with respect to the duration of life, with taking into account the real value of the coefficient of interference  $\beta = 1$ , we arrive at a quadratic equation:

$$\frac{W_w + W_f}{V_{zk} \cdot n_a} (W_s + W_d + W_z + W_t) T_N^2 - \left[ (W_s + W_d + W_z + W_t) + m(W_w + W_f) \right] T_N - mV_{zk} \cdot n_a = 0. \quad (22)$$

Equation (22) has two solutions. The first solution, which illustrates the duration of the tool life in terms of the wear of abrasive grains, is as follows:

$$T_G = \frac{m \cdot V_{zk} \cdot n_a}{W_s + W_d + W_z + W_t}. \quad (23)$$

The second solution, which represents the duration of the wheel life in terms of bond spalling, is described by the following formula:



$$T_B = \frac{V_{zk} \cdot n_a}{W_w + W_f}. \quad (24)$$

Including dependence (23) in original equation (20) we arrive at expression which describes the intensity of grinding wheel wear in the form of:

$$W_N = (W_s + W_d + W_z + W_t) + (1 - m) \cdot (W_w + W_f). \quad (25)$$

The above formula comprises the whole of the tool wear both in terms of the intensity of grains wear and in terms of cracking of the bonding bridges. The intensity of wheel wear described in this way is valid if there is no dominance of whichever elementary wear process.

#### 4. The influence of elementary processes on the wear of grinding wheels

The above theoretical considerations allow us to define the interaction between elementary wear processes and their influence on the grinding wheel wear. Calculations based on them produced results describing the influence of elementary processes of grinding wheels wear in various grinding conditions. Characteristic quantities and the influence of the parameters on their shaping are known from a closer analysis of elementary processes carried out earlier [2, 4]. Thus the most important is the interrelation between these quantities [14]. For these reasons, summary diagrams are the best way to show them.

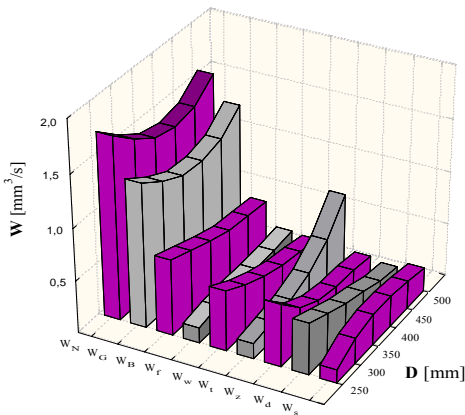


Fig. 2. The influence of grinding wheel (98C24K5V) diameter on the intensity of elementary wear processes

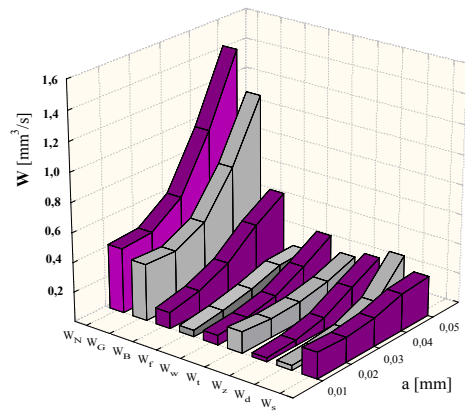


Fig. 3. The influence of grinding depth of the grinding wheel (98C24K5V) on the intensity of elementary wear processes

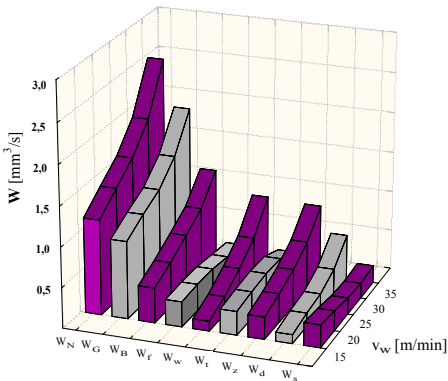


Fig. 4. The influence of workpiece velocity on the intensity of elementary wear processes for grinding wheel (98C24K5V)

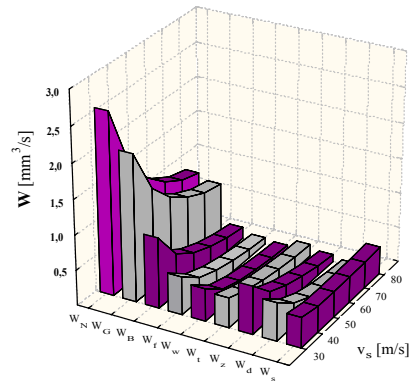


Fig. 5. The influence of grinding velocity on the intensity of elementary wear processes for grinding wheel (98C24K5V)

To illustrate a set of such results we consider the diagrams in Figures 2–5. These diagrams show the influence of variation in the parameters chosen, which characterize the grinding wheel and the grinding conditions, on shaping the wear intensity of standard grinding wheels according to individual elementary wear processes and their accumulated influence. Figure 2 shows the changes of the grinding wheel wear intensity defined according to various criteria in the function of the grinding wheel diameter. Figures 3, 4 and 5 present respectively the influence of the grinding depth, the workpiece velocity and the grinding velocity on the intensity of elementary wear processes.

The analysis of the elementary processes of abrasive grains wear and bond fracture allowed us to establish the influence of the contact zone of these quantities on the corresponding wear processes. If the wear of the whole grinding wheel is taken into account it is necessary to consider all elementary processes in its global wear. The influence of individual elementary processes on the grinding wheel wear is defined in (25), which describes the intensity of wear.

Figure 6 can exemplified the influence of selected machining conditions on shaping elementary wear processes and their share in the global wear of standard grinding wheels. From the diagrams in Figure 6 it appears that each individual influence can be described by the following general principles. In normal grinding conditions, the share of individual elementary processes in the global wear of standard grinding wheels is basically uniform. In the grinding conditions that ensure small mechanical load of abrasive grains in the wear of grinding wheels, the mechanical abrasion processes of the grains edges predominate. An increase in the mechanical load of abrasive grains in the grinding process intensifies the wear by immediate chipping of abrasive grain particles and immediate breaking of bonding bridges, contributing to the falling out of whole abrasive grains. The use of the wheels comprising too fine grains leads, in turn,

to a dominance of wear due to fatigue cracking of bonding bridges. The most intensive fatigue chipping of the abrasive material particles occurs for grains with a small degree of the cutting edges' wear.

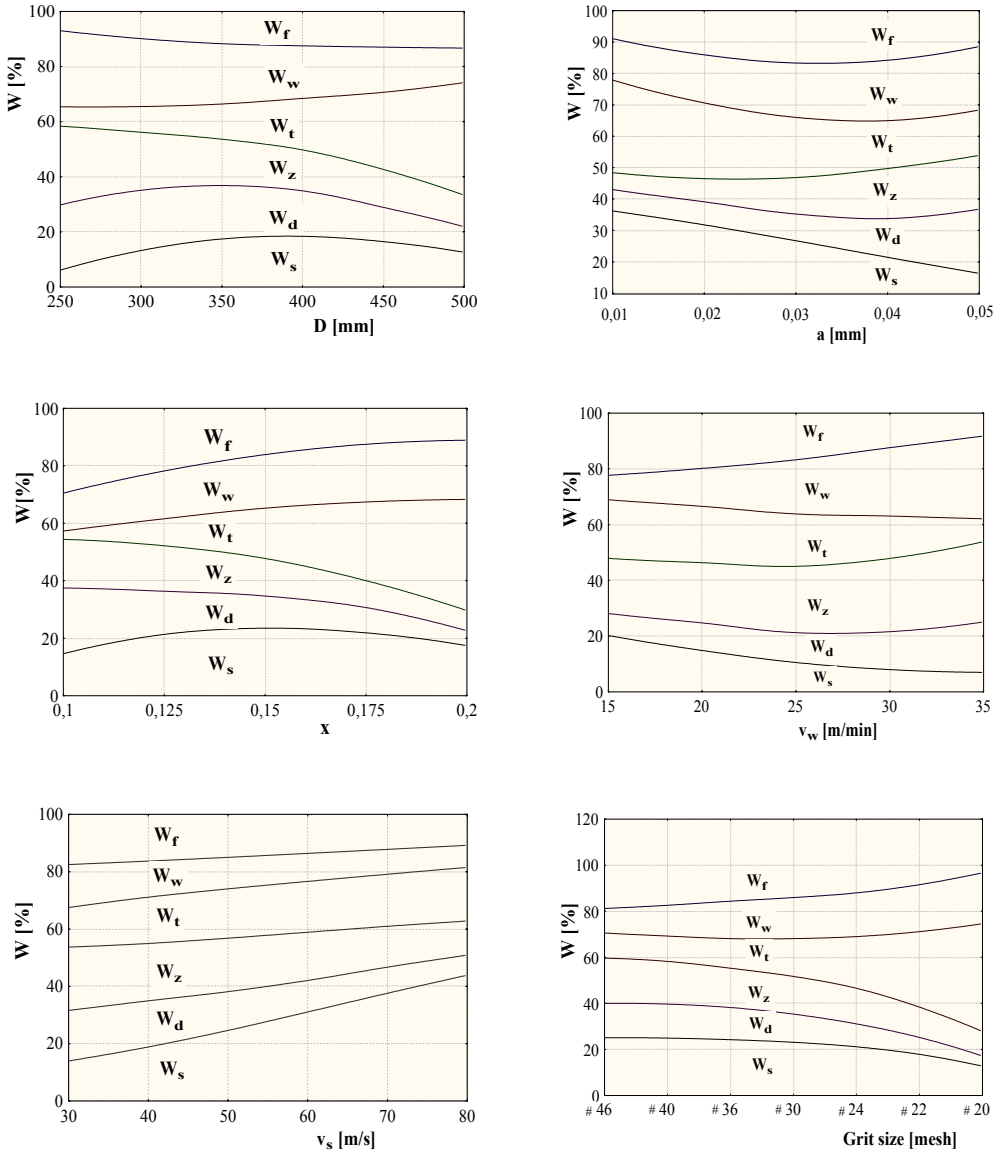


Fig. 6. The influence of selected parameters on percentage shares of elementary processes of individual silicon carbide grains and bond fracture of ceramic binder in the global wear intensity of grinding wheels 98C24K5V

With an increase in the abrasive grains wear the fatigue wear of grains diminishes. But the thermofatigue wear process of abrasive grains is intensified. Moreover, such changes of the grinding conditions that consist in elongation of the contact zone of abrasive grains with the workpiece contribute to a considerable intensification of the thermofatigue wear process. An increase in the grinding wheel width at a constant cross-feed does not cause any noticeable changes of its wear intensity. But an increase in the grinding wheel hardness, which does not considerably influence the degree of abrasive grains' wear, causes a considerable decrease in the grinding wheel wear due to bond spalling.

In average grinding conditions [8], the interaction of individual elementary wear processes is generally uniform. Only in special grinding conditions one of these processes becomes dominant. For these reasons in a complex evaluation of grinding wheel wear, possibly all wear processes should be taken into account. Investigation of some selected elementary wear processes only can be the cause of considerable divergences and, consequently, wrong conclusions.

## 5. Summary

The theory presented in this paper allows us to analyze the processes of grinding wheels wear, taking account of the influence of the most important elementary processes. If we consider the wear of the whole grinding wheel it is necessary to take into account all elementary processes. Investigation of selected processes only, because of their various influences, can be the reason of grave divergences which, in consequence, leads to wrong conclusions.

Selection of the individual elementary quantities that affect the wear intensity of the grinding wheels provides an opportunity to define the grinding wheel behaviour and makes it easier to control properly the grinding process, thus it enables us to minimize the grinding wheel wear and to select proper forms of wear.

## References

- [1] Borkowski J.: *Zużycie i trwałość ściernic*, PWN, Warszawa, 1990.
- [2] Borkowski J., Borkowski P.: *Physical bases of bond fracture in grinding wheels*, Scientific Publication of Mechanical Department: Modern techniques and technologies, Technical University of Koszalin, Koszalin, 2001, pp. 39–53.
- [3] Borkowski J., Borkowski P.: *Physical aspects of attritious grain wear in grinding conditions*, Scientific Publication of Mechanical Department: Modern techniques and technologies, Technical University of Koszalin, Koszalin, 2001, pp. 54–66.
- [4] Borkowski J., Szymański A.: *Uses of abrasives and abrasive tools*, Ellis Horwood Ltd., New York–London–Toronto–Sydney–Tokyo–Singapore, 1992.
- [5] Brinksmayer E., Werner F.: *Monitoring of grinding wheel wear*, Annals of the CIRP, Vol. 41, 1992, No. 1, pp. 373–376.

- [6] Brockhoff T.: *Grind-hardening: a comprehensive view*, Annals of the CIRP, Vol. 48, 1999, No. 1, pp. 255–260.
- [7] Guo C., Malkin S.: *Analytical and experimental investigation of burnout in creep-feed grinding*, Annals of the CIRP, Vol. 43, 1994, No. 1, pp. 283–286.
- [8] Inasaki I., Karpuschewski B., Lee H.-S.: *Grinding chatter – origin and suppression*, Annals of the CIRP, Vol. 50, 2001, No. 2, pp. 515–534.
- [9] Kacalak W., Kasprzyk M.: *Wybrane problemy modelowania stochastycznych procesów zużycia i trwałości ściernic*, XXIII Naukowa Szkoła Obróbki Ściernej, Rzeszów, 2000, s. 257–264.
- [10] Oczos K., Porzycki J.: *Szlifowanie. Podstawy i technika*, WNT, Warszawa, 1986.
- [11] Semba T., Fujiyama H., Sato H.: *Development of resin-bonded diamond wheels with improved by radio-frequency magnetron sputtering*, Annals of the CIRP, Vol. 47, 1998, No. 1, pp. 271–274.
- [12] Tönshoff H.K., Wobker H.-G.: *CBN grinding with small wheels*, Annals of the CIRP, Vol. 44, 1995, No. 1, pp. 311–316.
- [13] Ueda T., Sato M., Sugita T., Nakayama K.: *Thermal behavior of cutting grain in grinding*, Annals of the CIRP, Vol. 44, 1995, No. 1, pp. 325–328.
- [14] Weiss Z.: *Szlifowanie szybkościowe*, Wydawnictwo Politechniki Poznańskiej, Poznań, 1987.

### Wpływ zjawisk elementarnych na zużycie ściernic

Przedstawiono zależności opisujące intensywność zużycia ściernic spowodowanego przez elementarne zjawiska zużycia ziaren ściernych oraz wykruszanie mostków spoiwa. Jako elementarne procesy zużycia ziaren ściernych wyodrębniono:

- ścieranie wierzchołków ziaren o intensywności  $W_s$ ,
- doraźne wykruszanie cząstek ziaren o intensywności  $W_d$ ,
- zmęczeniowe wykruszanie cząstek ziaren o natężeniu  $W_z$ ,
- termozmęczeniowe wykruszanie cząstek ziaren o intensywności  $W_t$ .

Główne zaś elementarne procesy zużycia ściernic spowodowane wyruszeniami spoiwa są wywoływane przez:

- doraźne pękanie mostków spoiwa o intensywności  $W_w$ ,
- zmęczeniowe pękanie mostków spoiwa o intensywnością  $W_f$ .

Zbadano także współdziaływanie tych wielkości podczas szlifowania, rozpatrując globalne zużycie ściernicy jako wypadkową zużycia ziaren i wykruszania mostków spoiwa. Zużycie ziarna sprawia, że starciu bądź wykruszeniom podlega zawsze jedynie część ziarna ( $mV_{zk}$ ), co osłabia jego utwierdzenie w narzędziu, powodując wypadnięcie pozostałej części ziarna. Pękanie zaś mostków spoiwa jest przyczyną wypadania całości ziarna z czynnej powierzchni ściernicy bez względu na aktualny stopień jego zużycia. Takie rozumowanie pozwoliło podać wzory opisujące wynikową intensywność zużycia ściernicy, które obliczano dla różnych warunków szlifowania. Zaprezentowane wyniki umożliwiły dokonanie oceny wpływu wybranych parametrów i wielkości charakterystycznych na intensywność zużycia ściernic oraz udziały procentowe elementarnych zjawisk zużycia.

Zaprezentowana teoria pozwala przeanalizować procesy zużycia ściernic z uwzględnieniem udziału wszystkich zjawisk elementarnych. Rozpatrywanie bowiem tylko wybranych zjawisk zużycia, z racji ich różnorodnego oddziaływania, może być powodem rozbieżności, co w konsekwencji prowadzi do błędnych wniosków. Wyodrębniając wpływ poszczególnych elementarnych

wielkości zużycia, można określić zachowanie się ściernicy, a także świadomie sterować procesem szlifowania, minimalizując zużycie narzędzi i wpływając na odpowiednie formy jego zużycia.



## Thermodynamical aspects of high-pressure water-ice jet formation

J. BORKOWSKI, P. BORKOWSKI, G. CHOMKA

Technical University of Koszalin, Rac<sup>3</sup>awicka 15–17, 75-620 Koszalin

Theoretical analysis of thermodynamical conditions of water-ice jet formation is presented. It was assumed that ice material constitutes the model of grain made of ball-shaped particles of crushed ice H<sub>2</sub>O of different sizes. The conditions of transport of such “ice abradant” to the cryo-sprinkler and of pre-cooling of high-pressure water jet in the cryogenic technological plant are thoroughly analysed. This study is aimed at establishing main directions of research undertaken in order to construct experimental devices allowing formation of an effective water-ice jet. This work will make the jet increasingly erosive and will by the same token make a cutting tool more efficient.

Keywords: *high-pressure water-ice jet, thermodynamical analysis, temperature of ice grains*

### 1. Introduction

Nowadays removal of different kinds of impurities from technological surfaces is considered to be a serious problem. Besides the methods of cleaning being used most often, including sand blasting, new methods have been recently developed. They are based on making use of a high-pressure water jet often doped with abrasive grains and/or ice particles or using a high-pressure cryogenic jet, as for example liquid nitrogen or ammonia jets [10], etc.

The cryogenic abrasive jets [5] with addition of crushed ice H<sub>2</sub>O [9, 11] or dry-ice CO<sub>2</sub> pellets [12, 13] are gaining in popularity. Soon after publishing the first works [3] and applying high-pressure water jets doped with crushed ice we undertook the tests [2] on formation of pre-cooled water-ice and gas-ice jets (CO<sub>2</sub>). Results of the thermodynamic analysis [2] proved to be coincident with later simulation works [6, 7] in Japan. At present, proper crushers [4, 14] and technological plants [1, 8] with cooling systems are applied to production of ice grains H<sub>2</sub>O; however, they need the constant temperature control of a working medium.

The present work is devoted to thermodynamical analysis of the water-ice jets doped with grains of crushed ice H<sub>2</sub>O.

## 2. Method of formation of high-pressure water-ice jets

The water-ice jet can be used for cleaning technological surfaces. If this jet is efficient, the end temperature of ice grains should be possibly the lowest. To produce such a water-ice jet the suitable experimental plant [11], exemplified by Figure 1, is to be applied. This plant includes a valve 1 supplying municipal water to a cooler 2 where it is pre-cooled. A high pressure pump 3 enables us to obtain a water jet at an adequate pressure which is stabilized by a control system 4. This jet is once again cooled in a cooler 5, then it flows to a high-pressure spray gun 6 and a cryo-sprinkler 7. A high-pressure water jet flowing through a cryo-sprinkler 7 produces a negative pressure in a tube 9 sucking in ice grains from a container 10 situated in a room of a controlled temperature. If an air temperature is higher than the triple point of water, the ice grains will melt and then will form large chunks of ice clogging the suction pipe.

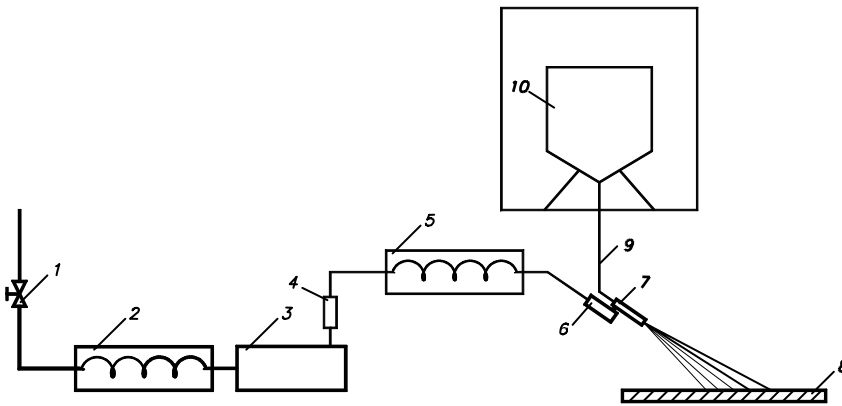


Fig. 1. Sample test-stand for high-pressure water-ice jet formation

To avoid aggregation of small ice particles into great chunks in the container or during the transport to a cryo-sprinkler 7, the air around the system should have a temperature below the ice point. It should be also taken into account that under conditions of high pressure, the water-ice phase transitions are proceeding at different temperatures [14] than under the so-called standard physical conditions. Ice grains sucked up from a container 10 to a nozzle of a cryo-sprinkler 7 are accelerated by a high-pressure water jet and formed in a water-ice jet sprayed on a workpiece 8.

## 3. Thermodynamical analysis of water-ice jet

To evaluate the suitability of ice particles for cleaning one has first of all to get to know a temperature which they will have at respective stages of the process that leads to the water-ice jets. A model of a thermal transient conduction in a system of weak



thermal resistance was used to determine a temperature of ice particles. Regarding the complexity of the process the following simplifying assumptions were accepted: ice particles are balls of diameter  $d$ , their weight, volume and area are constant in time, whereas temperatures of air and water are constant.

In the case of heat exchange between ice grain (solid) and a fluid jet (gas or liquid) flowing through it, we deal with taking up the heat. Then the intensity of a thermal flow can be described by Newton's equation:

$$q = \alpha(T_f - T_i), \quad (1)$$

where:

- $\alpha$  – coefficient of heat absorption,
- $T_f$  – liquid temperature (air  $T_p$  or water  $T_w$ ),
- $T_i$  – ice temperature.

Moreover, if the heat is taken up by a fluid jet, then  $T_f < T_i$  and  $T_i - T_f$  should be substituted for  $T_f - T_i$  in Equation (1).

The total amount of heat exchanged through the area  $F$  of ice grain in the time  $t$  can be calculated by solving the following equation:

$$Q = Q_{ht} = qFt = \alpha F(T_f - T_i)t, \quad (2)$$

where  $Q_h$  is the quantity of heat transferred by the element with the surface  $F$  in unit time.

To obtain an equation allowing calculation of the final temperature of ice grains the energy balance should be drawn up. Because the heat exchange proceeds at a constant pressure, the expression determining the internal energy of ice grain is on the right-hand side of the equation. So, a mathematical expression of the energy balance is given by the equation:

$$\alpha F(T_f - T_i)dt = -c\rho VdT, \quad (3)$$

where:

- $c$  – specific heat of ice,
- $\rho$  – ice density,
- $V$  – volume of ice grain.

After transformation of Equation (3) we obtain:

$$\frac{dT}{T_f - T_i} = -\frac{\alpha F}{c\rho V} dt. \quad (4)$$

The initial condition, i.e. ice-grain temperature, at the beginning is constant, therefore:

$$T_l = T_0 = \text{const.} \quad (5)$$

After heating up of ice grain by air it reaches a temperature of heated ice ( $T_{lp}$ ), and therefore:

$$T_l = T_{lp}. \quad (6)$$

Knowing that:

$$dT = d(T_f - T_l), \quad (7)$$

$$x = T_f - T_l, \quad (8)$$

$$\frac{dx}{x} = -\frac{\alpha F}{c\rho V} dt, \quad (9)$$

and integrating Equation (9) we obtain the expression:

$$\ln|x|_{T_0}^{T_{lp}} = -\frac{\alpha F}{c\rho V} t, \quad (10)$$

which after a necessary transformation will take the form:

$$\frac{T_f - T_{lp}}{T_f - T_l} = e^{\frac{-\alpha F}{c\rho V} t}. \quad (11)$$

From Equation (11) it is possible to determine a temperature of ice heated by air during its transport from a container to a sprinkler, which is determined by the formula:

$$T_{lp} = T_f - (T_f - T_l) \cdot e^{\frac{-\alpha F}{c\rho V} t}, \quad (12)$$

where:

$\alpha$  – coefficient of taking over a heat from ice grain surface during pneumatic transportation,

$t$  – time of ice grain flow during pneumatic transportation,

$T_f = T_p$  in the case of ice grain heating up during transportation.

The end temperature of ice grain, after heating by high-pressure water jet, can be calculated from relation (12), which takes a form:

$$T_{ik} = T_w - (T_w - T_{lp}) \cdot e^{\frac{-\alpha F}{c\rho V t}}, \quad (13)$$

where:

$\alpha$  – coefficient of taking over a heat from ice grain surface during flowing through the high-pressure water jet,

$T_w$  – temperature of high-pressure water jet.

#### 4. Results of thermodynamical analysis

On the basis of Equations (12) and (13) a series of calculation were done which enabled us to determine a suitability of ice grains for the process of cleaning. In part one of the paper, an influence of the temperature of air transporting the ice grains and water temperature on the final temperature of ice grains was determined. According to Figure 2 a rise in the air temperature brings about a rise in the final temperature of ice. For example, for an ice grain of 2 mm diameter and at a water temperature  $T_w$  of 323 K the final temperature of ice grain  $T_{ik}$  is 229.3 K (at an air temperature  $T_p = 293$  K), whereas for  $T_p = 243$  K a temperature  $T_{ik} = 226.9$  K is measured. It follows from this example that a change in the air temperature of 50 K gives rise to the final temperature of ice grain not more than 2.4 K.

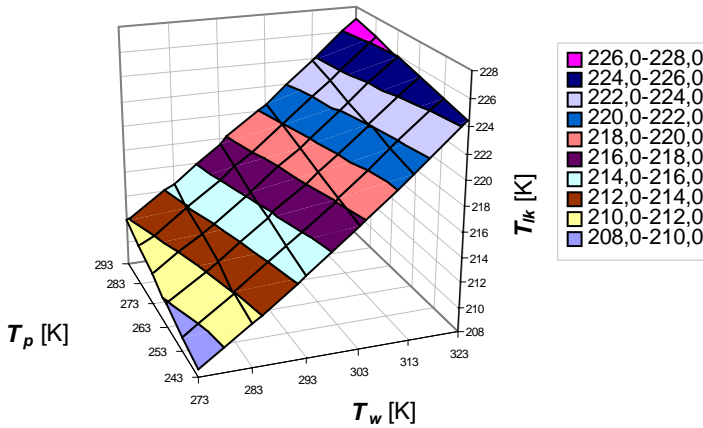


Fig. 2. Relation between final temperature of ice and temperature of water jet and temperature of air used for transport of ice grains. Water pressure  $p = 20$  MPa, length of suction hose  $l_1 = 5$  m, diameter of ice grain  $d = 2$  mm, initial temperature of ice  $T_1 = 193$  K, distance between water-ice jet outlet from sprinkler tube and work material  $l_2 = 250$  mm

The second factor which in a present technological plant exerts an influence on a change in the final temperature of ice grain is a temperature of a high-pressure water

jet (Figure 2). For ice grain of 2 mm diameter and at air temperature  $T_p = 243$  K, the final temperature of ice grain changed from  $T_{lk} = 210.1$  K at a temperature of water  $T_w = 273$  K to  $T_{lk} = 226.9$  K at  $T_w = 323$  K. Therefore a change in a water temperature of 50 K will produce a change in the final temperature of ice grain of 16.8 K. This means that a temperature of water has a greater influence on the final temperature of ice grain than the temperature of air.

The factor which also influences the final temperature of ice grain is a water pressure. The increase in pressure of a water jet gives rise to negative pressure in a suction pipe which shortens both time of an ice-grain flow through this pipe and time of an ice-grain flow in a water jet. The effect of a water-jet pressure – from the beginning of water-ice jet formation to the moment of the contact of ice particles with the surface being cleaned – on the final temperature of ice grain is presented in Figure 3. One can observe from this graph that as a water pressure increases the final temperature of ice grain drops. For instance, for an ice grain of 2 mm diameter and at water jet pressure  $p = 10$  MPa the final temperature of ice grain  $T_{lk}$  was 233.6 K, whereas for  $p = 50$  MPa this temperature was lower by 9.7 K ( $T_{lk} = 223.9$  K). This final temperature of ice grain differs much more from that measured when a temperature of air is changed, and is by 7.1 K lower than that obtained at a temperature of an adequate water pre-cooling.

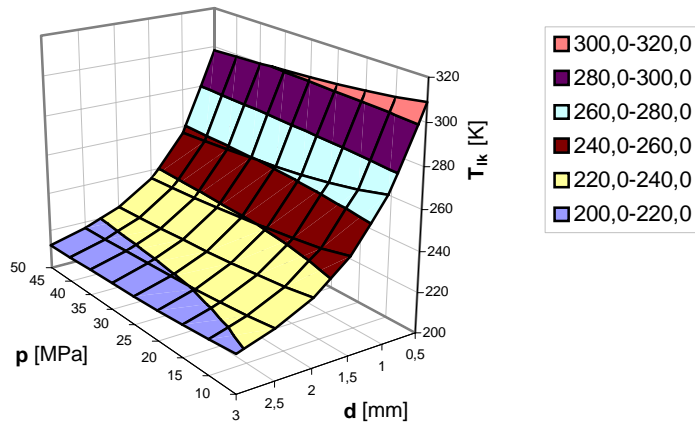


Fig. 3. The effect of water pressure on final ice temperature for different ice grain diameters. Air temperature  $T_p = 293$  K and water temperature  $T_w = 323$  K,  $p = 20$  MPa,  $T_1 = 193$  K,  $l_1 = 5$  m,  $l_2 = 250$  mm

In order to shorten the time of heat exchange between ice grains flowing through a suction pipe and air, which is connected with a shortening of a flow rate time, this pipe should be shortened. However, a rise in air temperature does not induce an essential change in the final temperature of ice grain. An influence of a suction pipe length on the final temperature of ice grain at different temperatures of water is shown

in Figure 4. A change in a suction pipe length, from 5 m to 1.5 m on an average, results in a drop of temperature not more than 2 K.

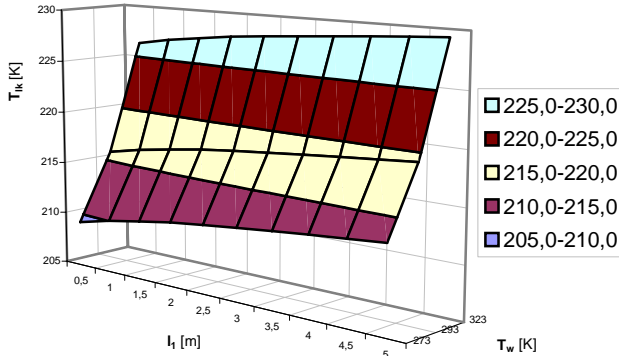


Fig. 4. Relation between final temperature of ice and length of suction hose used for transporting ice grains at changing temperature of water. Ice grain diameter  $d = 2$  mm,  $T_l = 193$  K,  $T_p = 293$  K,  $p = 20$  MPa,  $l_2 = 250$  mm

A diameter of a ice grain has the greatest influence on its final temperature, independently of the value of the water-jet pressure. Smaller grains of ice (to 0.25 mm) usually take up a temperature of water jet, and graphical representation of the changes of the final temperature of ice grains having larger diameters resembles a hyperbola (Figure 5).

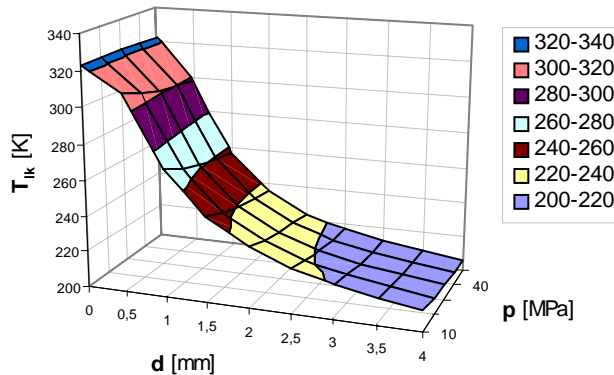


Fig. 5. The influence of ice grain diameter on final ice temperature at different water pressure values.  $T_l = 193$  K,  $T_p = 293$  K,  $T_w = 323$  K,  $l_1 = 5$  m,  $l_2 = 250$  mm

As an example, ice grains of 0.1 mm diameters at the water pressures as above and their temperature equal to 323 K reach a temperature of water. An increase in an ice-grain diameter to  $d = 1$  mm at a water pressure  $p = 20$  MPa brings about the final

temperature of ice  $T_{lk} = 264.8$  K, whereas for  $d = 2$  mm we have  $T_{lk} = 229.3$  K, and for  $d = 3$  mm –  $T_{lk} = 216.0$  K. However, a further increase in the diameter of ice grains will not produce such essential changes in their final temperature. However, the greater the ice grains are, the longer they maintain the final temperature of ice at a low level. A change in an ice-grain diameter  $d$  in the range from 1 mm to 2 mm will bring about a drop in the final temperature of ice up to 35.5 K. Therefore a change in an ice-grain diameter will cause the strongest effect on the final temperature of ice.

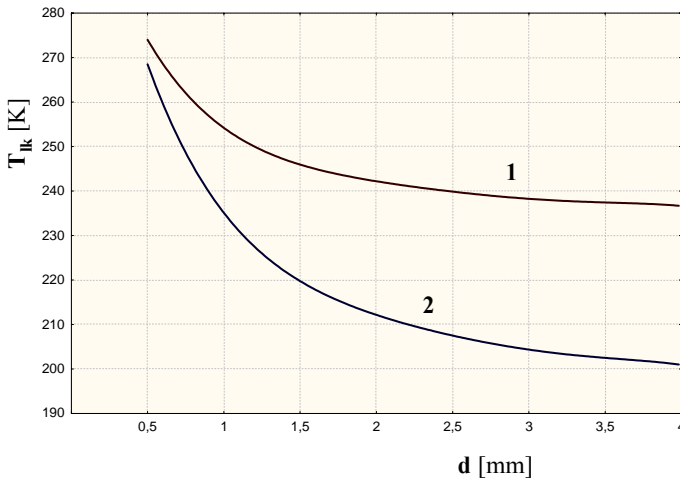


Fig. 6. Ice-grain diameter and the effect of its initial temperature on final ice temperature: 1 –  $T_i = 233$  K, 2 –  $T_i = 193$  K.  $T_p = 293$  K,  $T_w = 323$  K,  $p = 20$  MPa,  $l_1 = 5$  m,  $l_2 = 250$  mm

The next factor being analysed was the influence of the initial temperature of ice grain on its final temperature at different diameters of these grains. The analysis was based on the changes of air and water temperature, their pressure and a length of the suction pipe. The results obtained allow one to state that if the lowest initial temperature of ice grain is maintained, the lowest end temperature is obtained. However, for small ice grains these differences are slight. An example of these relations is presented in Figure 6.

In general, a shorter time of heat exchange between ice grains and water is advantageous. Reducing the distance between a water-ice jet outlet of a sprinkler tube and the work material ensures the lowest final temperature of ice grains. For example, for ice grain, whose diameter  $d$  is 2 mm, a change in a water-ice jet length from 0.5 m to 250 mm will produce a drop in the final temperature of ice grains up to 21.7 K.

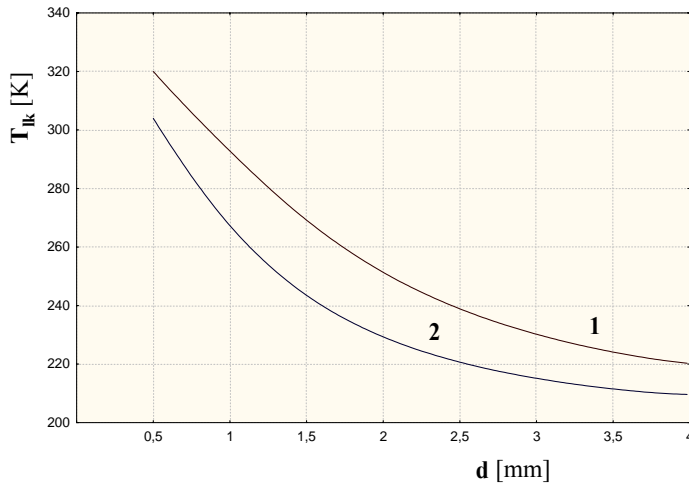


Fig. 7. Relation between the final temperature of ice and ice grain diameter at different distances between water-ice jet outlet of sprinkler tube and work material: 1 –  $l_2 = 500$  mm, 2 –  $l_2 = 250$  mm.  $T_i = 193$  K,  $T_p = 293$  K,  $T_w = 323$  K,  $p = 20$  MPa,  $l_1 = 5$  m

On the basis of the above analyses one can state that the initial temperature of ice grain is a factor most strongly affecting the final temperature of ice grain. The other factors which have a significant effect on the end temperature of ice grains, are the size of the grains and a distance between a water-ice jet outlet of a sprinkler tube and the work material. A slighter influence on the final ice temperature exerts a temperature of water, and the next factor is the water pressure which affects a jet rate and therefore its time of “heating up” the ice grains. A temperature of air has a little influence on the final temperature of ice, and the influence of the suction pipe length is the slightest. All these factors are essential for an appropriate construction of an experimental plant.

## 5. Foredesign for experimental technological plant of a new type

Based on the calculations and the analyses of the results obtained we created a fore-design for the experimental technological plant allowing formation of a water-ice jet. An apparatus for ice-grain production (Figure 8) is situated in a multi-chamber isolated case supplied with cold air. Chunks of ice in a cooler 10 are directed to a crusher-granulator 11 where grains of the size required are obtained. These grains drop to a super-cooled tank 13 being stabilized thermally from which they are sucked up at the rate determined by a vibrator 14. Remaining elements of this plant are identical with those discussed earlier (Figure 1).

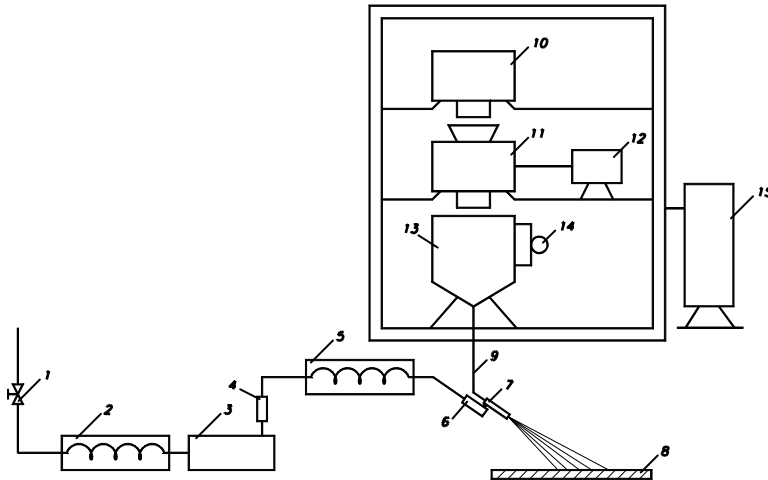


Fig. 8. Schematic drawing of experimental technological plant of new type: 1 – valve cutting off water supply, 2 – initial water cooler, 3 – high-pressure pump, 4 – pressure-control system, 5 – cooler of high-pressure water jet, 6 – high-pressure spray gun, 7 – cryo-sprinkler, 8 – workpiece, 9 – suction pipe, 10 – cooler of ice chunks, 11 – crusher-granulator, 12 – motor, 13 – container of crushed ice with liquid nitrogen cooling, 14 – vibrator, 15 – air cooler

The present plant in comparison with that described earlier is superior because it allows us to obtain ice grains of low initial temperature. Moreover, the crusher-granulator applied produces ice grains of specified size which also has a significant effect on the quality of jet. Therefore, both erosive effectiveness of water-ice jet and efficiency of treatment will increase.

## 6. Summary

Based on the analyses of calculation results simulating different conditions of formation of the high-pressure water-ice jet the following conclusions can be drawn:

- Drop in the initial temperature of coarse ice grains (diameter exceeding 1 mm) is advantageous since it allows us to obtain a significantly lower final temperature of ice grains.
- High quality of ice grains is promoted by their shorter staying in a water jet, therefore it is necessary to reduce a distance between an outlet of the sprinkler tube and the work material to about 250 mm.
- A drop in a temperature of the high-pressure water jet affects strongly both drop in the final temperature of ice grains and their mechanical properties.
- The increase in water-jet pressure is also advantageous because it makes the time of staying of ice grain both in an air environment (in a suction pipe) and in a water jet shorter.



- Both the drop in a temperature of air and the length of the suction pipe have relatively slight effect on the final temperature of ice grains. So these parameters are not essential for experimental design for the technological plant.

The above conclusions and remarks are of vital practical importance because they enable us to develop a foredesign for the present plant producing the high-pressure water-ice jet with a high efficiency of treatment.

## References

- [1] Borkowski J., Borkowski P.: *Chosen issues of creation and application of high-pressure water-ice jet*, Int. Conf. on Water Jet Machining, Cracow, 2001, pp. 127–140
- [2] Borkowski J., Borkowski P., Czyżniewski A., Lenz Z.: *Badania możliwości stosowania kriogenicznego wysokociśnieniowego strumienia płynu jako potencjalnego narzędzia erozyjnego*, I Forum Prac Badawczych: *Kształtowanie części maszyn przez usuwanie materiału*, Koszalin, 1994, s. 288–298.
- [3] Galecki G., Vickers G.W.: *The development of ice-blasting for surface cleaning*, Proc. of the 6th International Symposium on Jet Cutting Technology, Surrey, U. K., 1982, paper B-3, pp. 59–78.
- [4] Geskin E.S., Tisimenetskiy L., Li F., Meng P., Shishkin D.: *Investigation of icejet machining*, Proc. of the 9th American Water Jet Conference. Vol. I, Dearborn, Michigan, 1997, pp. 281–290.
- [5] Hashish M., Dunskey C.M.: *The Formation of Cryogenic and Abrasive-Cryogenic Jets*, Proc. of the 14th International Conference on Jetting Technology, Brugge, Belgium, 1998, pp. 329–343.
- [6] Kiyohashi H., Hanada K.: *A study of production of ice particles by the heat of vaporization of cryogenic liquefied fuels and their application in ice jets, and so on*, Proc. of the International Symposium on New Applications of Water Jet Technology, Ishinomaki, Japan, 1999, pp. 51–60.
- [7] Kiyohashi H., Kobayashi R., Hanada K.: *Numerical simulations of growth of ice particles for ice abrasive jets*, Proc. of the 4th Pacific Rim Int. Conf. on Water Jet Technology, Shimizu, Japan, 1995, pp. 175–186.
- [8] Li F., Geskin E.S., Tisimenetskiy L.: *Development of ice jet machining technology*, Proc. of the 8th American Water Jet Conference. Vol. II, Huston, Texas, 1995, pp. 671–680.
- [9] Li F., Geskin E.S., Tisimenetskiy L.: *Development of icejet machining technology*, Proc. of the 13th International Conference on Jetting Technology, Sardinia, 1996, pp. 725–734.
- [1] Liu H.T., Fang S., Hibbard C., Maloney J.: *Enhancement of ultrahigh-pressure 0] technology with LN<sub>2</sub> cryogenic jets*, Proc. of the 10th American Waterjet Conference. Vol. I, Huston, Texas, 1999, pp. 297–313.
- [1] Shishkin D. V., Geskin E. S., Goldenberg B.: *Development of a technology for 1] fabrication of ice abrasives*, Proc. of the 2001 WJTA American Waterjet Conference, Minneapolis, Minnesota, 2001, paper No. 27.
- [1] Spur G., Uhlmann E., Elbing F.: *Experimental research on cleaning with dry-ice blasting*, 2] International Conference on Water Jet Machining “WJM ‘98”, Cracow, 1998, pp. 37–45.

- [1 Spur G., Uhlmann E., Elbing F.: *Dry-ice blasting for cleaning: process, optimization and application*, Wear, Vol. 233–235, 1999, pp. 402–411.
- [1 Truchot P., Mellinger P., Duchamp R., Kim T.J., Ocampo R.: *Development of a cryogenic waterjet technique for biomaterial processing applications*, Proc. of the 6th American Water Jet Conference, Huston, Texas, 1991, pp. 473–480.

### **Termodynamiczne aspekty tworzenia wysokociśnieniowej strugi wodno-lodowej**

Usuwanie z powierzchni technicznych różnego rodzaju zanieczyszczeń stanowi czasami istotny problem. Do skutecznego czyszczenia stosuje się obecnie metody oparte na wykorzystaniu wysokociśnieniowej strugi wody domieszkowywanej często ziarnami ściernymi czy cząstkami lodu bądź wysokociśnieniową strugę kriogeniczną, jak np. struga ciekłego azotu lub amoniaku. Ostatnio szczególnie zainteresowanie budzi metoda czyszczenia strumieniem ziaren lodu, w tym również obróbka powierzchniowa wysokociśnieniową strugą wodno-lodową.

Skuteczność takiej obróbki istotnie zależy od temperatury końcowej ziarna lodu, która powinna być jak najniższa. Dzięki temu bowiem wzrasta skuteczność erozyjna strugi wodno-lodowej, a tym samym i wydajność obróbki. Aby określić temperaturę cząstek lodu, posłużono się modelem nieustalonego przewodzenia ciepła w układzie o małym oporze cieplnym. Na tej podstawie przeprowadzono termodynamiczną analizę strugi wodno-lodowej, której wyniki pozwoliły określić przydatność ziaren lodu w procesie czyszczenia.

Opierając się na analizach teoretycznych, stwierdzono, że początkowa temperatura ziaren lodu jest czynnikiem najsilniej oddziałującym na ich temperaturę końcową. Następnymi w kolejności pod względem wielkości wpływu na końcową temperaturę ziaren lodu jest ich wielkość oraz długość strugi wodno-lodowej między tryskaczem a materiałem obrabianym. Mniejszy wpływ na temperaturę końcową wywiera temperatura wody, a następnie ciśnienie wody, które oddziałuje na prędkość strugi, a więc i na czas „podgrzewania” ziaren lodu. W małym zaś stopniu na temperaturę końcową ziaren lodu wpływa temperatura powietrza, a w najmniejszym stopniu – długość przewodu ssawnego.

Wszystko to jest istotne, aby poprawnie skonstruować eksperymentalną instalację technologiczną przeznaczoną do wytwarzania strugi wodno-lodowej, a także efektywnie ją stosować.

## Cutting surface of the grinding wheel as a component of tribological system

L. DĄBROWSKI, M. MARCINIAK

Warsaw University of Technology, al. Niepodległości 222, 00-663 Warszawa

K. E. OCZOŚ

Rzeszów University of Technology, ul. Wincentego Pola 2, 35-959 Rzeszów

The results of comparative studies of the roughness profile of cutting surface of grinding wheel, based on the profilograms obtained from 2-D and 3-D measurements, were analysed. It was indicated that the cutting surface of the grinding wheel could be considered as a surface of one element of a tribological pair of elements, whose highest peaks are essential in decohesion of the grinded material. The number of these peaks were established based on theoretical model of a grinding wheel and experimentally verified. Evaluation of the tribological process effectivity was conducted based on the mass of material transferred from one tribological element.

Keywords: *grinding, 3-D surface topography, tribological system*

### 1. Introduction

Destruction of the machined material and a tool wear in grinding process are caused by mechanical and physical/chemical factors. Sliding friction, ploughing and microcutting are the most important mechanical factors. Adhesion, diffusion and fatigue are the most important physical/chemical factors. Analysis of the heights of grains placed on the working surface of the grinding wheel has shown that only about 10% of grains were involved in cutting, 30% in ploughing and more than 50% were sliding over the material of the machined part. The size of chips generated by the cutting grains is dependent on the parameters of the grinding process and on the conditions of the chip upsetting. The contribution of the work of cutting to the energy balance is from 5% to 35%. The most of this energy (65% to 95%) is consumed by the classical tribological system presented in Figure 1a.

At the contact area (A), the workpiece material is particularly under flow (Figure 1b). In the primary deformation zone (B), the material confluence changes to shear a process that leads to chip formation. During grinding of ductile materials the area of material separation is located near the tip of grain. But due to material properties and structure this can also happen in the primary deformation zone (C), which is already under thermal and mechanical strain. As soon as the mechanical stress, owing to the meshing grain, exceeds the inner strength of the material compound, breaking and

cracking accompany these processes of chip and surface formation. On the other hand, the cutting process also includes material deformation which does not lead to a material removal. Because of the compressive strain underneath the grain, the material dislocations lead to microplastic flows along grain marks.

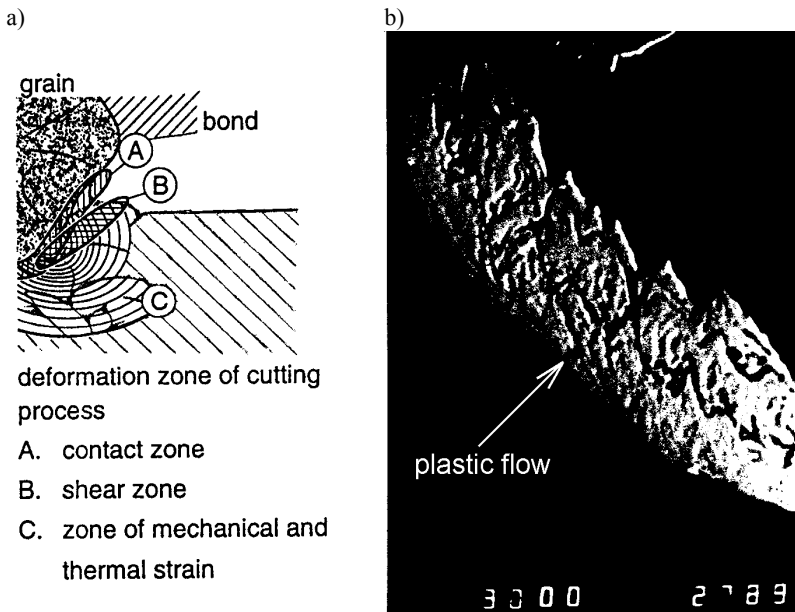


Fig. 1. Basic elements of a tribomechanical system (a), and particles generated by this system (b)

The final surface topography of a grinding wheel is determined by the particular truing and dressing operations it is subjected to, though it is the dressing operation which imparts the fine scale topography to the grinding wheel. The actual topography is due to the process of grit fracture or bond fracture. The wheel topography and the grinding parameters affect the kinematic interactions between the abrasive grains and the workpiece [1]. The wheel topography and the conditions under which it is prepared have a profound effect upon the grinding performance as characterized by grinding forces, power consumption, temperature and surface finish of components. Clearly, a detailed knowledge of the nature of the topography of the grinding wheel would enable improved control of the grinding process in general.

The productivity of the grinding process is influenced directly by the number of the highest tops of the grains which penetrate into the ground material to the level of 5–10% of the maximum roughness value of the grinding wheel (Figure 2) [2]. Because the grains are randomly distributed in the grinding wheel, we propose to describe their cutting ability by statistical parameters [3]. As regards the use of a data processing system, the bearing ratio curve (b.r.c.) and its special parameters [6] are a convenient

way to treat this aspect. In this case, the b.r.c. is calculated from the surface roughness profiles recorded along the grinding wheel circumference.

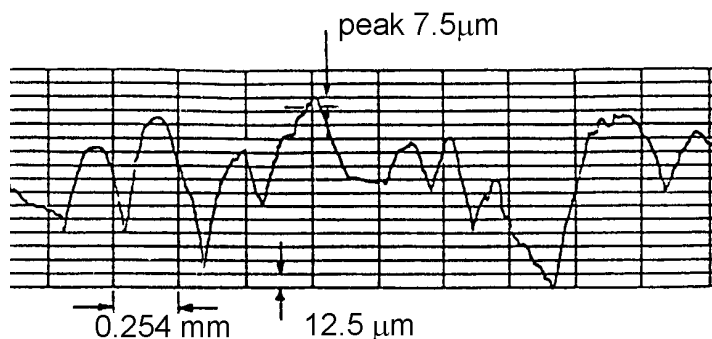


Fig. 2. The peak of the cutting grain

The point of interest is the variation in slope of Abbott's b.r.c. For this purpose, a new standard has been developed with special parameters describing the shape of curve [4]. These parameters divide the total peak-to-valley height of a surface profile into three portions corresponding to three heights:  $R_K$ , the kernel or core roughness;  $R_{PK}$ , the reduced peak height; and  $R_{VK}$ , the reduced valley depth. The division of the b.r.c. into three separate portions is illustrated in Figure 3. For the calculation of these three portions a straight-line tangent of 40% bearing ratio (b.r.) is moved from the top of the curve along its slope to a position of the smallest gradient. At this position the straight-line tangent is fixed. The lengthening of this line to the intersection points of 0 to 100% b.r. defines two parameters  $M_{R1}$  and  $M_{R2}$  whose height difference is  $R_K$ . Subsequently,  $R_{PK}$  and  $R_{VK}$  are evaluated in the same way. At first the area bounded by 0% b.r., the b.r.c. and the height line of  $M_{R1}$  is calculated. As a next step, this area is replaced by a triangle of the same area. The height of the triangle gives the parameter  $R_{PK}$ .  $R_{PK}$  is said to describe the fraction of the profile height contained in the peaks of the profile,  $R_{VK}$  describes one of the valleys, and  $R_K$  describes the central region of the profile which is neither peaks nor valleys. In this paper, the sum of the three heights  $R_K$ ,  $R_{PK}$  and  $R_{VK}$  is defined as a new parameter, the reduced roughness  $R_{Ges}$ :

$$R_{Ges} = R_{PK} + R_K + R_{VK}. \quad (1)$$

In contrast to  $R_t$ , the value of which is determined by single grains and single pores,  $R_{Ges}$  gives a statistical information about the whole surface trace [5]. The b.r.c. after dressing is approximately normally distributed leading to similar values for  $R_{VK}$  and  $R_{PK}$ . If the peak and valley distribution of the grinding wheel topography changes influenced by grain wear or wheel loading, the value of  $R_{Ges}$  decreases. This process is accompanied by a change of the relation between  $R_{PK}$  and  $R_{VK}$ , depending on the type

of wheel wear.  $R_{Ges}$  as a conventional feature of the grinding wheel performance is disadvantageous quality because the grinding wheel profilograms do not give a chance to recognize the grains tops and edges and summits formatted by the bond.

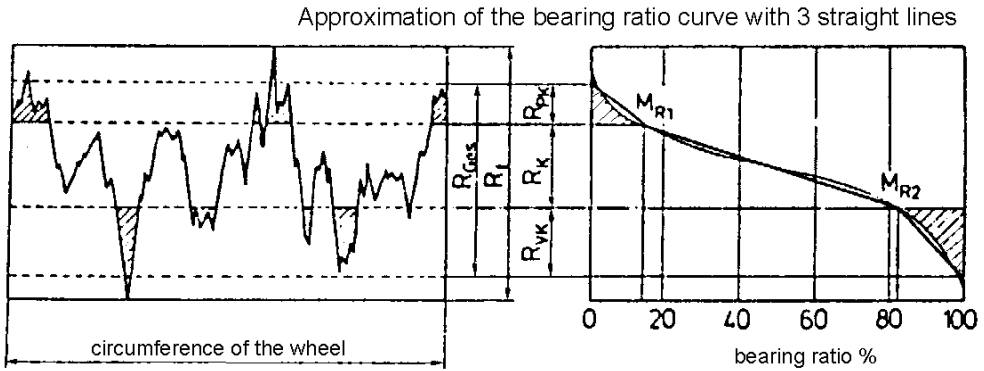


Fig. 3. Parameters of bearing ratio curve.  $R_{PK}$  – reduced peak roughness,  $R_K$  – kernel roughness,  $R_{VK}$  – reduced valley roughness,  $M_{R1}$ ,  $M_{R2}$  – the smallest and the biggest profile bearing portion of the kernel profile [5]

As a result, generalizations or estimations are difficult to make with any degree of accuracy. Therefore, it has been necessary to develop techniques for examining details of the grinding wheel topography in order to ascertain quantitative measurements of cutting edges. A review of the available techniques contains: scanning electron microscopy techniques, three-dimensional imprint methods, two-dimensional stylus profilometry and dynamic techniques, such as acoustic emission, thermocouple and razor blade techniques. Usui et al. [6] developed a triangulation laser reflectance system for in-process two-dimensional grinding wheel characterization.

However, it is becoming increasingly obvious that a full compatibility between surface topography and functional performance can only be realized if a three-dimensional approach to surface characterization is utilized. The emergence of the three-dimensional approach to surface analysis is largely due to the limitations of two-dimensional surface analysis and also as a result of the development of modern powerful microcomputers [5].

In order to differentiate between the total number of cutting edges and those that actually do work, Verkerk et al. [7] proposed that two parameters be used. These are  $C_{stat}$  (total number of “static” cutting edges) and  $C_{dyn}$  (those cutting edges involved when dynamics is included in the assessment). A third subscript is also introduced. This is  $C_{kin}$  (kinematic), which also considers the penetration angle of the cutting edges. The report also suggests that on any one grain, there is often more than one cutting edge. Thus, to differentiate between grains and cutting edges, a second parameter is introduced along with  $C$ , i.e.  $G$  (grains).

There emerges some evidence which suggests that the differences between static and dynamic measurements are much less in practice than the theory would predict, particularly in the case of active grain measurement ( $G_{\text{stat}}$  and  $G_{\text{dyn}}$ ), where the two values may be very similar [8].

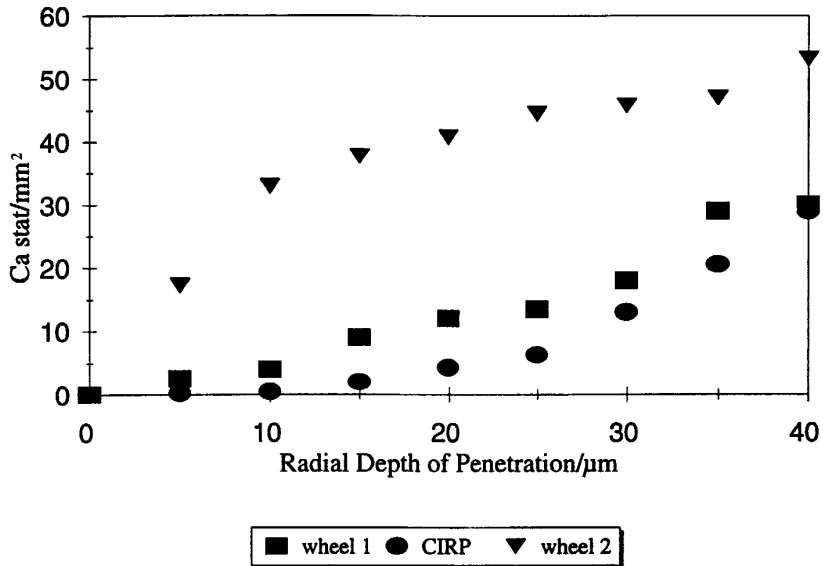


Fig. 4. Relationship between cutting edge density and radial depth of penetration for wheel 1 (WA60H6VG), wheel 2 (WA100H6VG) and wheel used in CIRP [7] work measured under identical conditions

Another factor influencing the result is that typical two-dimensional longitudinal and transverse profiles of a wheel are reasonably dissimilar. For example, the characteristic wavelength component of the longitudinal roughness was found to be by over seven times larger than that in the traverse direction, and the values for  $Ra$  are larger across the lay than along it. This is recognized in two-dimensional surface measurement standards. Thus, it is even more difficult to simplify the spacing of the cutting points in such a way as to obtain an “ideal” from a profile in only one direction. Clearly, some of these problems are the result of shortcomings of two-dimensional techniques and have the potential for removal if a three-dimensional technique is employed.

This analysis was achieved by truncating the three-dimensional surface map at increasing depths, simulating the radial depth of penetration, and counting the number of peaks intersecting the plane of truncation. A peak is defined as a point in the data array which is higher than its eight nearest neighbours.

Figure 4 shows a graph of the present results and the “converted” CIRP figures. Note that the measurement sample spacings and wheel preparations of wheel I and the wheels used in the CIRP work are as close as possible to allow comparisons.

## 2. Topography model of the grinding wheel

Completed research has proved that the stereometry of the cutting surface of grinding wheel manufactured according to standard requirements is closely related to its structure, characteristic grain size and volume of the bond [9, 10]. It has been proved that the grinding efficiency tests are strictly connected with the maximum height parameter of the roughness profile of cutting surface of the grinding wheel. The investigations demonstrate that this height parameter is dependent upon the average grain size and the average distance between grains in the grinding wheel.

3-D structural model of a grinding wheel is presented in Figure 5. The abrasive grains of the average size  $a$  are encircled by the tightly condensed balls ( $Cb = 74\%$ ). The ball diameter is equal to the distance between the neighbouring grains  $L_{av}$ . The unit volume of the grinding wheel can be filled with  $\bar{n}$  grains of the individual volumes  $V_i = \pi a^3/6$

$$\bar{n} = \frac{6(62 - 2N)}{100\pi a^3}. \quad (2)$$

The average distance between the grains is:

$$L_{av} = a \left( \frac{74}{62 - 2N} \right)^{1/3}, \quad (3)$$

where  $N$  is the structure number featuring the volume of grains in the grinding wheel, X-X cross-section plane defines two cutting faces CS1 and CS2, each containing half of the total grain number in this cross-section.

The expectation  $E\{n_c\}$  of the grain number along the unit length is as follows:

$$E\{n_c\} = \frac{1}{2} E \left\{ \frac{1}{L_{av}} \right\}, \quad (4)$$

$$n_c \cong \frac{(62 - 2N)^{1/3}}{8.4a}. \quad (5)$$



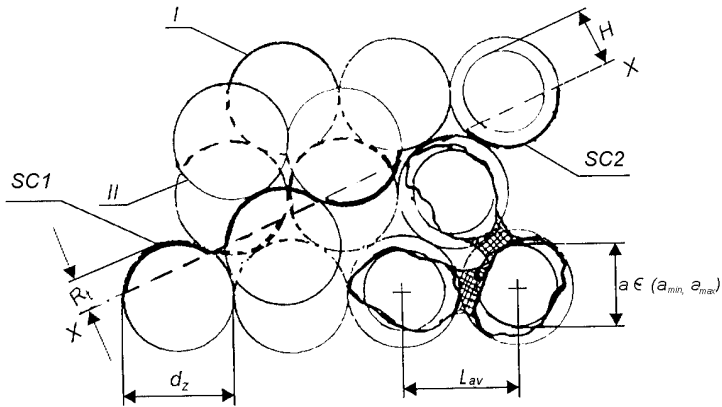


Fig. 5. 3-D structural model of the grinding wheel ( $d_z$  – imaginable ball diameter)

The maximum roughness height  $R_t$ , according to the model explained in Figure 5, is influenced mainly by the grain size  $a$  and also by the relative share  $V_{sp}$  of the bond surrounding the grains, which can be expressed as  $V_z/V_{sp}$ , where  $V_z$  is volume of the grains.

### 3. Experiment

The procedures for making profilograms do not give a chance of getting the true shapes of asperities (Figure 6a). The shapes of elevations obtained for the same vertical and horizontal enlargement are similar to the shapes of the grain fragments sticking out from the bond (Figure 6b).

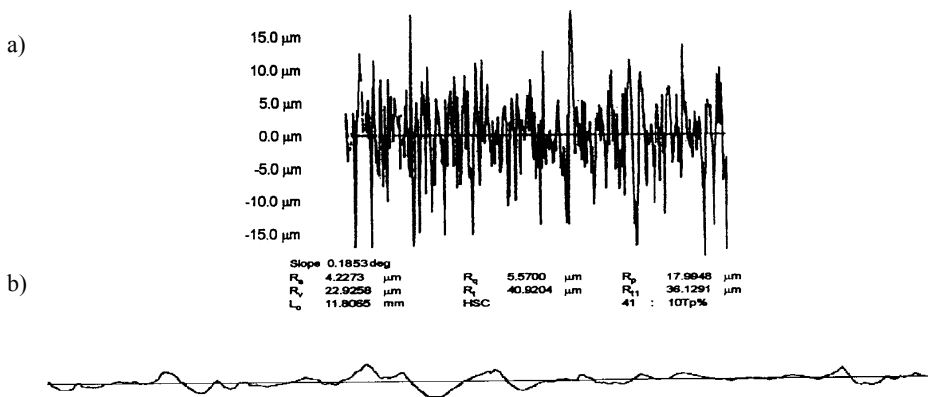


Fig. 6. 2-D structure of the grinding wheel: a) standard profilogram, b) this same profile with the equal vertical and horizontal magnification

The number of grains determined in (5) has been verified by defining the HSC number for the peaks in the profilogram (Figure 6a), where the higher-order components are automatically filtered out. The wheels being investigated are specified in the Table.

Table. Wheel roughness conditions

Type of wheel		Parameters $R_t$ (2-D) and $sR_t$ (3D)					
		36.O.6	60.O.5	80.K.6	80.O.6	100.Q.7	120.O.6
SiC grains	$R_t$ (2-D)	143.3	115.2	95.3	85.5	60.7	36.9
	$sR_t$ (3-D)	243.0	199.0	222.0	198.0	158.0	107.0

Figure 7 testifies to a good conformity of the results obtained for grinding wheel.

Based on the measurement results the roughness heights  $R_t$  have been described by the following regression equations:

- 2D profilogram .....  $R_t = 1.35a^{0.72}(V_z/V_s)^{0.22}$ , (6)

- 3D profilogram .....  $R_t = 1.41a^{0.74}(V_z/V_s)^{0.17}$ . (7)

The coefficient values of multiple correlation for (6) and (7) are  $R = 0.905$  and  $R = 0.936$ , respectively, and the Fisher test numbers are  $F = 27.129$  and  $F = 42.575$ , respectively. A statistical evaluation of relationships (6) and (7) shows the important difference between two measurement types.

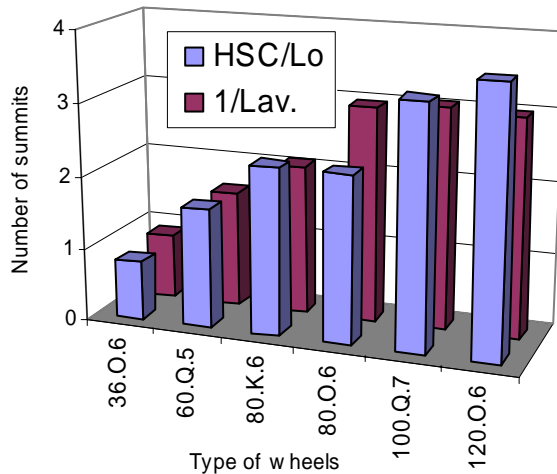


Fig. 7. Comparative number of summits (1/Lav) obtained from relationship (3) and from measurements of the wheel roughness (HSC/Lo, Lo – cut off)

Figures 8a and 9a show perspective drawings of the surfaces of wheel SC60.O.5 and wheel SC120.O.6, respectively. The maps clearly show the nature of the wheel surface and give an excellent visual perception. Unfortunately, the technique cannot distinguish between grits and bond material. However, the grits protruding above the general surface are clearly visible.

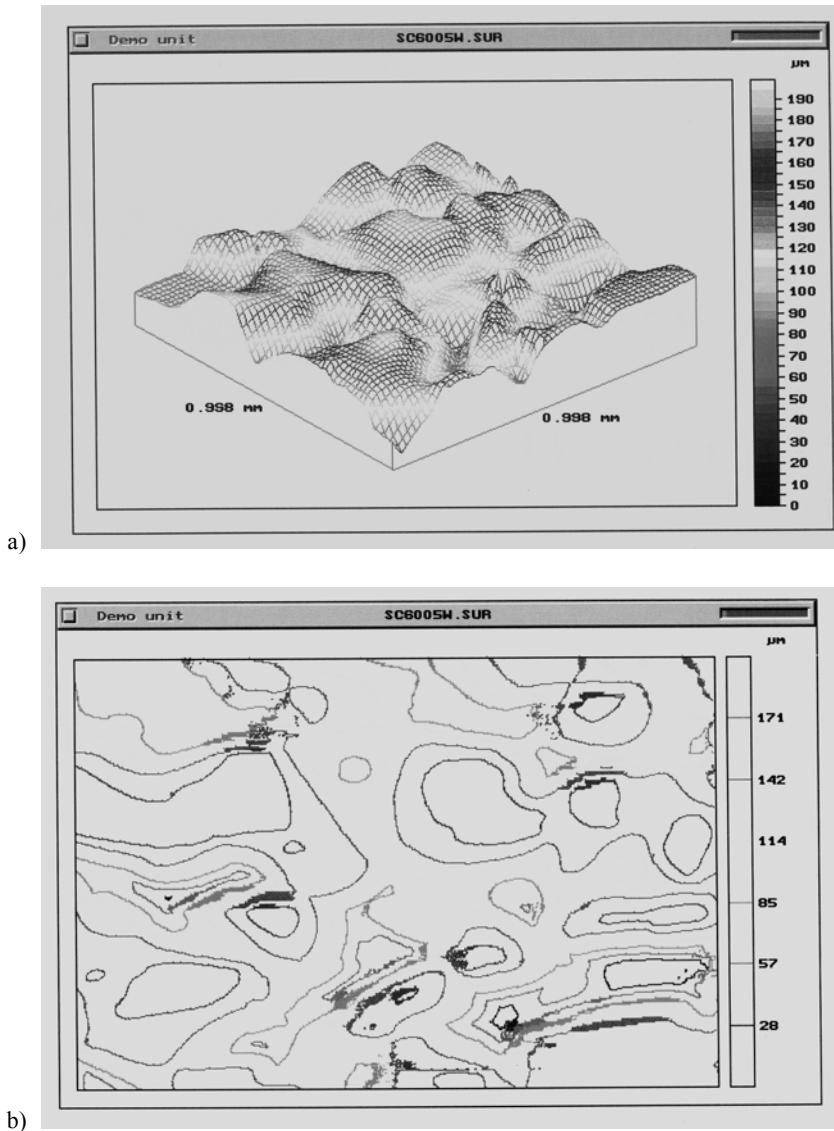


Fig. 8. 3-D surface measurement and characterization of the wheel SC60.O.5: a – 3-D profilogram , b – map

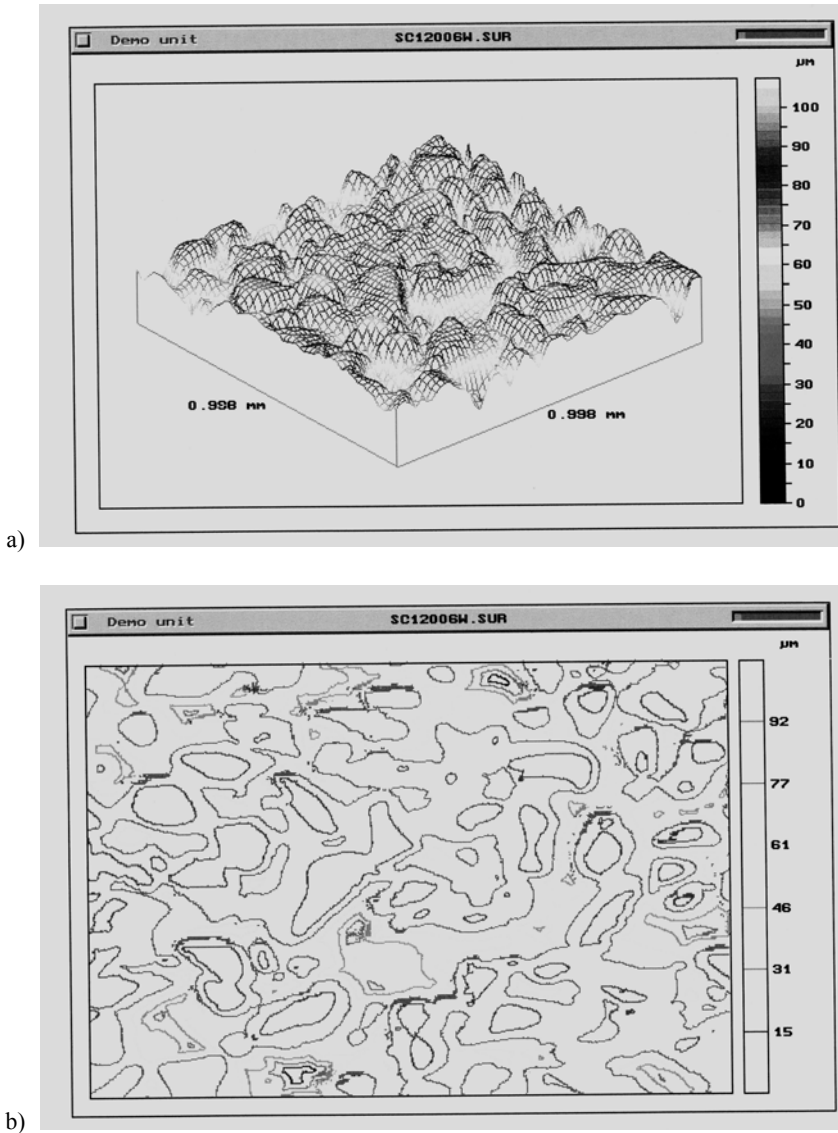


Fig. 9. 3-D surface measurement and characterization of the wheel SC120.O.6: a – 3-D profilogram, b – map

The number of peaks per the unit length (area) of the roughness profile of a grinding wheel surface and the maximum profile depth describe the tribological contact of the wheel with the ground surface and consequently the productivity of grinding. The 3-D visualization of the wheel surfaces when applying grain numbers 36 and 120 presented in Figures 8a, b and Figure 9a, b is a good representation of the tribological

contact between the surface of the grain tops (Figures 8a, 9a) and contact areas at various penetration levels (Figures 8b and 9b). These conditions influence unit pressures which, at the constant normal grinding force  $F_n$ , are dependent on the grain number  $n_c$  defined by the Equation (5).

The unit pressure has been defined as  $F_n/n_c^2$  and then the specific volume removal rate  $Q'_w$  [ $\text{mm}^3/\text{mm}\cdot\text{min}$ ] has been determined for the samples of bearing steel 100Cr6 of Rockwell hardness 54 and for wheels specified in Table 1 (for  $v_c = \text{const}$ , the  $F/F_{cr}$  ratio equals 4.415):

$$Q'_w = 0,46 - 2,83 \cdot 10^{-2} Rt + 2,54 \cdot 10^{-2} t + 5,08 \frac{F_n}{n_c^2} - 2,42 \left( \frac{F_n}{n_c^2} \right)^2. \quad (8)$$

The graphical representation of relationship (8) is presented in Figure 10 for the constant grinding time  $t = 60$  s.

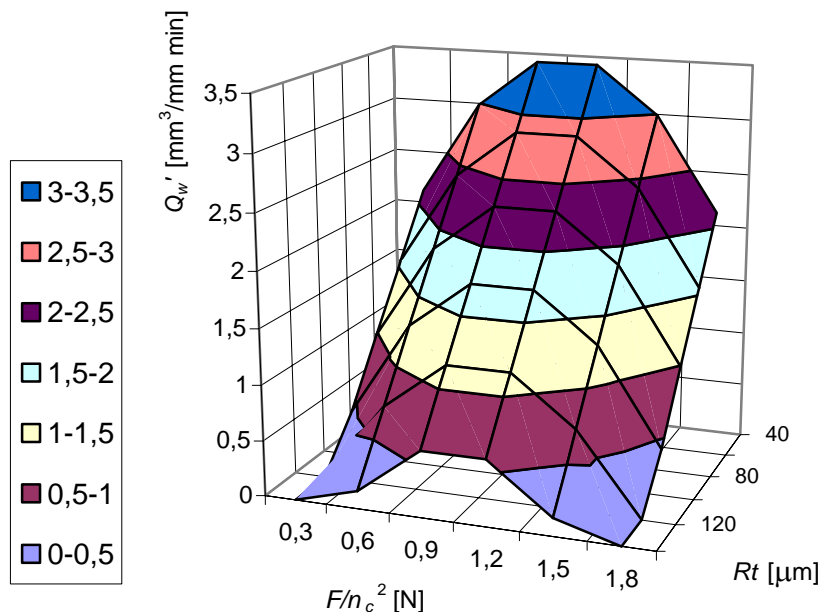


Fig. 10. The influence of the tribological load ratio of  $F/n_c^2$  and the maximum roughness  $Rt$  on the grinding removal rate  $Q'_w$

The  $sRt$  parameter specified in the Table that describes the highest of peaks being recorded in a 3-D measurement yields relationship (8) with the enhanced reliability ( $F/F_{kr} = 5.915$ ).

## 4. Summary

By acquiring a quantified characterization of the topography of both grinding wheel and ground surface, an insight into various factors, which may influence the finished surface of a workpiece, can be gained. In practical terms, if more can be learned of how loaded wheels affect the finished surface, estimations of the expected surface texture obtainable from a measured wheel can be made, and a more predictive approach to the optimum timing of redressing can be taken.

The functional performance of many grinding wheel surfaces can now be further quantified in terms of roughness, and these measurements associated with conventional tribological techniques of microscopy proved to be invaluable.

## Acknowledgement

The Polish State Committee for Scientific Research (Research Grant # 8 T07D 04221) is gratefully acknowledged for their support. Authors also acknowledged Mr. Z. Lechniak for their assistance in this study.

## References

- [1] Marciniak M.: *Non-Conventional Grinding as a Tribological System*, Abrasives Magazine, June/July, 1996, p. 14, USA.
- [2] Shaw M., Komanduri R.: *The Role of Stylus Curvature in Grinding Wheel Surface Characterization*, Ann. CIRP 25 (1), 139–140, 1997.
- [3] Tönshoff H.K., Wobker H.G., Wetner F.: *Analysis of Wheel Waviness and Grain Wear in Grinding*, Transaction of NAMRI/SME, Volume XXI, 1993, p. 145.
- [4] Standard DIN 4776.
- [5] Blunt L., Ebdon S.: *The Application of Three-Dimensional Surface Measurement Techniques to Characterizing Grinding Wheel Topography*, Int. J. Mach. Tool Manufact, Vol. 36, No. 11, pp. 1207–1226, Great Britain, 1996.
- [6] Usui E., Obikawa T., Hagiwara S.: *Study on Edge Fracture of Abrasive Grain During Grinding with Applying the Theory of Markov Process*, Bull. Japan Soc. of Proc. Eng., Vol. 22, No. 2, June 1988.
- [7] Verkerk J. et al.: *Final Report Concerning CIRP Cooperative Work on Characterisation of Grinding Wheel Topography*, Ann. CIRP 26, 2, 1977.
- [8] Malkin S.: *Grinding Technology; Theory and Applications of Machining with Abrasives*, Ellis Horwood, Chichester, 1989.
- [9] Dąbrowski L., Marciniak M.: *Tribological Aspects of the Grinding Process*, Advances in Manufacturing Science and Technology, quarterly, Polish Academy of Science, Vol. 24, 2, 2000.
- [10] Marciniak M., Oczós K.E.: *Tribological Aspect of Grinding 3D Cutting Surface Wheel*, Collection of Works XXIV Scientific School of Abrasive Machining, Łopuszna, Poland, 2001.

### **Czynna powierzchnia ściernicy jako element systemu tribologicznego**

Zanalizowano wyniki badań porównawczych profilu chropowatości czynnej powierzchni ściernicy na podstawie dwu- i trójwymiarowych profilogramów (2-D, 3-D). Wykazano, że czynną powierzchnię ściernicy można traktować jako powierzchnię jednego z dwóch elementów pary tribologicznej, której najwyższe wierzchołki odgrywają zasadniczą rolę w procesie dekohezji materiału szlifowanego. Liczbę tych wierzchołków określono na podstawie modelu teoretycznego struktury ściernicy i zweryfikowano doświadczalnie. Wpływ tych czynników na efektywność procesu trybologicznego oceniono, badając siłę normalną  $F_n$  i wydajność właściwą szlifowania  $Q'_w$ .

## Advisory system for grinding operation planning

R. DĘBKOWSKI, M. URBANIAK

Department of Production Engineering, Technical University of Łódź, ul. Stefanowskiego 1/15,  
90-537 Łódź

A system, which improves a decision-making process during grinding operation planning, is described. It should favour the selection of grinding wheel, dressing conditions and grinding conditions. The system was designed as an artificial intelligence hybrid system. Wheel selection is realised by an expert system, while forecasting of grinding results is performed by means of a grinding process model based on artificial neural network.

Keywords: *grinding conditions, artificial intelligence, selection*

### 1. Introduction

Development of design, control and optimisation of intelligent systems in grinding is well grounded because:

- The costs of grinding process need to be decreased. This can be achieved by the decrease of tool wear rate (especially important when using superhard wheels), reduction of reject number and quality assurance of workpieces being ground.
- Elimination of human participation in arduous actions is desired.
- Frequent changes of production profile and place of production should not affect high quality of workpieces.

Tasks of the system, which would fulfil the above mentioned requirements, are described in Figure 1 [14]. The search for optimum grinding conditions requires application of adequate solutions in scope of the process controlling and monitoring in terms of grinding efficiency and ground-surface quality. Good results of process optimisation depend also on initial conditions, being selected during process planning, which is the first stage of optimisation process.

The research was carried out using artificial intelligence methods, as they are the most efficient tools in simulation and modelling of manufacturing processes. They are helpful in design of grinding process models, which enable process monitoring [15–19, 21–23]. They are also the part of integrated control and inspection systems, [7, 10, 14, 20], grinding condition selection systems [1–6, 24, 25], and advisory systems of grinding process optimisation [11–13].



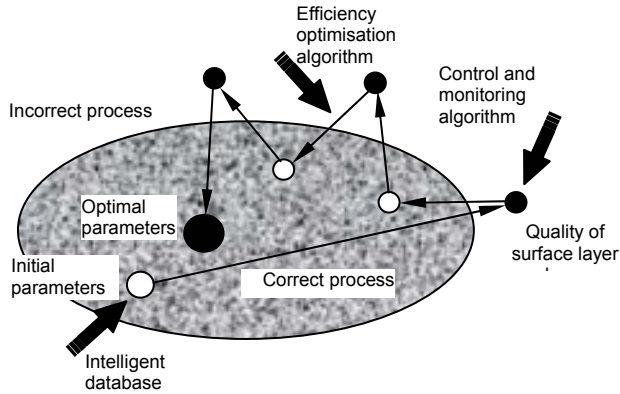


Fig.1. Tasks of intelligent grinding system [14]

In the paper, an intelligent database created for selection of machining conditions at the beginning of grinding operation is described. The examples of such systems can be found in [1–6, 24, 25]. When analysing an available literature one can notice an increasing number of artificial intelligence tools in the systems which are more universal and contain deeper knowledge. For example, Rowe [5] proposed a hybrid system. He described an integrated system based on artificial neural network model (for selection of wheel characteristics), database (containing solutions) and knowledge base (containing rules which relate dressing and grinding conditions to grinding results and type of grinding wheel). Similar hybrid system was described by Rojek-Mikołajczyk [6]. In the system, wheel selection was carried out with the aid of neural network, while the selection of grinding parameters was realised by an expert system. In order to automate grinding process design, Chen [25] described a system, in which neural networks and fuzzy logic were applied to optimise cutting conditions.

Application of combined artificial intelligence tools and their different tasks make a complex problem easier to solve. This is why a database described below has been designed as a hybrid system, whose architecture is different from that presented in [5, 6, 25]. The system is based on artificial neural network (ANN) used for grinding process modelling, expert system (ES), which selects wheel characteristics, and standard database that contains solutions and facts which enable description of grinding operations.

## 2. A concept of advisory system structure

The project was designed in order to create a system, which allowed selection of grinding wheel characteristics, dressing and grinding parameters for given machining task and thus obtaining the desired machining results. It can be realised by assignation of different tasks to different artificial intelligence modules, being part of the hybrid system.

## 2.1. Expert module

Expert systems with knowledge base in the form of rules are developed in order to solve non-algorithmic problems in scope of detailed knowledge defined by man. They simulate human expertise in a given, narrow field. In our research, an expert system was applied to decision-making process according to technical characteristics of the wheel. Facts which need to be collected are unequivocal and permanent. Scope of knowledge, according to the task, is constant (during long period of time). It contains ability to relate wheel characteristics to machining task described by:

- type of ground surface,
- grinding method,
- type of workpiece material and its hardness,
- accuracy of grinding.

Such an expert knowledge can be found in catalogues of grinding wheel producers and in other sources connected with application of abrasive products. This knowledge, if it is accumulated in knowledge base, may be used for selecting wheel characteristics by expert system. Description of machining task (by the above-mentioned parameters) will be a basis for inference. Task of the expert system is described in Figure 2. Expert systems can be characterised by overt presentation of knowledge. It can be extended and improved by both expert and system user. When new tools, materials or machining methods are available, the knowledge base can be easily supplemented by addition of a new rule or modification of existing one.

## 2.2. Artificial neural networks

Knowledge bases, which use rules, have limited potential due to countable number of recognisable events. They cannot select correct conclusion and they are not able to make a decision about new problems, where new facts appear. Knowledge bases based on artificial neural networks are more flexible.

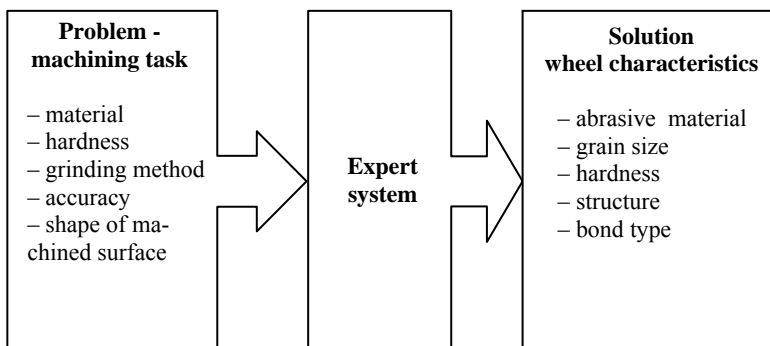


Fig. 2. Task of expert system

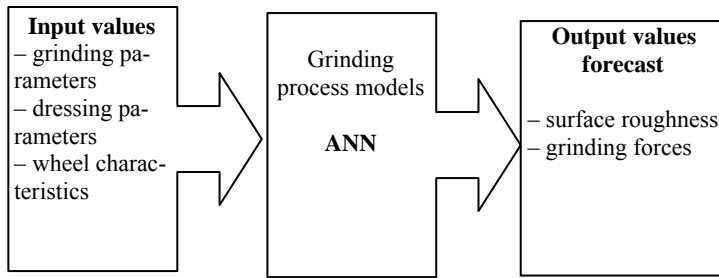


Fig. 3. Neural model task

They can apply unclear and incomplete knowledge. This kind of knowledge is typical of grinding process, which is highly complicated and influenced by several factors. For this reason empirical model of grinding process, which describes relationship between input and output parameters, is based on artificial neural networks. Tasks of the neural models are shown in Figure 3. Results of grinding process are forecasted on the basis of input values – grinding parameters, dressing parameters, wheel characteristics. The surface roughness and grinding forces are the values being forecasted.

### 2.3. Control software

Knowledge bases described above were introduced into one hybrid system controlled by the control software. The software starts an inference process in an appropriate base and participates in the exchange of information between the bases. The tasks of software are as follows:

- identification of machining task,
- transfer of the problem to an expert system,
- transfer of solution (from ES) to ANN with grinding and dressing parameters,
- verification of forecasted (by ANN) output values of grinding process.

The scheme of system structure and its functionality are shown in Figure 4.

The above-mentioned tasks are realised in three modules.

*Task identification module* enables a detailed description of machining task (type of material, type of dresser, surface roughness parameters, grinding methods, etc). Facts, which are important for beginning the inference in ES, are introduced into the module's memory during conversation with the system user.

*Grinding condition generation module* delivers wheel characteristics and grinding and dressing parameters (for the task defined) to artificial neural network on the basis of ES answer.

*Forecast verification module* verifies the quality of workpiece surface layer on the basis of ANN forecast according to the surface roughness parameters  $R_{aANN}$  and tangential component of the grinding force  $F_{LANN}$ .

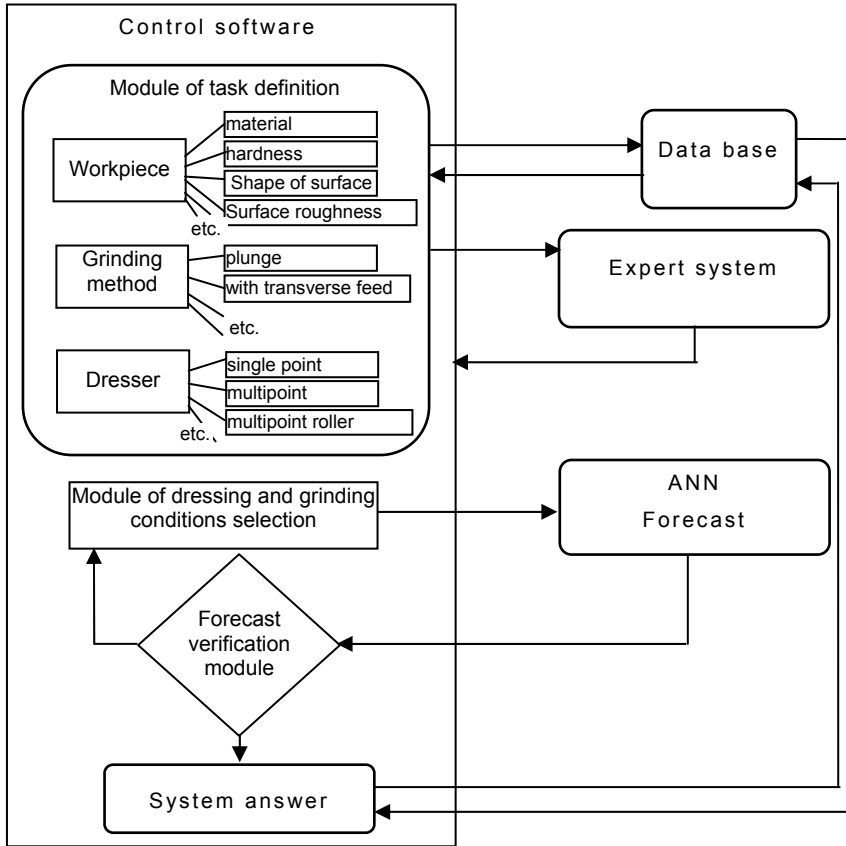


Fig. 4. Structure and functionality of the hybrid expert system

Surface roughness is found to be correct if  $R_{aSSN}$  does not exceed the value defined by the system user. Smaller values are correct as long as they do not reach the values, which characterise higher class of surface roughness. These conditions are described by the following relation:

$$1 \leq \frac{R_a}{R_{a(SSN)}} < 2. \quad (1)$$

Physical and mechanical properties are verified using the second parameter – tangential component of a grinding force. The value of the component influences

value of the factor  $B_p$ , which corresponds with energy of the machining process. In the case of surface grinding, the factor value can be calculated from the following equation:

$$B_p = \frac{v_s \cdot F_t}{v_p \cdot b}. \quad (2)$$

A clear relationship between the factor  $B_p$  and the properties of surface layer was found in [8, 9]. Grinding process is efficient and high quality surface is obtained until a certain limit value of the factor is exceeded. Beyond this point unfavourable changes in the surface layer of a workpiece are observed (high stress level, changes of micro-hardness, burns, micro-cracks).

On the basis of equation (2) one can calculate the value of a tangential component of grinding force, for which the value  $B_p$  does not exceed permissible range. The value of the force component can prove that the surface layer has appropriate properties. It should correspond with the value  $F_{tANN}$  forecasted by ANN.

### 3. Advisory hybrid system for grinding process planning

The system's concept was realised according to the surface grinding of high-speed steel by means to vitrified alumina wheels. The following software was applied during development of the system:

- artificial intelligence package Sphinx 3.0,
- database creator MS Access,
- scientific calculation software Matlab 5.3.

Communication between these environments was maintained by SQL database language and the mechanism of Dynamic Data Exchange (DDE).

#### 3.1. Expert module

Expert system PC-Shell, being a part of Sphinx 3.0 package, was applied to create a knowledge base and the system supervising software. The system insures separation of expert knowledge from control procedures.

PC-Shell can convert knowledge, so the system user needs to introduce expert knowledge into knowledge base together with the description of the way of how the knowledge should be applied. The knowledge is represented by facts and rules in the form of: (conclusion) if (conditions).

Table architecture of PC-Shell System enables application of several knowledge sources (KS). Whole knowledge about a given aspect can be divided into smaller pieces (about appropriate problems) and described by separate sources. Knowledge on

wheel selection for a given workpiece material group was then introduced into several knowledge sources.

PC-Shell knowledge conversion subsystem realises the so-called back inference. The system selects rules (concerning a given problem, e.g. the relationship between wheel characteristics and description of machining task) from knowledge source and inspects conditions of the rule. If there is a condition, which cannot be confirmed, the system searches for solution, which might confirm the condition. If among selected rules one can find the rule where all conditions are fulfilled, the conclusions become the solution of the problem – the system generates wheel characteristics for machining a task required.

*Supervising software* controls an appropriate knowledge utilisation. It consists of a set of instructions (in the Sphinx environment language), starts the inference processes in an adequate knowledge source and saves solutions in computer memory. This result becomes a part of whole solution or is a basis for inference, using different source. The software recalls an adequate source of knowledge, in which rules of an appropriate group of workpiece material are stored. This enables continuous development of the system by elaboration of new knowledge sources.

### 3.2. Neural model of grinding process

Model of grinding process was designed using an artificial neural network. Multi-layer perception (MPL) network with one hidden layer was used to model the process. In order to activate neurons in both hidden and output layers, an arctg function was used. Conditions and results of 114 grinding tests were applied to train the network. Test conditions are shown in the Table. Wheel characteristics and dressing conditions were the model input values. Grinding results (surface roughness parameter  $R_a$ ) and grinding force tangential component  $F_t$  achieved after a few grinding passes were the output values.

Table. Grinding wheel measurement conditions

Characteristics of the wheel made by KORUND: 38A, 46/60/80, J/K/L, VBE	
Dressing conditions	
Dresser type	single diamond dresser
Diamond width [mm]	0.8–1.1
Number of dressing passes	5
Dressing depth [mm]	0.005, 0.015, 0.025
Overlap ratio $k_d$	1.2–2.5
Grinding conditions on the SPG 30 surface grinder	
Wheel speed [m/s]	26.5
Workpiece speed [m/s]	0.16–0.33
Infeed [mm]	0.005–0.025
Number of passes	4
Coolant	4% oil emulsion
Workpiece material	SW7M 60HRC

### 3.3. Task identification

Introduction of the input values, which enable an artificial intelligence to draw inferences, is realised by database created in database creator – MS Access. The base contains tables with values and definitions describing grinding operation. The control software takes an appropriate range of notions from database and saves adequate values as facts after communication with a user. They can be used in further stage of communication or applied during inferring. Database structure is shown in Figure 5.

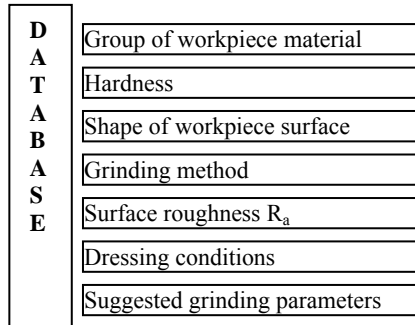


Fig. 5. Database structure

The base has also in memory the solutions that have been found earlier. Connection between the base and task definition module ensures fast access to solutions if the system meets the same problem.

### 3.4. Generation of grinding and dressing parameters

Solution obtained from ES, including grinding wheel characteristics, needs to be completed with grinding and dressing parameters. An adequate selection of these parameters decides whether the result of the process is successful. Information about the results is presented by neural network. In order to generate a forecast, the network is supplied with the set of parameters, corresponding with defined process of grinding and dressing. Surface grinding process and dressing operation with a single diamond dresser are characterised here by:

- grinding infeed  $a_e$ ,
- workpiece speed  $v_{fb}$ ,
- dressing infeed  $a_d$ ,
- overlap ratio  $k_d$ .

Values of these parameters are taken (by control software) from files, where intervals of their variations in discrete form are kept.

The parameters  $a_e$ ,  $v_{fb}$ ,  $a_d$ ,  $k_d$  are arranged in groups “each one with the other” and send to ANN together with a wheel characteristics.

### 3.5. Correct grinding criteria

On the basis of information on the values of grinding process parameters and on the neural model forecast concerning the surface roughness parameter  $R_a$  and grinding force component  $F_{tSSN}$ , the control software checks whether condition (1) is fulfilled. Then the factor  $B_p$  is computed. The width of a machined material is represented by the parameter  $b$ . It was assumed that grinding conditions would be correct if the result of computing did not exceed 2. Such a value of  $B_p$  was suggested by authors of publication [9] (to obtain correct properties of workpiece surface layer) during grinding of SW7M steel using grinding wheel designated as 38A46J8VK.

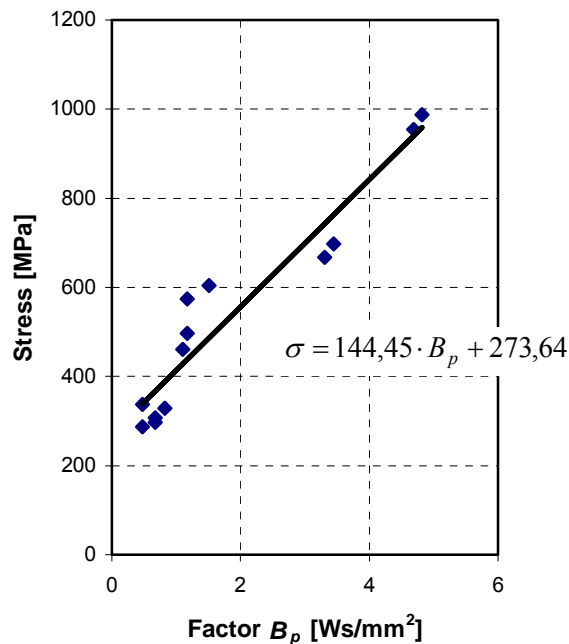


Fig. 6. Relationship between stress level in workpiece top layer and the factor  $B_p$  during grinding process of SW7M (60HRC) with 38A46J8VK wheel [9]

Research described in [9] showed the possibility of applying the factor  $B_p$  to evaluation of stress level in workpiece surface layer after machining process. The relationship derived is described in Figure 6. Information about residual stress in the workpiece surface layer enables further optimisation of grinding condition selection, which seems especially important when the number of solutions is high. In the system, minimum stress level in workpiece surface layer was proposed as a criterion of correct grinding conditions. The system user is informed about the solutions which fulfil the criterion.



### 3.6. Results of the system action

Due to the system action we arrive at the propositions of grinding wheels together with grinding and dressing conditions. The information is completed with the forecast of stress level which may occur in the workpiece surface layer after machining process. Example of the system report is shown in Figure 7.

## 4. Conclusions

Continuous search for solutions, which enable optimisation of grinding process, leads to application of new modelling methods and new techniques of knowledge base manipulation. This enabled design of the above intelligent advisory system for selection of grinding and dressing conditions. The system can operate in a wide range of workpiece materials; however, the tests are narrowed down to high-speed steel.

Department of Production Engineering Technical University of Łódź	27th January, 2002
<b>PC-Shell 3.0 systemu report</b>	
Grinding task	
Workpiece material	High-speed steel
Hardness [HRC]	>60
Ground surface	plane
Accuracy	fine grinding
Desired surface roughness $R_a$ [ $\mu\text{m}$ ]	0.63
Type of dresser	single point
<b>Suggested grinding conditions</b>	
$a$ – infeed [mm]	
$v_p$ – workpiece speed [m/min]	
$k_d$ – overlap ratio	
$a_d$ – dressing infeed [mm]	
$\sigma$ – forecasted stress in surface layer [MPa]	
<b>1) 38A60I8VBE</b>	
$a = 0.005$ , $v_p = 8.0$ , $k_d = 1.0$ , $a_d = 0.025$ , $\sigma = 340.3$	
<b>2) 38A60I8VBE</b>	
$a = 0.005$ , $v_p = 8.0$ , $k_d = 1.2$ , $a_d = 0.025$ , $\sigma = 344.8$	
<b>3) 38A60I8VBE</b>	
$a = 0.005$ , $v_p = 6.0$ , $k_d = 1.2$ , $a_d = 0.015$ , $\sigma = 350.0$	

Fig. 7. Artificial intelligence system report

One of the system advantages is the possibility of further development of the system by introduction of new knowledge bases in form of:

- rules which relate wheel characteristics with its application,
- neural models that describe grinding process (due to data dynamic exchange system (DDE), even if created in different softwares, which realise artificial neural networks),

- databases which enable description of wide range of machining tasks and correct grinding criteria ( $B_p$ ).

Neural models, applied in the system, complete expert knowledge. They are the best form of compressed empirical knowledge, which delivers fast and precise forecast of machining process results without simplifications. The system can be a part of larger intelligent grinding system. It can play a role of tool for selection of machining conditions, which are then optimised using algorithms supervising grinding process. Further research should lead to extension of expert and empirical knowledge bases stored in neural models. Also algorithms, which optimise the grinding conditions selected, should be introduced into the system.

## References

- [1] Sakakura M., Inasaki I.: *A Neural Network Approach to the Decision-Making Process for Grinding Operations*, Annals of the CIRP, 41(1992)1, 353–356.
- [2] Sakakura M., Inasaki I.: *Intelligent Data Base for Grinding Operations*, Annals of the CIRP, 42(1993), 1, 379–382.
- [3] Liao T.W., Chen L.J.: *A Neural Network Approach for Grinding Processes: Modeling and Optimization*, Int. J. Mach. Tools Manufact., 34(1994)7, 919–937.
- [4] Li Y., Mills B., Rowe W.: *An Intelligent System for selection of Grinding Wheels*, Journal of Engineering Manufacture, 211(1997), B8, 635–641.
- [5] Rowe W., Li Y., Chen X., Mills B.: *An Intelligent Multiagent Approach for Selection of Grinding Conditions*, Annals of the CIRP, 46(1997), 1, 233–238.
- [6] Rojek-Mikołajczyk I., Weiss Z.: *Inteligentna baza danych w planowaniu operacji szlifowania*, XXIII Naukowa Szkoła Obróbki Ściernej, Rzeszów, 2000, 310–315.
- [7] Rafałowicz J., Leżański P., Lajmert P.: *Sterowanie i nadzorowanie procesu szlifowania kłowego walków*, XXIII Naukowa Szkoła Obróbki Ściernej, Rzeszów, 2000, s. 89–117.
- [8] Wójcik R.: *Wpływ gęstości strumienia energii szlifowania na stan naprężeń własnych w warstwie wierzchniej*, praca doktorska, Politechnika Łódzka, Łódź, 1996.
- [9] Wójcik R., Kruszyński B.: *Wpływ gęstości strumienia energii na właściwości warstwy wierzchniej przy różnych odmianach kinematycznych szlifowania*, Projekt Badawczy KBN Nr 7T07D00815, 2000.
- [10] Adamko K., Musiał W., Plichta J.: *Możliwości wykorzystania metod sztucznej inteligencji w procesie mikroszlifowania plastycznego*, XXII Naukowa Szkoła Obróbki Ściernej, Gdańsk, 1999, s. 9–14.
- [11] Vishnupad P., Shin Y.C.: *Intelligent optimization of grinding processes using fuzzy logic*, Proceedings of the Institution of Mechanical Engineers, Part B: Journal of Engineering Manufacture, Vol. 212, No. B8, 1998, pp. 647–660.
- [12] Brinksmeier E., Toenshoff H.K., Czenkusch C., Heinzl C.: *Modelling and optimization of grinding processes*, Journal of Intelligent Manufacturing, Vol. 9, No. 4, 1998, pp. 303–314.
- [13] Lee Cheol W., Shin Yung C.: *Improved generalized intelligent grinding advisory system*, American Society of Mechanical Engineers, Manufacturing Engineering Division, MED, Vol. 10, 1999, pp. 473–480.

- [14] Inasaki I.: *Sensor fusion for monitoring and controlling grinding processes*, International Journal of Advanced Manufacturing Technology, Vol. 15, No. 10, 1999, pp. 730–736.
- [15] Susic E., Grabec I.: *Characterization of the grinding process by acoustic emission*, International Journal of Machine Tools and Manufacture, Vol. 40, No. 2, Jan. 2000, pp. 225–238.
- [16] Nathan R.D., Vijayaraghavan L., Krishnamurthy R.: *Intelligent estimation of burning limits to aid in cylindrical grinding cycle planning*, Heavy Vehicle Systems, Vol. 8, No. 1, 2001, pp. 48–59.
- [17] Shi J.F., Hong Z.C., Cao J.: *On-line intelligent identification in grinding process based on rough sets theory*, Key Engineering Materials, Vol. 202–203, 2001, pp. 189–192.
- [18] Gong Y.D., Liu G.J., Wang W.S.: *Research on grinding wheel intelligent dressing system*, Key Engineering Materials, Vol. 202–203, 2001, pp. 181–184.
- [19] Dong T., Li Y., Hou L.: *Modeling of real-time monitoring and forecasting system about grinding temperature*, Nanjing Li Gong Daxue Xuebao/Journal of Nanjing University of Science and Technology, Vol. 24, No. 5, Oct. 2000, pp. 398–401.
- [20] Mamalis A.G., Grabchenko A.I., Fedorovich V.A., Grinko S.A., Paulmier D., Horvath M.: *Development of an expert system of diamond grinding of superhard polycrystalline materials considering grinding wheel*, International Journal of Advanced Manufacturing Technology, Vol. 17, No. 7, 2001, pp. 498–507.
- [21] Kobayashi Futoshi, Arai Fumihito, Fukuda Toshio, Onoda Makoto, Hotta Yuzo: *Sensor selection based on possibility measure for grinding system*, IEEE International Conference on Fuzzy Systems, Vol. 1, 1999, IEEE, Piscataway, NJ, USA, pp. I.492–I.497.
- [22] Kwak J.S., Song J.: *Trouble diagnosis of the grinding process by using acoustic emission signals*, International Journal of Machine Tools and Manufacture, Vol. 41, No. 6, May 2001, pp. 899–913.
- [23] Wang Z., Willett P., DeAguiar P.R., Webster J.: *Neural network detection of grinding burn from acoustic emission*, International Journal of Machine Tools and Manufacture, Vol. 41, No. 2, Jan. 2001, pp. 283–309.
- [24] Park M.W., Park B.T., Rho H.M., Kim S.K.: *Incremental supervised learning of cutting conditions using the fuzzy ARTMAP neural network*, Annals of the CIRP, 49/1/2000, p. 375.
- [25] Chen Y.T., Kumara S.R.T.: *Fuzzy logic and neural networks for design of process parameters: a grinding process application*, International Journal of Production Research, Vol. 36, No. 2, February 1998, pp. 395–415.

### **Doradczy system do projektowania operacji szlifierskiej**

Opisano system wspomagający podejmowanie decyzji przez technologa podczas projektowania operacji szlifierskiej w zakresie doboru ściernic, warunków obciążania i szlifowania. Zaprojektowano go jako hybrydowy system sztucznej inteligencji. Dobór ściernic do zadania obróbkowego powierzono systemowi ekspertowemu natomiast prognozowanie wyniku szlifowania modelowi procesu szlifowania zbudowanemu w oparciu o sztuczne sieci neuronowe.

## **Ecological methods of cooling in grinding processes**

T. KARPIŃSKI, J. SIENIAWSKI

Technical University of Koszalin, ul. Raławicka 15-17, 75-620 Koszalin

It is possible to reduce considerably manufacturing costs by the application of modern ecological grinding processes. In their paper, the authors present the current state-of-the-art of such processes. They have discussed the following modern and ecological methods of cooling: cooling by means of holes purposely formed in grinding wheels and reducing a flow zone of fluid supply; cooling by the use of injectors and “shoe” sprinklers; change in abrasive-wheel processes properties due to specially formed working surface. The authors in the present paper depict their initial studies in this field.

Keywords: *grinding, methods, cooling*

### **1. Introduction**

The main feature, which distinguishes grinding from other methods of machining, is a large contact area between the grinding wheel and the work piece and strong friction between abrasive grains, bond and work surfaces. Such a contact area and high rotational speed of a grinding wheel makes it difficult to supply the fluid to the grinding zone. This can lead to thermal cracks of sub-superficial layers [2]. An increase in grinding output leads to a substantial loading of cutting edges, mainly with heat loads. Emission of heat results in substantial stresses in the workpiece and in the grinding wheel. In order to avoid these unwanted effects, an “optimal” cooling is required. The optimal cooling is connected with supplying a necessary amount of grinding fluid to the grinding zone. This brings about a substantial reduction of the consumption of grinding fluid which at the same time enables us to obtain economical and ecological advantages.

Furthermore, the authors present the results of their own studies in reference to cooling in the grinding processes making use of grinding wheels with radial holes arranged inside the wheel and cooling with the application of slot and radial injectors.

### **2. Ecological aspects of cooling methods in grinding processes**

Ecological and economical reasons and also an increase in the grinding output are essential in reducing the amount of grinding fluid supplied to the grinding zone. Costs of fluid management constitute from 7 to 17% of manufacturing costs, Figure 1 [6, 8, 10]. Only in Germany, about 800000 t of grinding fluid are used up per year. It is qualified as

a special waste disposal which is very costly (about 1 billion DEM per year) [7, 8]. A considerable effort has been made to solve the problem of supplying fluid to the grinding zone, Figure 2 [1, 2, 7]. Supplying the fluid to the contact area between the grinding wheel and the workpiece is considered to be one of the main tasks which make the removal of the heat from the grinding wheel and the workpiece possible.

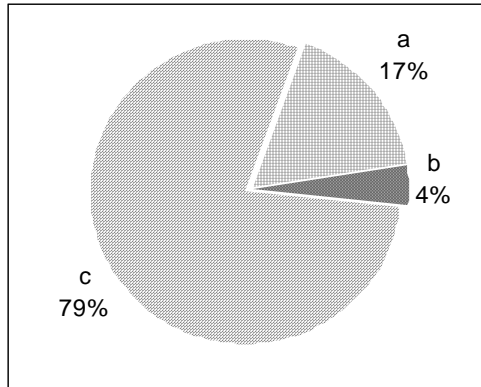


Fig 1. Share of grinding fluid costs in manufacturing costs: a) cost of fluid, b) cost of tools, c) others [10]

The most important requirement regarding this issue is avoiding the unused fluid jets flowing in the contact area between the grinding wheel and the workpiece.

The optimal system supplying the cutting fluid to the grinding zone should greatly reduce the amount of this fluid.

Depending on the amount of the fluid supplied, we distinguish the following modes of fluid supply: the conventional ways of supplying, the supplying with a substantial reduction of the fluid consumption and the minimum-quantity lubrication [9]. All those modes of fluid supply specified have should result in the reduction of friction in the zone of contact between the grinding wheel and the workpiece. The fluid is always supplied by means of conventional nozzles. A drawback of this method is deflection of a fluid jet from the grinding wheel and an increase in energy consumption induced by the demand for a large amount of fluid at the pressure equal to 20–30 bars.

A formation of an “air cushion” connected with the rotation of the grinding wheel is considered to be a very disadvantageous phenomenon in the process of grinding (Figure 3). A thickness of this cushion increases along with a rotational speed of the grinding wheel because the fluid has to flow through this area. According to Figure 3, there is a column of fluid in the front of the grinding wheel. In order to overcome a resistance of this column, the nozzle should be positioned at a minimal distance from the grinding wheel and at the same time the flow velocity of fluid  $v_c$  should be increased in order to be close to a rotational speed of the grinding wheel  $v_s$  [7].

Another mode often applied in investigation of the cooling systems in the grinding processes is a shoe sprinkler (Figure 4) [1, 7]. An extremely interesting way of cooling is the cooling through radial openings purposely made in the process of grinding-wheel formation [7]. In both methods, the cooling occurs at a reduced flow rate. It is due to surrounding the grinding wheel on three sides and a direct fluid supply (under the influence of centrifugal forces) to the cutting surface of the grinding wheel [1, 7]. These ways enable us to reduce the consumption of the grinding fluid (by about 2 dm<sup>3</sup>/min) [7]. However, one has to take into account a larger cost of the grinding wheel with a special fixture.

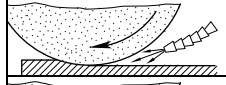
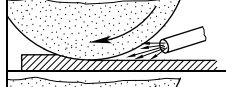
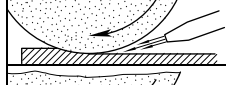
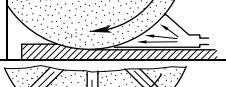
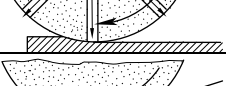
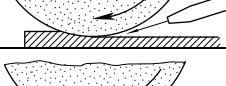
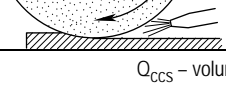
Flooding nozzles		A. Flexible segmented hose	Conventional fluid supply ( $Q_{CCS} = 20-40 \text{ l/min}$ )
		B. Tube	
		C. Free jet nozzle	
		Shoe nozzle	Fluid supply with a distinct reduction in its rate ( $Q_{CCS} < 2 \text{ l/min}$ )
		Internal supply	
		Spray nozzle	
		Spot jet nozzle	Minimal lubrication ( $Q_{CCS} = 50-100 \text{ ml/h}$ )
$Q_{CCS}$ - volumetric fluid supply			

Fig. 2. Basic ways of grinding fluid supply in grinding processes [2]

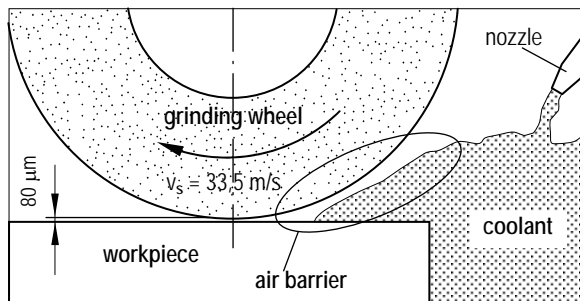


Fig. 3. Influence of air barrier on coolant supply [1]

Another interesting way of fluid supply is minimum lubrication and cooling (Figure 5). This concept consists in liquid supply to the cutting surface of the grinding wheel at a rate of  $Q_{ccs} \cong 50\text{--}100 \text{ cm}^3/\text{h}$  [7]. And also in this case, the fluid has to lubricate the grinding zone. The cooling effect due to a small amount of the liquid is minimized. This mode allows us to reduce the costs connected with waste disposal, management of grinding fluid, removal of chips and sludge. In this case, a cooling function of the grinding zone must be taken up by an appropriately designed grinder [4, 7].

In many parts of the world, the researchers carry out the tests on graphite as a lubricating medium in grinding [3], the cooling the grinding wheel by means of liquid nitrogen [3, 9] and the application of grinding wheels with discontinuous cutting surfaces [4, 5]. The use of graphite, according to the references, can replace the cooling by means of the grinding fluid in the process of steel grinding. Graphite in the form of blocks is forced against the grinding wheel in order to coat the abrasive grains before their cutting into the work material.

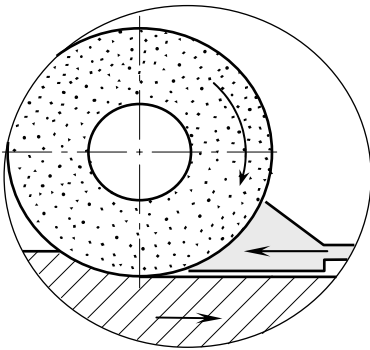


Fig. 4. "Shoe" nozzle

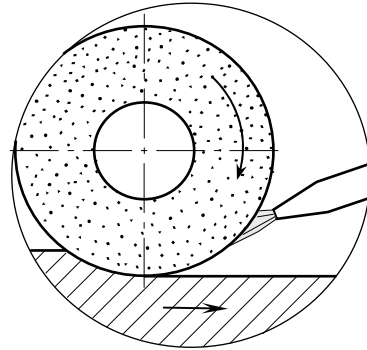


Fig. 5. Minimal lubrication

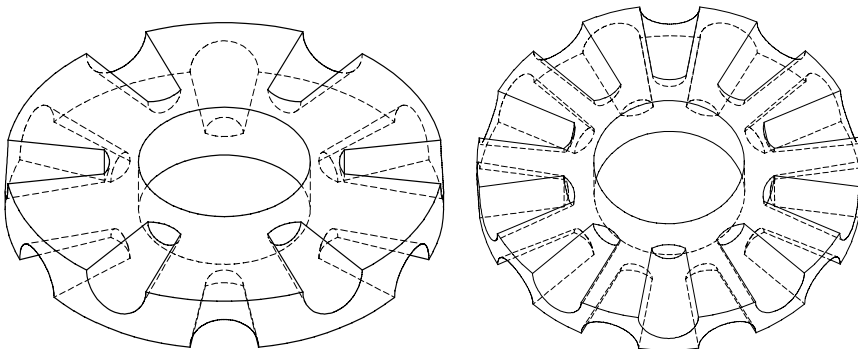


Fig. 6. Grinding wheels with discontinuous cutting surfaces

In the case of grinding the wheel surface being lubricated with graphite, the surface roughness of the workpiece is similar to the roughness obtained at lower wear of the grinding wheel [11]. However, this method can only be applied to grinding processes with lower outputs [3]. Investigation of the application of liquid N<sub>2</sub> in grinding confirmed the advantages of liquid-nitrogen cooling, especially a drop in temperature, reduction in components of grinding forces and a favourable shape of chips [9].

On the other hand, investigations of the grinding process with the use of grinding wheels with discontinuous cutting surfaces (Figure 6) revealed a considerable reduction in cutting forces (20–35%) and a drop in temperature in the grinding zone from 30 to 40% [4, 5]. However in this case, investigations of the conventional mode of cooling have not been carried out. The investigations more often confirmed that the life of grinding wheels with discontinuous cutting surfaces is longer (from 30 to 35%) compared to the life of grinding wheels with uniform surfaces [4].

### 3. Methods applied to research

Our tests on the effects of fluid supply on grinding efficiency in the grinding zone were carried out using the following methods of cooling:

- a) cooling through openings in the grinding wheel (at the 1<sup>st</sup>–3<sup>th</sup> flow rate within 990–14400 cm<sup>3</sup>/min), Figure 7,
- b) cooling through spot injectors (holes from 0.5 to 2 mm in diameter at a flow rate from 155 to 1460 cm<sup>3</sup>/min), Figure 8,
- c) cooling through slot injectors (holes from 0.5 to 1.34 mm in width at a flow rate from 3720 to 9000 cm<sup>3</sup>/min), Figure 8,
- d) flood cooling (conventional),
- e) grinding without cooling.

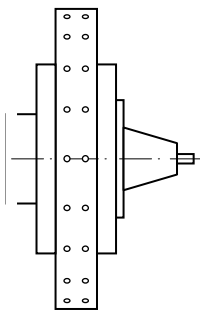


Fig. 7. Pictorial view of grinding wheel with internal holes

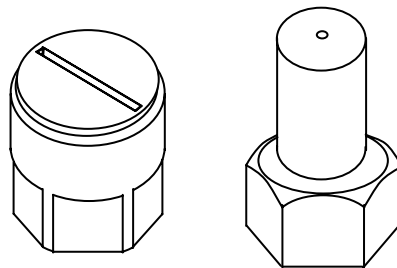


Fig. 8. Pictorial view of spot and slot injectors

Tests were carried out on the flat specimens made of 15 HGM steel after an appropriate heat treatment (hardness  $52 \pm 2$  HRC). Grinding parameters for the surface



grinding while testing were as follows: the wheel speed  $v_s = 36$  m/s, the tangential feed speed  $v_{ft} = 8$  m/min, the axial feed  $f_a = 0.02$  mm/stroke, the number of working strokes  $i = 1$ , the number of sparking-out passes  $i_1 = 3$ , dressing of grinding wheels – 2 strokes of a single-point diamond dresser at a constant dressing feed.

#### 4. Experimental results

Measurements of force distribution during surface grinding are presented in Figure 9 and the Table. Close analysis of the plots (Figure 9) and the data (the Table) shows that in the case of cooling through holes in the grinding wheel, the grinding forces decrease with an increase in the rate of fluid flow. In the case of cooling through point and slot injectors the situation is diametrically different; with an increase in the rate of fluid flow the grinding forces also increase. This can be interpreted as follows: while cooling through the holes in the grinding wheel the fluid is supplied under the influence of centrifugal forces directly to the grinding zone which causes a considerable “reduction in binder”.

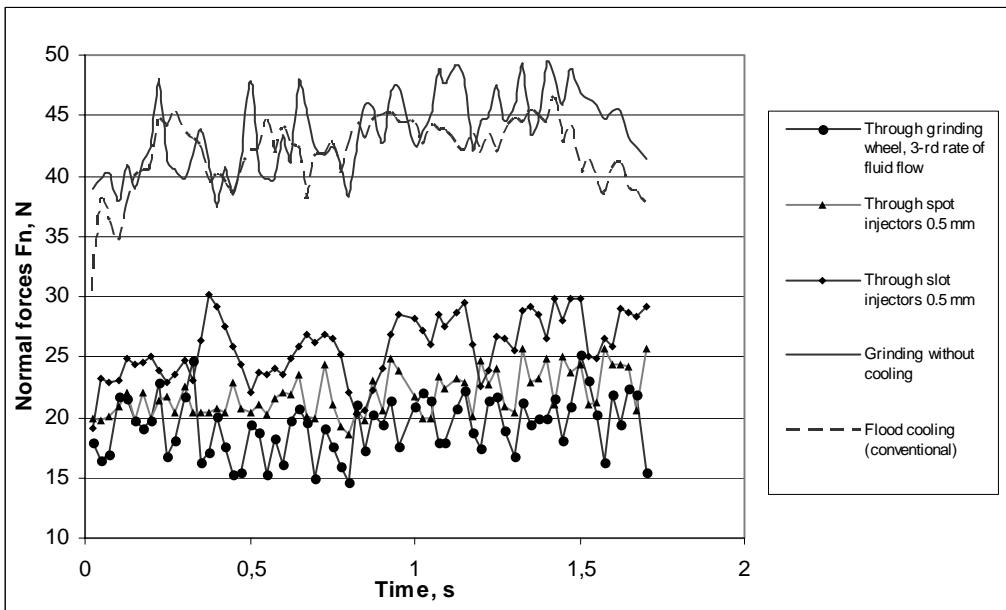


Fig. 9.  $F_n$  forces distribution, depending on various ways of supplying a grinding fluid

In the case of cooling through injectors, our initial tests showed that injectors with the nozzles smaller in size produced higher rates of fluid flow in comparison with larger ones. Further investigations are necessary to explain this phenomenon and we

consider to apply the pressure control to the fluid. In the test carried out, we could only change a diameter of the nozzle.

In the case of cooling through injectors, we have to apply an additional filter to the grinding fluid. In the tests with slot injectors, we observed an interrupted fluid flow. This phenomenon also required more detailed analysis. The tangential forces  $F_t$  showed a similar distribution but they were by 15 N higher.

Table. Medium grinding forces  $F_n$ , depending on various ways of fluid supply

No.	Cooling method	Medium normal grinding force $F_n$ [N]
1	Through grinding wheel at the 1 <sup>st</sup> rate of fluid flow	28.83
2	Through grinding wheel at the 2 <sup>nd</sup> rate of fluid flow	24.08
3	Through grinding wheel at the 3 <sup>rd</sup> rate of fluid flow	19.27
4	Through spot injectors, 0.5 mm diameter	21.91
5	Through spot injectors, 1.5 mm diameter	24.59
6	Through spot injectors, 2 mm diameter	27.33
7	Through slot injectors, 0.5 mm diameter	25.78
8	Through slot injectors, 0.77 mm diameter	25.94
9	Through slot injectors, 1.34 mm diameter	28.03
10	Flood cooling (conventional)	35.84
11	Grinding without cooling	41.05

Furthermore, analysis of vibrations of the grinder fixed headstock also showed that only in the case of fluid supply through the holes in the grinding wheel, an amplitude of vibrations slightly increased at the initial stage of the fluid supply. Then vibrations became stabilized at a level of 0.04  $\mu\text{m}$ .

Previous studies showed that grinding fluid had different effects on a decrease in friction forces in the process of grinding.

## 5. Summary

On the basis of the initial results of our investigations of the effects of various modes of grinding fluid supply during of the grinding process the following conclusions have been drawn:

- the best method of cooling is a mode of fluid supply through the holes in the grinding wheel;
- in the method of cooling through holes in the grinding wheel (at a flow rate equal to 14 400  $\text{cm}^3/\text{min}$ ), the grinding forces are two times smaller than those in a flooded method (at the same flow rate);
- an efficient method of cooling was fluid supply through a spot injector of 0.5 mm in diameter at a fluid flow rate of 155  $\text{cm}^3/\text{min}$ ;

- in the case of conventional cooling (flooded method), a necessary rate of fluid flow is by about 90 times higher than in the case of a cooling by the use of an injector of 0.5 mm in diameter;
- additional fluid filter and an appropriate pump allowing us to force the fluid to the grinding zone at a required pressure should be assembled in the grinder;
- during the tests with different fluid supply to the grinding zone any increased vibrations of the grinder were not observed;
- the flood cooling (conventional) is the least economical way of cooling.

## References

- [1] Brinksmeier E., Heinzl C., Wittman M.: *Effektive Zuführung des Kühlschmierstoffs beim Schleifen*, IDR, 34. Jahrgang, 2/2000.
- [2] Brinksmeier E., Heinzl C., Wittman M.: *Friction, Cooling and Lubrication in Grinding*, Annals of the CIRP, 48/2, 1999, pp. 581–598.
- [3] Hoffmeister H.-W., Langemeyer A.: *Auf dem Weg zum Trockenschleifen., Minimalmengenschmierung Stickstoffkühlung und Graphit-schmierung.*, VDI-Z, 1998, Vol. 140, No. 5, pp. 43–46.
- [4] Jakimov A.B.: *Abrazivno-almaznaja obrabotka fazonnych poverchnostej*, Moscow, Mašinostroenie, 1984, pp. 117–124, 280–288.
- [5] Jakimov A.B.: *Optimizacija processa šlifovanija*, Moscow, Mašinostroenie, 1975, pp. 64–74.
- [6] Klocke F., Eisenblätter.: *Dry Cutting*, Annals of the CIRP, 46/2, 1997, pp. 519–526.
- [7] Klocke F., Schulz A., Gerschwiler K.: *Saubere Fertigungstechnologien – Ein Wettbewerbsvorteil von morgen?* [in]: *Wettbewerbsfaktor Produktionstechnik – Aachener Perspektive*, AWK Aachener Werkzeugmaschinen-Kolloquium. VDI Verlag, Düsseldorf, 1996.
- [8] Oczos E.K.: *Obróbka na sucho i ze zminimalizowanym smarowaniem*, Mechanik, 1998, No. 5–6, pp. 307–318.
- [9] Paul S., Chattopadhyay A.B.: *The Effect of Cryogenic Cooling of Grinding Forces*, Int. J. of Mech. Tools and Manuf., 1996, Vol. 36, No. 1, pp. 63–72.
- [10] *Schnell und trocken*, Werkst. u. Betr., 1997, Vol. 130, No. 5, pp. 356–357.
- [11] Weinert K.: *Schleifen mit Graphit als Schmierstoff. Umweltfreundliche und wirtschaftliche Alternative zu konventionellem Kühlschmierstoff*, VDI-Z, 1998, Vol.140, No. 1/2, pp. 46–49.

## Ekologiczne metody chłodzenia w procesach szlifowania

Koszty procesów wytwarzania można znacznie obniżyć, stosując nowoczesne ekologiczne procesy szlifowania. Przedstawiono wyniki badań własnych i innych uczonych dotyczące takich właśnie procesów. Do nowoczesnych i ekologicznych metod chłodzenia autorzy zaliczają: chłodzenie z wykorzystaniem otworów świadomie wykonanych w ściernicy i ogranicze-

nie strefy przepływu podawania płynu, chłodzenie inżektorowe i trzewikowe, zmianę właściwości ściernicy poprzez specjalnie ukształtowaną powierzchnię roboczą.

Ustalono, że najbardziej efektywną metodą jest chłodzenie przez otwory w ściernicy (zafornowane w trakcie jej wytwarzania). Drugą w kolejności jest metoda chłodzenia z użyciem inżektorów. Odpowiedzi na pytanie, o ile zmniejszy się (w odniesieniu do metody zalewowej) zużycie płynu chłodzącego, będzie można udzielić po zakończeniu badań.

Autorzy w niniejszym artykule przedstawiają wyniki badań wstępnych w tym zakresie.



## **Abrasive Electrodischarge Grinding (AEDG) of advanced materials**

J. KOZAK

Warsaw University of Technology, Al. Niepodleglosci 222, 00-663 Warszawa  
University of Nebraska Lincoln, USA

The main objective of this investigation is to study the Abrasive Electrodischarge Grinding (AEDG) process performance while machining such advanced materials as polycrystalline diamond (PCD), metal matrix composite Al-SiC, polycrystalline cubic boron nitride (PCBN) and electric conductive ceramics. AEDG machining characteristics obtained with oil and deionized water have been compared. The effects of current, pulse on-time and wheel speed on the grinding have been studied. Application of neural network modelling for determination of performance characteristics of AEDG and the comparison of neural network prediction with multiple regression analysis are presented. The study also sheds light on self-dressing effect in AEDG process.

Keywords: *electrical discharge, grinding, self-dressing, neural network*

### **1. Introduction**

Shaping of superhard materials such as polycrystalline diamond (PCD) and polycrystalline cubic boron nitride (PCBN) tool blanks is challenging due to their inherent properties of high strength and high toughness. Diamond grinding is one of the commonly used techniques. Low G ratios, high cutting forces, high wheel costs and limited scope for complex tool edge configurations are some of the problems associated with diamond grinding of PCD/PCBN [1]. In order to remove the material from the PCD/PCBN blanks, the diamond layer of the grinding wheel must be renewed frequently by a dressing operation, resulting in rapid wear of the wheel. Hence, classical grinding is suitable only to a limited extent for production of PCD/PCBN profile tools. The high costs associated with machining ceramics /composites and damages generated during machining are major impediments to the implementation of these materials. In some cases, conventional machining methods cannot be used and innovative techniques or modifications of existing methods are needed.

The electrodischarge machining (EDM) process offers a lower cost alternative with inherent higher accuracy. Published data on the use of die-sinking EDM, wire EDM and electrodischarge grinding (EDG), which incorporates graphite wheel for PCD tool fabrication, is extremely limited. The major PCD manufacturers (General Electric,

DeBeers, and Sumitomo Electric) have reported using wire-EDM to slice their products into segments for subsequent use by tool fabricators [2]. Extensive experimental results along with possible material removal mechanism during wire EDM of PCD and determination of the manufacturing characteristic have been reported in [3]. The effects of wheel speed and pulse settings in EDG on material removal rate (MRR) and surface integrity problems such as the generation of heat-affected layer have been studied in [4, 5].

The technological improvement of machining processes can be achieved by combining different physical-chemical action on the material being treated. In particular a mechanical action, which is used in conventional material removal processes, can be combined with electrical discharge or electrochemical interactions in abrasive hybrid machining such as Abrasive Electrical Discharge Grinding and Abrasive Electrochemical Finishing.

The reasons for developing hybrid machining processes (HMP) are to make use of the combined or mutually enhanced advantages, and to avoid or reduce some adverse effects the constituent processes produce when they are individually applied [6].

Abrasive Hybrid Machining (AHM) processes are the most commonly used in industry. These can be classified in three main subgroups: Abrasive Electrical Discharge Machining (AEDM), Abrasive Electrochemical Machining (AECM), and Abrasive Electro-Chemical-Discharge Machining (AECDM).

Depending on type of tool and working movements that are used in particular process, there are various methods such as: Abrasive Electrochemical Grinding (AECG), Abrasive Electrical Discharge Grinding (AEDG), and Electrochemical Honing (ECH) which use abrasive tool with metallic bond. Abrasive Electrochemical Finishing (AECF), Abrasive Electrical Discharge Finishing (AEDF), and Ultrasonic Electrochemical Machining (USECM) use free abrasive grains.

## **2. Abrasive Electrical Discharge Grinding (AEDG)**

AEDG process, where synergistic interactive effect of combination of electrical discharge machining and grinding process is employed to increase machining productivity [7–16]. The contribution of conventional grinding and electrodischarge grinding (EDG) to AEDG illustrates Figure 1.

In the AEDG process, metallic or graphite electrode used in electrical discharge grinding (EDG) process has been replaced with metallic bond grinding wheel. Therefore, material is removed by the combined effect of electro-erosion and micro-cutting process (mechanical effect of abrasives). An increase in performance measures of the AEDG process becomes evident when machining super-hard materials, engineering ceramics, sintered carbides and metal composites.

Thus, the AEDG is a controlled electrodischarge process assisted by mechanical grinding. In order to achieve mechanical grinding action in the rotary EDM, grits in the wheel are in contact with the workpiece, but this contact does not result in short

circuits between the tool and the workpiece because of the non-conductive diamond grits. The abrasion action in this process helps to speed up the removal of electrically non-conductive components when machining electrical conductive composites like PCD and PCBN. The abrasion can also smooth off the protrusions of the non-conductive ingredients, which insulate the interelectrode gap, so that the electroerosion can be accelerated. The process can be controlled either in grinding dominant state with a relatively less contribution of electrical erosion to acquire a reduced heat-affected surface layer, or in EDM dominant state with a relatively less contribution of grinding to reduce machining force, or in a well balanced state between the grinding and the erosion. Simultaneously electrical discharge interactions on the metal bond superabrasive-grinding wheel lead to its self-dressing in process.

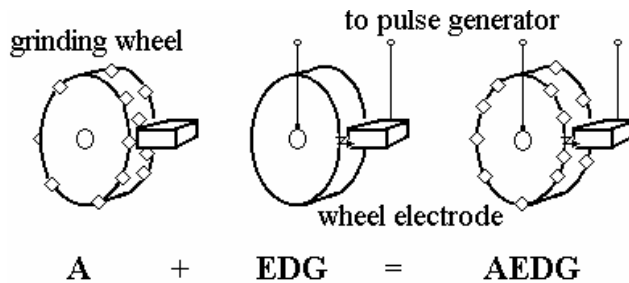


Fig. 1. Principle of Abrasive Electrical Discharge Grinding (AEDG)

Additional benefits include grinding forces, lower grinding wheel wear, and an effective method for dressing of grinding wheel during machining process [7, 8, 15]. Electro-erosion process could also be applied in profiling of super-hard metal bonded wheel [8]. This process has also been found to be effective in preventing chipping of the brittle workpieces [9]. AEDG of titanium alloy (Ti-6Al-4V), Inconel 601, Al-SiC (DURALCAN F3S.20D), PCD, and PCBN have been reported in references [10, 13, 14]. Main parameters influencing the process were peak current, pulse on-time and wheel speed. The enhancement of the material removal rate on introducing abrasion into the process has been studied in comparison to conventional EDM and EDM with a rotating graphite electrode (EDG). The experimental results of DURALCAN and Ti-6Al-4V indicated that AEDG resulted in higher material removal and better surface finish as compared to EDM or EDG [10]. There is an increasing requirement of exploring means to reduce or eliminate the adverse effect of cooling or working fluid (dielectric in EDM) in metalworking industry. One of the grand challenges for the current and future manufacturing industries is to reduce production waste and minimize the related environmental impact to “near zero”. In die-sinking EDM, EDG, and AEDG, hydrocarbon oils are used as dielectric fluid to constrict the discharge channel, cool the erosion zone and flush away debris from the inter-electrode gap. The dielectric oil has a long operating life, but the debris collected

during machining needs an appropriate disposal. Therefore, the research involves the comparative study of the AEDG performance (metal removal rate and surface quality) obtained with oil and deionized water to investigate the feasibility of replacing oil with water as the dielectric fluid. The investigations of AEDG using deionized water in place of commonly used dielectric oil have been reported in [14, 15]. These experiments carried out with different polarities of tool-electrode show that the better quality of machined surfaces was obtained at positive polarity of tool-wheel; therefore, this polarity has been used in further experiments. The PCD blanks were machined with oil and water using 240 grit size grinding wheel when the wheel is connected to positive polarity. MRR obtained with oil is 20–30% more than with water for the same experimental range of current and for wheel speed below 2500 rpm. Surface finish obtained from AEDG of Compax 1600 PCD with water is better compared to all other PCD grades. The  $R_a$  values of surface roughness obtained with water are 2–2.5 times less than those with oil at maximum MRR (i.e. at wheel speed of 2000 rpm) [14].

### 3. Experimental procedure

Experimental investigations have been performed on modified Coborn EM1 EDG machine tool by incorporating a dielectric system for deionized water developed at University of Nebraska. Figure 2 shows the scheme of the machine and experimental system [14, 15 and 16].

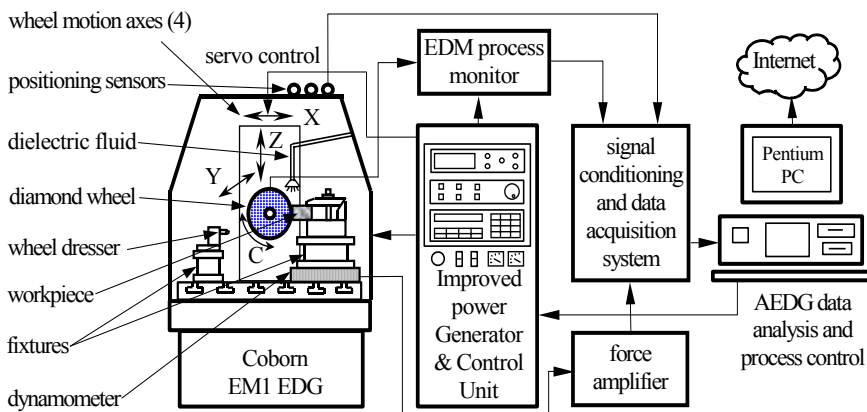


Fig. 2. Schematic diagram of experimental AEDG [14]

The EM1 machine from Coborn (UK), actually an erosion discharge grinding (EDG) machine, is predominantly used by the diamond and polycrystalline diamond (PCD) industries. Although the machine is specially suited for producing PCD tooling, it can be modified for other applications. An extensive study has been done on the



process characterization and machining of PCD using “Reolec 138” as the dielectric fluid during the research in the past few years [10, 13–15].

The research presented was conducted using deionized water as the dielectric fluid. To incorporate the water-based dielectric system the existing pipelines, which carried the oil from dielectric tank to the machine and vice versa, were disconnected. A separate tank with a pump is used along with deionizing chambers and a filter.

The copper-based metal-bonded diamond wheels of 240 and 320 grit sizes (grain size 63 and 32  $\mu\text{m}$ , respectively) have been used for the experiments of this study. Workpiece specimens of the dimensions of  $17 \times 17 \times 3.85$  mm made of COMPAX 1600 Polycrystalline Diamond, BZN 6000 Compacts with polycrystalline cubic boron (PCBN) from GE Superabrasives, DURALCAN F3S.20S and silicon nitride ( $\text{Si}_3\text{N}_4 + \text{TiN}$ ). COMPAX 1600 Polycrystalline Diamond has been machined to compare the machining characteristics.

Material Removal Rate (MRR) was measured by the difference of weight of the workpiece before and after the machining using a Sartorius E-12005 precision scale having a maximum capacity of 1210 g and a precision of 0.001 mg. The surface roughness was measured by a Surtronic 3+ skid and stylus type profilometer having an accuracy of 0.01  $\mu\text{m}$  from Rank Taylor Hobson Co.

Figure 3 shows the selected parameters for a comprehensive experimental investigation. The effect of pulse frequency is presented by the duty factor defined as the ratio of pulse on-time to pulse period.

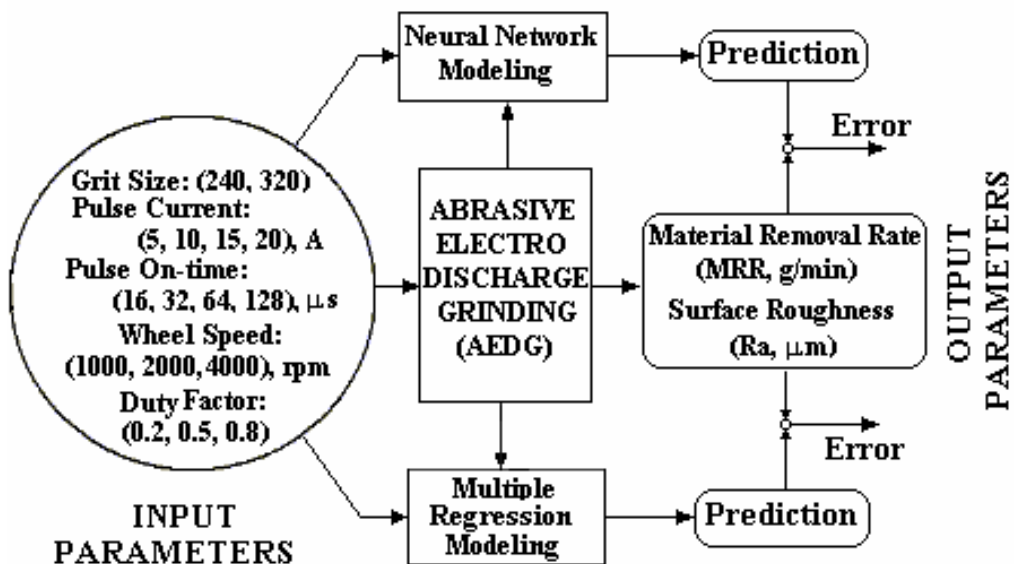


Fig. 3. Input and output parameters at investigation of AEDG

The experimental results are used to compare the use of deionized water with the use of dielectric oil and to train the neural network for prediction of performance characteristics and to study self-dressing process during AEDG.

#### 4. Neural network modelling

Artificial Neural Network (ANN) software, called NeuroShell Predictor, from Ward Systems Group, Inc. has been used for developing prediction models for AEDG process and for determination of machining characteristics, i.e. relationship between operating parameters and performance measures such as MRR and surface roughness. The neural and genetic training strategies are tried and the best model is used for prediction of the AEDG process output parameters. The trained prediction models were used to predict the material removal rate (MRR) and surface roughness ( $Ra$ ). The effect of various input variables on them was analyzed using Neural Network with schematic structure presented in Figure 4. The same experimental data from AEDG was also used to predict material removal rate and surface roughness by multiple regression analysis.

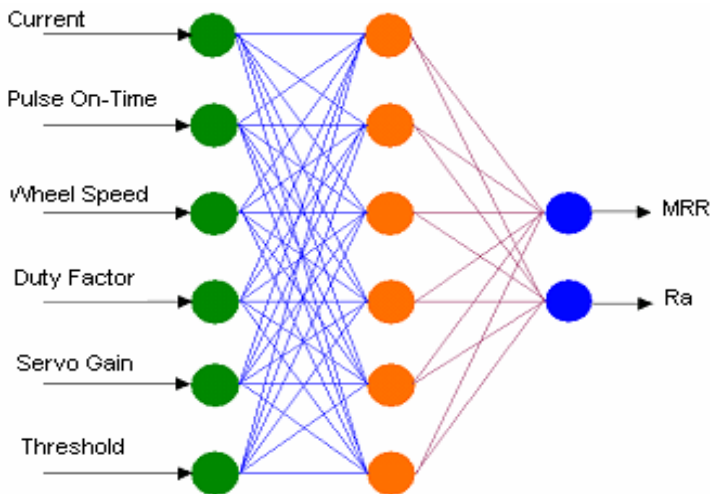


Fig. 4. The structure of neural network for AEDG process

Previous research indicates that the prediction of neural network is good if the training set consists of large number of observations. The higher the number of patterns in the training data set, the higher the prediction accuracy of the model built. In this study, an attempt was made to investigate the effect of size of training set on accuracy of predicted values for optimizing the modelling procedure (learning of the network).

The network used consisted of 30 observations in the case of  $\text{Si}_3\text{N}_4 + \text{TiN}$  and 31 observations in the case of DURALCAN materials [16]. The size of patterns (observations) was varied to obtain different neural network models. These models were used to predict the remaining rows in that data set. First, 10 rows were trained to build the model and remaining rows (i.e. 20 values) were predicted. Then, the size of training set was increased in step of five rows and the accuracy of the predicted values achieved in each model was compared and studied. Four models were created for each output, where the last model consisted of 25 trained rows and 5 predicted rows. For comparison, a model was also created where all the rows were used for training. The predictions of the neural network were also compared with multiple regression analysis results. Training rows, which were used for building the neural network model, were also used to develop the multiple regression models.

Figure 5 shows the relationship of training sets with the prediction of entire data for MRR. In order to achieve a prediction error less than 8%, only 15 rows are needed for training in ANN, whereas in the case of multiple regressions, even using training set of 30 rows, a prediction error greater than 12% was noticed. Hence, fewer experiments would be sufficient for accurate prediction by neural networks.

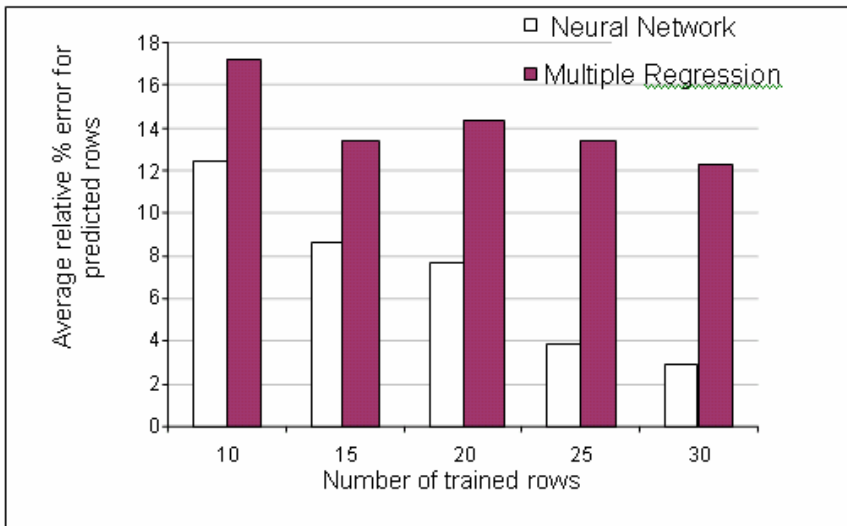


Fig. 5. Effect of training data set on accuracy MRR - prediction model for  $\text{Si}_3\text{N}_4 + \text{TiN}$  [15]

Thus, ANN reduces overall cost and saves valuable time. As the size of the training data set increases, the accuracy of the prediction model also increases. For example, in neural network, when the number of training rows was increased from 10 to 25, the error was reduced by nearly 3 times, whereas in multiple regression, the error was reduced only by 1.3 times. When the model was trained with 30 patterns, neural networks proved to be 4 times better than multiple regressions.

On modelling of relationship for surface roughness parameter  $R_a$ , for a prediction error less than 8% only 15 rows were used in training of ANN, and in multi-regression modelling, 15 and larger number of rows gave the same value of prediction error (Figure 6).

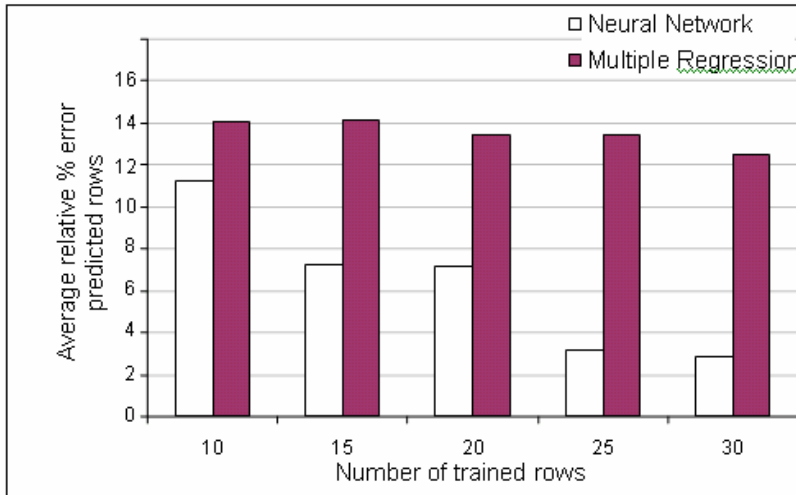


Fig. 6. Effect of training data set on accuracy  $R_a$  - prediction model for  $\text{Si}_3\text{N}_4 + \text{TiN}$  [15]

As the size of the training data set increases, accuracy of the prediction model also increases. For example, in neural network, when the number of training rows was increased from 10 to 25, the error reduced almost 3.7 times, whereas, in multiple regression, the error was reduced only by 1.2 times. Thus, the neural network prediction is better than that given by the multiple regression analysis in all cases.

In these studies, ANN trained with 25 rows was used for determination of machining characteristics of AEDG process.

## 5. Performance characteristics of AEDG

After validating the neural network model, ANN was used for determination of machining characteristics of AEDG, i.e. relationship between operating parameters and performance measures such as MRR and surface roughness. The trained prediction model (with 25 trained rows) was used to predict the material removal rate while machining silicon nitride using AEDG. Several graphs were plotted using ANN predicted values to validate the model. Figures 7–10 show the effect of various significant factors on MRR using ANN predicted values [16]. These ANN values were compared with experimental values and were found closer to experimental values. Material Removal Rate (MRR) achieved for DURALCAN F3S.20S,  $\text{Si}_3\text{N}_4 + \text{TiN}$ ,

PCD and PCBN increases with an increase in current. MRR is more with 240 grit size wheels than with 320 grit size wheels. At low currents and higher wheel speeds better surface finish values were obtained with wheel of 320 grit size.

Effect of wheel speed on the MRR of silicon nitride is shown in Figure 7. A higher wheel rotating speed leads to a faster material removal because of the enhanced mechanical abrasion. As the wheel speed increases, material removal rate increases. Increase in MRR effect is also due to improved hydrodynamic flushing action at the spark gap. At high wheel speed there is a transition in material removal mechanism from predominant EDM to grinding which leads to rapid material removal.

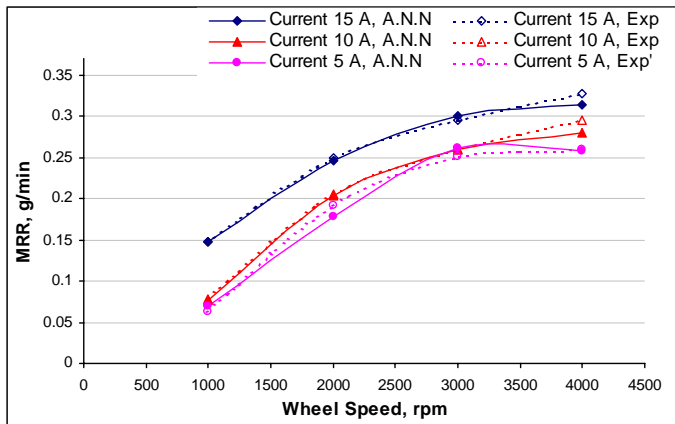


Fig. 7. Effect of wheel speed on MRR for  $\text{Si}_3\text{N}_4 + \text{TiN}$  at different currents (pulse on-time = 20  $\mu\text{s}$ , duty factor = 0.5, grit = 320)

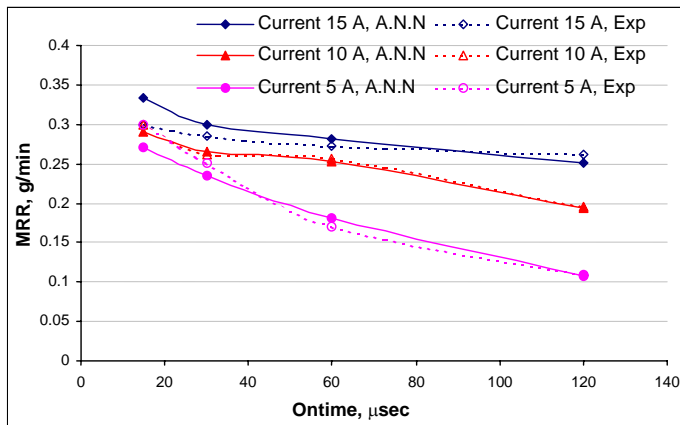


Fig. 8. Effect of pulse on-time on MRR for  $\text{Si}_3\text{N}_4 + \text{TiN}$  at different currents (wheel speed = 4000 rpm, duty factor = 0.5, grit = 320)

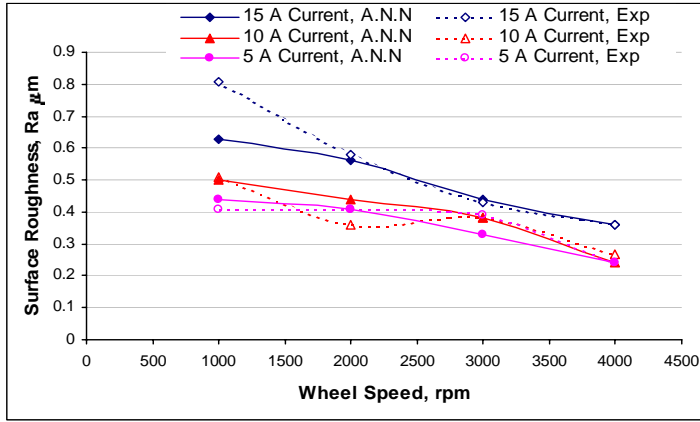


Fig. 9. Effect of wheel speed on surface roughness for  $\text{Si}_3\text{N}_4 + \text{TiN}$  at different currents (pulse on-time = 20  $\mu\text{s}$ , duty factor = 0.5, grit = 320)

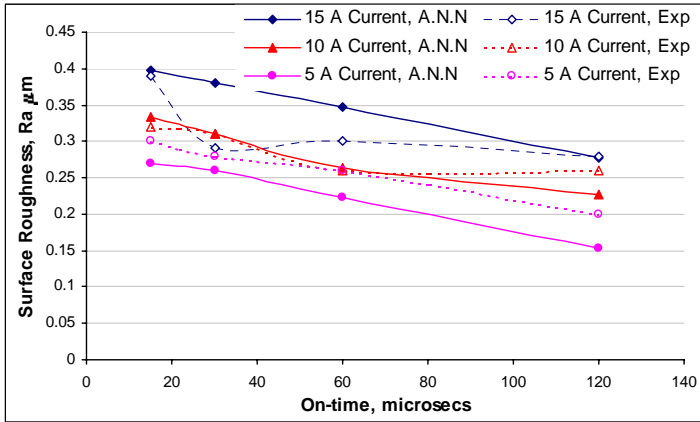


Fig. 10. Effect of pulse on-time on surface roughness for  $\text{Si}_3\text{N}_4 + \text{TiN}$  (wheel speed = 4000 rpm, duty factor = 0.5, grit = 320)

Figure 8 shows the effect of pulse on-time duration on material removal rate. At certain pulse energy, pulse duration being longer with the less current amplitude, more thermal energy is lost. This causes the decrease in material removal at longer pulse time. Shorter pulse duration has larger current amplitude, and the heat is much more concentrated. Thermal energy losses decrease and EDM action becomes higher at smaller pulse on-time. In addition, concentrated heat causes further thermal softening, leading to improved mechanical abrasion. Hence, material removal rate is high in the case of silicon nitride composite for smaller on-time pulse duration. One more reason for higher material removal rate at small pulse duration is that as the pulse on-time increases, the off-time also increases for a constant duty factor. Since the pulse off-

time is an unproductive duration, it causes total machining time to be increased and causes the MRR to be decreased. From graph (Figure 8), it is found that 20  $\mu\text{s}$  is the optimal pulse on-time for most discharge currents within the experimental range for AEDG of silicon nitride.

The surface texture is improved with the increase in wheel speed as shown in Figure 9. With an increase in wheel speed, as the number of abrasive–workpiece interactions per unit time increases, the number of spark discharges per unit grain decreases. Fewer craters are formed, leading to better surface finish. Moreover, at higher speeds, dominant grinding condition causes improved surfaced texture. Finer surface finish is obtained at 4000 rpm for all current settings.

It is seen in Figure 10 that as the pulse duration increases, the surface roughness tends to decrease. The surface roughness is higher at 20  $\mu\text{s}$  pulse time and it stabilizes at 60  $\mu\text{s}$  pulse on-time. With the further increase in pulse time, surface roughness remains almost constant. Although the crater size increases with the increase in pulse on-time, surface roughness decreases. This may be because erosion is comparatively less at higher pulse on-time values.

## 6. Study of self-dressing process during AEDG

In grinding process, the metal-bonded wheel loses its cutting ability after certain number of operations. Hence, to resume the efficient grinding process, frequent re-dressing of wheel becomes imperative. Conventional dressing methods of metal bonded grinding wheels are time consuming and lead to severe wear of the tool.

One of the most important benefits of AEDG process is self-dressing, where the electrical discharges simultaneously erode workpiece and tool (wheel). Therefore in AEDG the wheel is being dressed continuously [8, 12, 15, 16]. As the dressing of the wheel is continuous, there is no need to interrupt machining for dressing the wheel, thus saving the productive machining time.

Figure 11 shows a schematic diagram of workpiece and wheel contact region with abrasive grits, metallic bond and embedded or lodged workpiece chips in the wheel. These lodged chips melted due to the thermal energy generated by series of electrical discharges D and occasional short circuits SC.

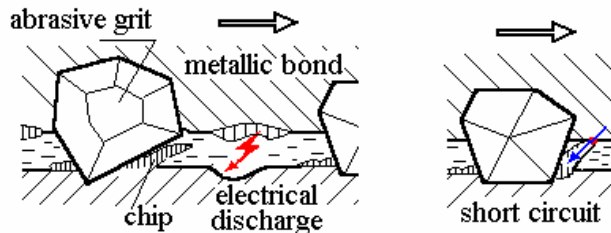


Fig. 11. Schematic diagram of electrical discharge and short circuit during contact of a chip with wheel bond

An experimental analysis of debris after machining has indicated that the chips have been melted. It was also observed that for certain values of pulse on-time and pulse current, the material removed during AEDG was in the powder form. These experimental observations indicate the occurrence of melting of embedded chips, within certain time that is shorter than applied pulse on-time. To verify this hypothesis, the following modelling and analysis have been done.

To estimate the time required for the chip temperature to reach melting point, the thermal model of a chip (length  $L$  under voltage  $U$ ) has been developed (Figure 12).

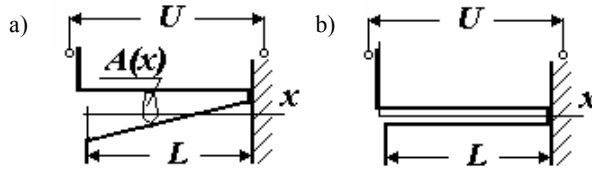


Fig. 12. Models of a chip

The following assumptions are made in developing the model for the heating of chips during electrical short circuit:

1. The cross-sectional area  $A$  of the chip in a general model “a” is changing along the length and in the model “b” value of  $A$  is constant throughout the length of the chip.

2. The changes in temperature, current density and electrical properties in the cross-section of the chip are negligible.

3. The changes in specific heat  $C$  and density  $\rho$  of the chip material with temperature are negligible.

4. The change in the electric resistance of the chip material is given by:  $r = r_0(1 + \alpha\theta)$ , where:  $r_0$  and  $\alpha$  are the electrical resistance and the temperature coefficient of resistance at a temperature  $T_0$ , respectively, and  $\theta = T - T_0$  is the increase in a temperature of the chip.

5. The current is determined by ohmic drop voltage, i.e. electromagnetic effects are neglected.

Considering the Joule heat, the increase in temperature of the chip can be described as:

$$\frac{\partial \theta}{\partial t} = \frac{a}{A} \frac{\partial}{\partial x} \left( A \frac{\partial \theta}{\partial x} \right) + r \frac{i^2}{\rho \cdot C}, \quad (1)$$

where  $i = \frac{I}{A(x)}$  is current density, and  $a$  is the thermal diffusivity.

The current  $I$  can be determined from Ohm’s law as follows:



$$I \left( r_0 \int_0^L \frac{1 + \alpha \cdot \theta}{A(x)} dx + R_C \right) = U, \quad (2)$$

where  $A$  is the cross-sectional area of the chip and  $R_C$  is contact resistance.

At increasing temperature of the chip and the assumption that copper bond of wheel plays the role of a perfectly good conductor, the contact resistance is approximately described by expression [17]:

$$R_C = r_0 \left( 1 + \frac{2}{3} \alpha \cdot \theta_c \right) / d, \quad (3)$$

where  $\theta_c$  is an increment temperature in the contact spot,  $d$  is the characteristic dimension of contact spot. For circular contact,  $d$  is the diameter of spot.

Upon transformation of Equation (2) and Equation (3), the current density can be estimated by:

$$i = \frac{U}{r_0 \left[ \frac{1 + 0.7\alpha \cdot \theta_c}{d} + \int_0^L \frac{1 + \alpha \cdot \theta}{A(x)} dx \right]}. \quad (4)$$

For simplification it is necessary to determine the magnitude of terms on the right-hand side of Equation (1) for typical condition of AEDG. For example, during machining cobalt matrix composite (such as PCD, tungsten carbides) needed for estimation the data are as follows: density  $\rho = 8900 \text{ kg/m}^3$ , specific heat  $C = 0.42 \text{ kJ/kgK}$ , specific electrical resistance  $r_0 = 5.81 \times 10^{-8} \text{ } \Omega\text{m}$ , melting point  $T_m = 1768 \text{ K}$ , thermal coefficient of electrical resistance  $\alpha = 0.004 \text{ 1/K}$ .

For voltage at short circuit  $U = 2.5 \text{ V}$ , grit size of 240 (grain size of  $63 \text{ } \mu\text{m}$ ) and the chip with  $L = 50 \text{ } \mu\text{m}$  and  $d = 20 \text{ } \mu\text{m}$ , the orders of mentioned magnitudes in K/s are

$$a \frac{\partial^2 \theta}{\partial x^2} \sim a \frac{T_m - T_0}{L^2} = 2.36 \times 10^7, \quad r \frac{i^2}{\rho \cdot C} = 4.28 \times 10^{16}.$$

Therefore, the first term, which is connected with heat conduction along the  $x$ -axis, can be neglected and Equation (1) after transformation becomes:

$$\frac{\partial \theta}{\partial t} = \frac{r_0 \cdot U^2}{\rho \cdot C \cdot A^2(x) \cdot \left[ \frac{1 + 0.7\alpha \cdot \theta_c}{d} + \int_0^L \frac{1 + \alpha \cdot \theta}{A(x)} dx \right]^2} \quad (5)$$

with the initial condition  $\theta(t = 0) = 0$ .

In Equation (5), the variable of  $x$  is treated as parameter and solution can be obtained using iterative procedures.

For AEDG process when voltage during short circuit is approximately stable and for model (b) with a constant cross-sectional area, after integrating Equation (5) and transforming and neglecting the second-order term, the time for melting can be estimated from

$$t = \frac{r_0 \cdot \rho \cdot C \cdot L^2 \cdot \theta}{U^2} \left[ 1 + \frac{1}{2} \alpha \cdot \theta + \left( 1 + \frac{1}{3} \alpha \cdot \theta \right) \frac{d}{L} \right]. \quad (6)$$

Figure 13 shows the changes in increment temperature during time for the example considered above.

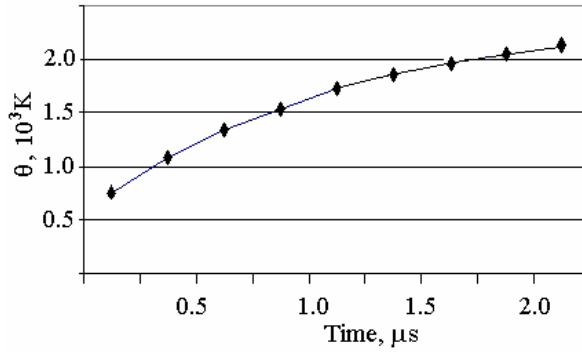


Fig. 13. Change in temperature of the chip with time

The time estimated for the chip temperature to reach melting point is  $t_m = 1.03 \mu\text{s}$ .

For the case of AEDG when pulse generator with constant amplitude of pulse current  $I$  is used, the heating can be approximately described by

$$\frac{\partial \theta}{\partial t} = \frac{r_0 (1 + \alpha \theta) i^2}{\rho \cdot C}, \quad (7)$$

$$\theta(t=0) = 0,$$

where  $i = \frac{I}{n \cdot A(x)}$ ,  $I$  is setting current and  $n$  is the number of chips contacted with the wheel bond.

Solution of Equation (8) for this case is

$$t = \frac{\rho \cdot C \cdot n^2 A^2}{\alpha \cdot r_0 \cdot I^2} \ln(1 + \alpha \theta). \quad (8)$$

For the example considered above, at pulse current  $I = 15$  Amp, the required time for melting a single chip is  $t_m = 25.5 \mu\text{s}$  for cross-sectional area  $A = 625 \mu\text{m}^2$  and  $t_m = 0.65 \mu\text{s}$  for  $A = 100 \mu\text{m}^2$ . Similar estimates for different workpiece materials using Coborn EM1 machine (pulse on time of  $16 \mu\text{s}$  to  $120 \mu\text{s}$  and pulse current of 5 Amp to 25 Amp) confirm that the embedded or lodged chips melt well before the end of the pulse on time. Visual observation and analysis of AEDG debris also verified this conclusion. An absence of chips was noticed at the end of machining as opposed to presence of chips after the grinding operation.

The presence of self-dressing can be concluded by the difference in material removal rates for grinding and AEDG processes [15]. Figure 14 shows the material removal rate for DURALCAN F3S.20S using metal bonded diamond wheel. During grinding the material removal rate is high in the initial few minutes of the experiments. However, as the machining time increases, the diamond abrasive grains become blunt and wheel gets loaded with the aluminum matrix. Due to this reason, the wheel loses its cutting ability and the material removal rate significantly decreases. After 10 minutes of grinding the MRR decreases to one half of the initial value. At the end of the 68-minute long experiment, the material removal rate is one fourth of the initial MRR.

For AEDG experiments with 15 Amp current, the material removal rate is almost constant (0.08 g/min) throughout the experiment. This constant MRR can be attributed to the self-dressing effect, i.e. the wheel getting dressed online continuously.

Additional experiments were carried out in the following sequence of grinding (G)–AEDG–G–AEDG–G (Figure 15).

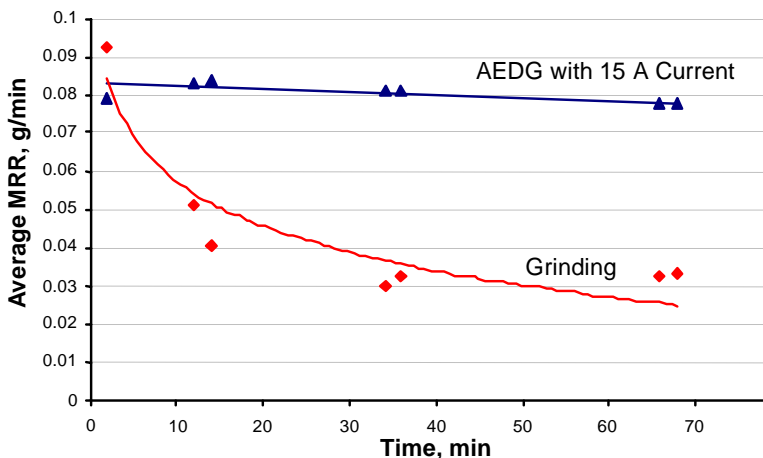


Fig. 14. Effect of machining time on MRR for Duralcan (F3S.20S) (speed = 4000 rpm, pulse on time =  $60 \mu\text{s}$ , duty factor = 0.5, grit size = 320) [15]

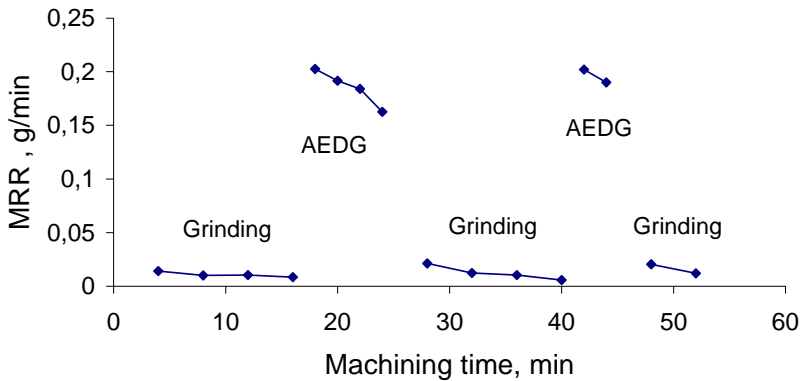


Fig. 15. Material removal rate (MRR) in G–AEDG–G–AEDG–G sequence

In the first stage of grinding, mechanically dressed wheel was used. After 16 minutes of grinding (current = 0 A), MRR decreased by 40%, from 0.014 g/min to 0.0085 g/min. Next the AEDG process was started with pulse current of 20 A, the initial MRR was 0.21 g/min which is 25 times higher than MRR of grinding process. After 8 minutes of AEDG process, the second stage of grinding was started, the initial MRR was 0.021 g/min, which is almost 1.5 times higher compared to the initial MRR of the first stage grinding when fresh wheel was used. This result shows occurrence of self-dressing phenomenon during AEDG. The similar results were observed when this sequence of operations was continued. Surface roughness during grinding processes were by 40% better compared to AEDG process.

Figure 16 shows the material removal characteristics for polycrystalline diamond (PCD). While performing machining on PCD at zero current (pure grinding), the material removal rate is high in the initial phase of the experiments. As the machining progresses beyond 10 minutes, almost no material removal takes place. The hard PCD workpiece destroys the cutting edges of the tool faster preventing any grinding action to occur. As there is no current, self-dressing does not occur and the wheel substantially loses its machinability. When the current of 15 Amp is used, the material removal rate gradually decreases with machining time. In this condition, the self-dressing occurs because the electrical sparks sharpen the blunt edges on the periphery of the wheel. However, it seems that electrical sparks were not sufficient to dress the wheel to the level required. This leads to a slight drop in the material removal rate over the machining time. Minimum MRR at 15 Amp current is almost equal to maximum MRR achieved when no current is used. At 20 Amp current, MRR was almost 1.5 times the MRR achieved at 15 Amp current and 3 times higher than MRR of grinding at the beginning of machining. The minimum MRR at 20 Amp current (i.e. after 70 min of machining) is almost 2 times higher than maximum MRR of grinding at the beginning.

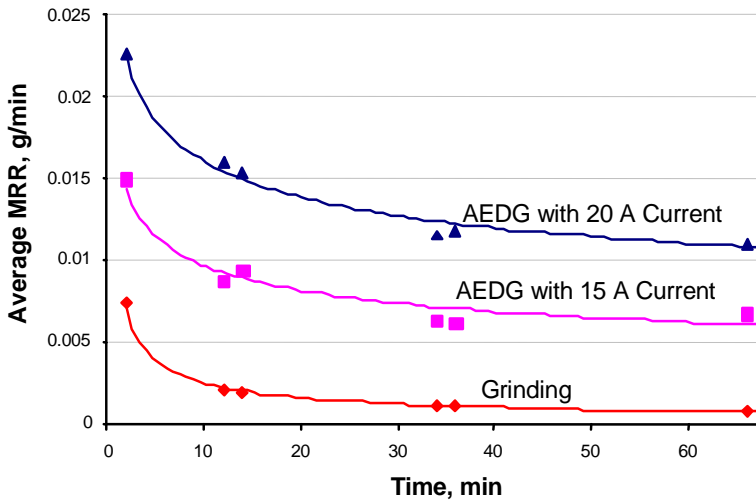


Fig. 16. Effect of machining time on MRR for PCD (speed = 4000 rpm, pulse on time = 60  $\mu$ s, duty factor = 0.5, grit size = 320) [15]

Thus, in the case of brittle materials, which consist of nonconductive PCD or PCBN particles, electrical discharges have significant contribution to material removal from workpiece. The investigation shows that G-ratio with AEDG depends on pulse current. For PCD, the values of G-ratio were less than one (0.3–0.8), which meant that more tool material was removed than workpiece material while machining PCD at given instance of time. These values were almost 5–10 times higher when compared to diamond grinding of PCD. Using the same sequence of operations (G–AEDG–G) for PCD, similar results were observed to those while machining Duralcon.

Therefore, in the sequence of AEDG–G operations a good surface quality and higher MRR can be obtained.

## 7. Summary

This paper reports a theoretical analysis and experimental investigations of self-dressing mechanism in Abrasive Electrodischarge Grinding (AEDG). A visual inspection of debris and quantitative comparison of material removal variation with grinding process support the theoretical analysis. An experimental study has been conducted to explore the feasibility and application of deionized water as dielectric medium instead of water to address the environmental aspects of the AEDG process. A comprehensive experimental study and subsequent neural network modelling are also reported. It is shown that the neural network model-based prediction is better than multiple regression even using limited data.

## Acknowledgement

The American National Science Foundation (Research Grant #DMI-9908219), the Polish State Committee for Scientific Research (Research Grant # 8 T07D 04221) and the State of Nebraska (Nebraska Research Initiative Fund) are gratefully acknowledged for their support. Author also acknowledges H.G. Khilnani and S. P. Santhanam for their assistance in this study.

## References

- [1] Werner P.G., Kenter M.: *Material Removal and Wheel Wear Mechanisms in Grinding of Polycrystalline Diamond Compacts*, Proceedings of the First International Symposium on Machining of Advanced Ceramic Materials and Components, 1987.
- [2] Anon: *Wire EDM Guidelines for Cutting COMPAX Diamond Tool Blanks and BZN Compacts*, General Electric Publication, 1987.
- [3] Kozak J., Rajurkar K.P., Wang S.Z.: *Material Removal in WEDM of PCD Blanks*, ASME Journal of Engineering for Industry, Vol. 116, No. 3 (1994), 363.
- [4] Aspinwall D.K., Fu S., Bennett M.: *Design and Initial Performance Aspects of EDG Equipment Developed for PCD Tool Fabrication*, Proceedings of the Machine Tool Design and Research Conference, 1986, 389.
- [5] Aspinwall D.K., Fu S., Menshawy F.E.: *Operating Parameters and Machinability Data for PCD Blanks Using EDG Equipment*, Proceedings of NAMRC, Vol. 15 (1987), 418.
- [6] Kozak J., Rajurkar K.P.: *Selected Problems of Hybrid Machining Processes*, Advances in Manufacturing Science and Technology, Vol. 24, No. 2 (2000), 5.
- [7] Grodzinskii E.Y.: *Grinding with Electrical Activation of Wheel Surface*, Mach. Tooling, Vol. 50 (1979), 10.
- [8] Pachlin J.A.: *Electro-Contact Diamond Grinding in Russian*, Maszynostrojenie, Leningrad, 1985.
- [9] Aoyoma T., Inasaki I.: *Hybrid machining – combination of electrical discharge machining and grinding*, Transactions of the North American Manufacturing Research Institution of SME, Vol.14 (1986), 654.
- [10] Rajurkar K.P., Wei B., Kozak J., Nooka S.R.: *Abrasive Electrodischarge Grinding of Advanced Materials*, Proceed. of the International Symposium for Electromachining, ISEM-X1, Lausanne, Switzerland, 1995, 863.
- [11] Zhang J.H., Ai X., Lee K.W., Wong P.K.: *Study on Electro-Discharge Diamond Wheel Grinding (EDGM) of Ceramic Materials*, Materials and Manufacturing Processes, Vol. 11, No. 5 (1996), 763.
- [12] Koshy P., Jain V.K., Lal G.K.: *Mechanism of Material Removal in Electrical Discharge Diamond Grinding*, Int. J. Mach. Tools Manufact., Vol. 36, No. 10 (1996), 1173.
- [13] Shrivastava S., Rajurkar K.P., Zhao W.S.: *Rotary Electrodischarge Machining of Polycrystalline Diamond*, Transactions of the North American Manufacturing Research Institution of SME, Vol. 17 (1999), 141.
- [14] Kozak J., Rajurkar K.P., Muruganandham R.: *Neural Network Prediction of Abrasive Electrodischarge Grinding (AEDG) Process Performance*, Proceed. of the International Symposium for Electromachining, ISEM-XIII, Vol. 1, Bilbao, Spain, 2001, 420.

- [15] Kozak J., Rajurkar K.P., Khilnani H.G.: *Performance Characteristics in Rotary Abrasive Electrodischarge Machining*, Transaction of the North American Manufacturing Research Institution of SME (NAMRI/SME), Vol. 30, 2002, 154.
- [16] Khilnani H.G.: *Abrasive Electrodischarge Grinding of Advanced Materials*, M.S. Thesis, University of Nebraska-Lincoln, 2001.
- [17] Holm R.: *Electric Contacts*, Springer-Verlag, New York Inc., 1967.

### Ścierne szlifowanie elektroerozyjne zaawansowanych materiałów

W obróbkach hybrydowych HMPs (*HMP – Hybrid Machining Processes*) do kształtowania elementów maszyn, narzędzi, elementów mikroelektronicznych i mikroelementów w układach mechatronicznych wykorzystuje się łączenie dwu lub więcej procesów obróbczych, często o różnych oddziaływaniach fizykochemicznych na materiał obrabiany. Dzięki temu można znacznie podwyższyć wskaźniki użytkowe kształtowania oraz zmniejszyć ujemne cechy i skutki występujące podczas indywidualnej realizacji sposobów, które połączono. W pracy przedstawiono wyniki badań ściernego szlifowania elektroerozyjnego (AEDG), w którym wykorzystuje się zarówno mikroskrawanie, jak i erozję elektryczną zachodzącą podczas wyładowań elektrycznych. AEDG prowadzono z zastosowaniem ściernicy diamentowej z wiązaniem metalowym i dejonizowanej wody jako dielektryka. W pierwszej części opisano wyniki badań nad wyznaczeniem podstawowych charakterystyk procesu, obejmujących powiązania parametrów obróbki z jej wskaźnikami użytkowymi podczas obróbki ceramiki technicznej. Wykazano przy tym efektywność zastosowania sieci neuronowej do modelowania procesu AEDG. W drugiej części omówiono wyniki badań teoretycznych i doświadczalnych procesu samoostrzenia się ściernicy wyładowaniami elektrycznymi w czasie obróbki materiałów supertwardych (PCD) i kompozytów metalowych (typu Duralcan). Przeprowadzone badania potwierdziły wysoką efektywność AEDG, w szczególności podczas obróbki takich materiałów zaawansowanych jak: PCD, PCBN, ceramika techniczna i kompozyty o osnowie metalowej.